Effects of Disc Injuries on the Mechanical Properties of the

Lumber Disc

A Thesis

Presented by

Tirad Sulaiman Alsharari

Supervisor: Associate Professor John Costi

Submitted in partial fulfilment of the requirements of the degree of

Master of Engineering (Biomedical)

College of Science and Engineering

Flinders University

October 2018

Declaration

I certify that this thesis does not incorporate without acknowledgment any material previously submitted for a degree or diploma in any university; and that to the best of my knowledge and belief it does not contain any material previously published or written by another person except where due reference is made in the text.

Signed: _____ On: _17____/__10__/_2018____

Tirad Alsharari

Abstract

Background

Intervertebral disc tears can cause spinal disorders such as chronic low-back pain (LBP) and are linked to increasing age and disc degeneration; 80% of the population suffer from them at some point in their lives (Andersson 1999; Buckwalter 1995; Adams & Roughley 2006). LBP is a condition frequently experienced throughout the course of many people's lifetimes and has major financial effects on the individual and society (White 1990). Its cause is ascribed to work-related injuries, to strenuous daily routine activities and to leisure activities, such as sports. The disorder has become a widespread problem and influences the quality of life of affected individuals (Urban & Roberts 2003). There are three distinct types of annular disc tears: rim lesions, concentric (circumferential) tears and radial tears. Rim lesions are more pronounced at the human spinal level T12/L1. Radial tears and concentric tears occur in equal frequency at level L4/L5 of the spine (Hilton et al. 1976; Thompson et al. 2000).

There have been limited in vitro studies investigating the effects of disc injuries on the mechanical behaviour of functional spinal units (FSU) in certain degrees of freedom (DOF) (e.g. flexion–extension, bending, axial rotation and compression). Under physiological conditions, mechanical tests have been conducted on FSUs with acute injuries inflicted on their discs to simulate annular disc tears. The findings show consensus in some areas, such as on the effects of tears in terms of various DOF; however, they lack agreement in others. For example, while FSU stiffness was found to decrease for rim lesions in axial rotation, it seemed to remain unaffected, to increase or sometimes to decrease for radial tears in flexion–extension (de Visser et al. 2007; Michalek& Iatridis 2012; Thompson et al. 2004; Thompson et al. 2000). The effects of the injuries were measured under varying simulated physiological conditions (e.g. inclusive or exclusive of a compressive preload and a posterior element) and sometimes in the presence of other potentially affecting factors (e.g. varying levels of disc degeneration and/or in combination with other injuries), which may explain any inconsistency found in the results. To the author's knowledge, no studies have examined the six degrees of freedom (6DOF) in terms of the functioning of FSUs with disc injuries.

Objectives

The primary aim of this thesis was to evaluate the effects of disc injuries, particularly rim lesions and radial tears, on the mechanical and viscoelastic properties of ovine lumbar FSUs. These properties were evaluated under 6DOF dynamic testing, mimicking three physiological disc conditions that occur during walking and through office work (Costi et al. 2008). This study also compared the failure peak loads of the specimens exhibiting the two types of injuries after being subjected to traumatic overload.

Methods

Sixteen healthy sheep L4/5 FSUs (vertebra–disc–vertebra with an intact posterior element) of ages ranging from one to three years were randomly assigned into two groups: (1) for radial tears and (2) for rim lesions. Before and after the creation of injuries, each FSU was immersed in a hydration bath overnight under a preload equivalent to its disc size; it was then subjected to 6DOF dynamic testing at 1 Hz. 0.1 Hz and 0.01 Hz. After this, traumatic overload was applied to achieve FSU failure. The stiffness (the force/translation or moment/rotation) and the phase angle (the temporal shift between loading and displacement) were calculated for each DOF and at each frequency using the collected data and considering the peak load at which each FSU failure occurred.

Results

Under 6DOF dynamic testing, radial tears and rim lesions significantly decreased FSU stiffness in axial rotation (mostly toward injury location) at 1 Hz and 0.1 Hz, and in left and right lateral shear at 0.1 Hz. Testing at the lower frequency 0.01 Hz did not seem to make variation in the effects of both injuries. However, FSU phase angle displayed significant variation by radial tears and no changes by rim lesions. The change in frequency appeared to significantly determine the directions affected by radial tears and the patterns of effect. This control was clear by radial tears when an increase in phase angle changed from left-right lateral shear at 0.1 Hz to flexion- extension at 0.01 Hz. Such change in frequency also showed a decrease in phase angle by radial tears in posterior-anterior shear. The ultimate failure loads between specimens of radial tears and rim lesions resulting from a traumatic failure were not significantly different.

Conclusion

These findings can be clinically beneficial for example to people diagnosed with radial tears or rim lesions in their intervertebral discs. It raises their awareness and better understanding on the effects of directions they need to avoid where FSU stiffness can be most affected. Fields such as tissue engineering can benefit from understating a viscoelastic property of disc under dynamic movement simulating that of the in-vivo condition.

Acknowledgements

Table of Contents

List of Figures

List of Tables

List of Abbreviations

6DOF	Six degrees of freedom
AF	Annulus Fibrosus
AoR	Axis of rotation
AP	Anterior–posterior
CPSD	Cross power spectral density
DOF	Degrees of freedom
FEM	Finite element method
FSU	Functional spinal units
GCS	Global coordinate system
ICC	Interclass correlation coefficient
LAT	Lateral side
LBP	Lower back pain
NATA	National Association of Testing Authorities
NP	Nucleus pulposus
PBS	Phosphate-buffered saline
PMMA	Polymethyl methacrylate
SP	Spinous process
TP	Transverse process
VB	Vertebral body
VEP	Vertebral endplate

Chapter 1: Introduction

The lumbar spine is a pivotal structure in the human body, comprising complex, specifically designed structures and tissues that together provide mobility, flexibility and loadbearing strength to the body (Ferguson & Steffen 2003). Among the many spinal disorders, lower back pain (LBP) is a frequent problem encountered over the course of most people's lifetimes. LBP in mild or chronic form can be ascribed to work-related injuries, to strenuous daily routine activities or to leisure activities, such as sports. This disorder has become a widespread problem and influences the quality of life of affected individuals (Urban & Roberts 2003). Thus, awareness of the events causing LBP and other spine-related disorders is imperative, not only to fully understand the underlying mechanisms of these disorders, but also to formulate new and advanced treatment modalities (Sengupta 2017).

The intervertebral disc degenerates rapidly and earlier than other musculoskeletal tissue in the body (Urban & Roberts 2003). Studies have suggested a link between increasing age and degenerative changes in the intervertebral joint of the spine (Buckwalter 1995; Adams & Roughley 2006) and it has been concluded that certain degenerative changes occur in functional spinal units (FSUs)—consisting of two vertebrae, an intervertebral disc and facet joints—that lead to altered mechanical behaviour and modifications to the viscoelastic properties of the spine (Urban & Roberts 2003). Notably, the formation of tears in the annulus fibrosus (AF) of the disc has been shown to lead to degenerative changes that take place overtime (Anderson et al., 2002, Osti et al., 1990). However, to examine spinal disorders, we need a thorough and deep understanding of the structure and biomechanical functioning of the spine and its integral components—that is, the intact FSU.

1.1 Anatomy of the Lumbar Spine

The spine is a complex 3D structure (see Figure 2.1). The spinal column is divided into five regions, comprising a total of 33 alternating (bony) vertebrae, connected to each other via intervertebral discs and the diarthrodial facet joints. The uppermost region in the spine is the cervical (with seven vertebrae), situated in the neck area; beneath it is the thoracic region (with 12 vertebrae). Below this region is the lumbar spinal region, which is in the lower back area of the body (Ferguson & Steffen 2003). Underneath the lumbar spinal region are the sacral region (with five vertebrae) and the coccygeal region (with four vertebrae) as shown below.
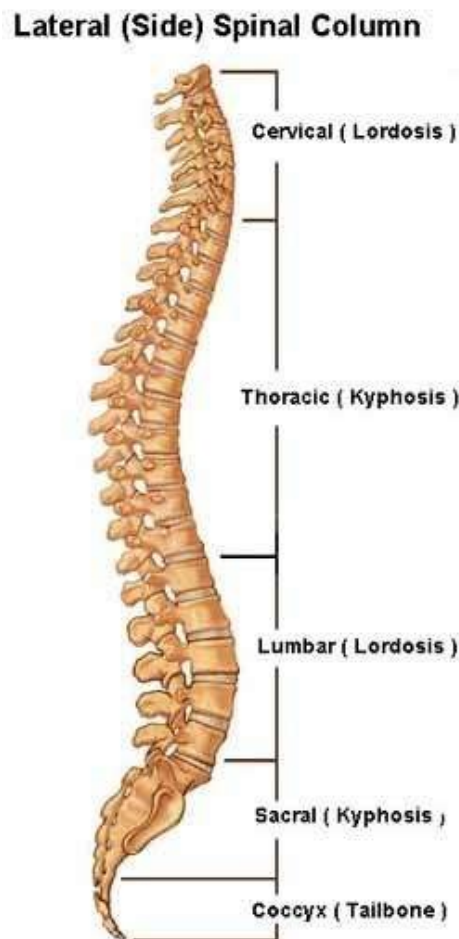
Figure 1.1: The Spinal Column

The lumbar spinal region comprises five intervertebral FSUs—L1 to L5, from top to bottom. Each FSU is composed of two vertebrae, the intervertebral disc sandwiched

between them and the facet joints that connect the vertebrae to the spine (Ferguson & Steffen 2003).

1.2 The Functional Spinal Unit

1.2.1 The vertebrae

The FSU consists of the vertebrae (the bony, hard part of the segment), the disc (the soft-tissue part of the spinal unit) and the facet joints (Bogduk 1997). In the anatomy of the FSU (see Figure 2.2) the vertebral body forms the anterior side and is the main loadbearing structure. The paired pedicles and laminae are at the arch of the vertebrae and the spinous process is formed from the posterior fusion of the laminae. The arch on both sides of the vertebrae comprises the transverse process, the inferior articular process and the superior articular process, which form the facet joints between the adjacent vertebrae (Ferguson & Steffen 2003). The vertebrae are designed to bear massive loads and the combined movements of the adjacent vertebrae allow for mobility in a range of directions.
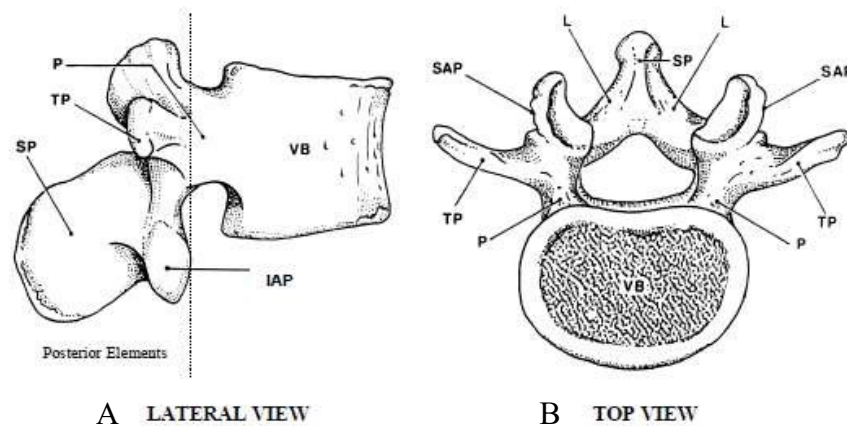
Figure 1.2: Anatomy of the Vertebrae: (A) Lateral View; (B) Top View

Note: VB: vertebral body; TP: transverse process; SP: spinous process; P: pedicle; L: lamina; SAP: superior.

1.2.2 The intervertebral disc

The disc can be defined as a joint connecting the vertebrae in the spine that act as fibrocartilage pads between the vertebral bones and transmit the mechanical load placed on the spine (Newell et al. 2017). The disc acts as a cushion and a shock absorber and is

composed of three distinct structural regions: the inner nucleus pulposus, the outer AF and the cartilage endplates (see Figure 2.3). This disc, along with the adjacent and adjoining ligaments, anchors to the spine to form the FSU , also know as the motion segment.
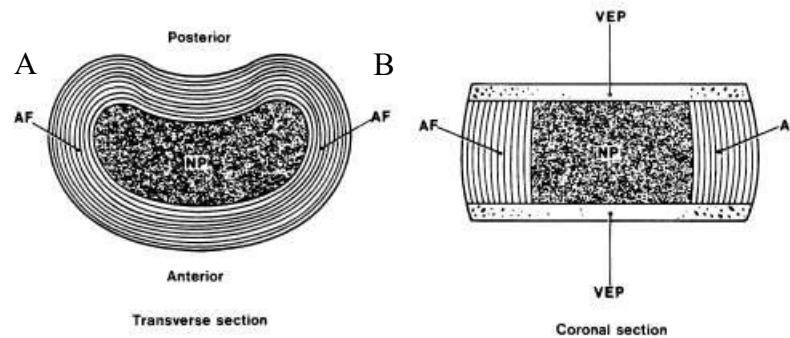
Figure 1.3 Anatomy of Intervertebral Disc (A) Transverse (B) Coronal

Note: AF: annulus fibrosus; NP: nucleus pulposus; VEP: vertebral endplate. Source: Bogduk (1997).

These discs are the largest non-vascularised structures in the human body, yet they are designed and serve to withstand the most difficult physiological conditions (Moore 2006). The integrity and organisation of these structures, governed by their constituents, plays a crucial role in the mechanical movements and changes in the disc structure that affect the mechanical properties of the spinal joint. The changes that take place in the disc over time, or as a result of some injury or movement, result in various spine-related disorders, the most common being LBP (Urban & Roberts 2003). Hence, familiarity with the structure and biomechanical function of the disc is necessary to understand the initiation and progression of spinal disorders.

1.2.2.1 Nucleus pulposus

A normal, healthy disc has an inner, spongy, jelly-like core termed the 'nucleus pulposus' (NP). The NP largely comprises water and proteoglycan, loosely held together by type II collagen and elastin fibres, thereby forming a matrix in the inner core. The dominant proteoglycan in the NP is aggrecan. The proteoglycan is present as aggregates in the nuclear matrix. These aggregates are entrapped in the network formed by collagen and elastin fibres. In a proteoglycan aggregate, the central hyaluronan is filled or attached with aggrecan and comprises a central core protein and side chains of

sulfated glycosaminoglycan. The inner nuclear core acts as a water bed and a cushion for the vertebrae during body movements. The glycosaminoglycan side chains of the aggrecan comprise keratin sulfate and chondroitin and possess hydration properties. A hydrostatic pressure builds in this region when a load is placed on the disc (Raj 2008). These hydration properties cause the NP tissues to swell and control the disc mechanics by balancing the tensile forces of the collagen fibre network.

1.2.2.2 Annulus fibrosus

The outer region of the disc, the AF, is a thick tough fibrous cartilaginous region around the NP. The AF is made up of bundles of type I and II collagen fibre sheets known as lamellae. A series of around 15 to 25 lamellae form a thick AF and these successive lamellae run in alternating directions at an approximate angle of 30 degrees (see Figure 1.4). The AF serves to protect the inner gel-like NP. The lamellae form a tough, exterior ring around the NP, protecting it and connecting the vertebrae together. The outermost lamellae of the annulus are innervated.
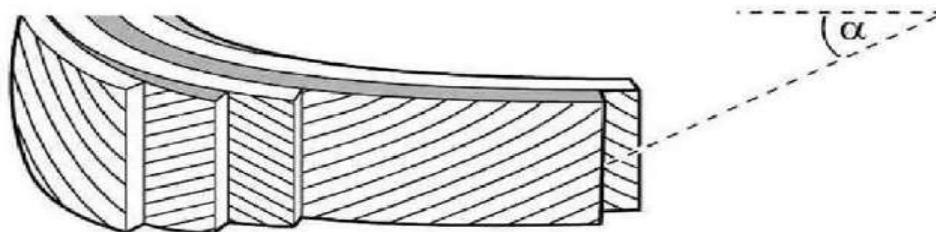
Figure 1.4: Arrangement of Lamellae in the Annulus Fibrosus (AF)

Note: These may be otherwise described as directed (at approximately 30°) collagen fibre bundles in lamellae sheets. Source: Adams and Roughley (2006).

1.2.2.3 Vertebral endplate

The cartilage endplate is the interface between the vertebral bone and disc. It is a thin layer of hyaline cartilage that lies horizontally on the superior and inferior surfaces of the disc (Raj 2008). Such endplates are typically less than 1 mm thick. The thickness of these endplates varies across the width of a single disc with the endplates usually being thinnest in the central region, next to the NP (Moore 2006). The role of the cartilage endplates is to protect the NP from protruding out into the adjacent vertebrae as well as to separate the intervertebral disc from the bone. They also function to absorb the

swelling pressure generated in the NP as a result of mechanical loading on the FSU and the entire spine. Biochemically, cartilaginous endplates are predominantly composed of collagen type II and are thought to be the most important type of endplate (Moore 2006). These endplates withstand dramatic loads during daily movements and activities and distribute these loads as well as intradiscal pressure.

Chapter 2: Literature Review

2.1 Annular Tears and Disc Degeneration

Annular tears produce chronic pain and 80% of the population will encounter an annular tear at some point in their lives (Andersson 1999). There are three distinct types of annular disc tears: rim lesions, circumferential tears and radial tears (see Figure 2.1). These tears occur in the outer AF region and are categorised by their locations in disrupted annular layers; they are most common after 10 years of age (Adams & Roughley 2006). According to Hilton et al. (1976) and a later study conducted by Thompson et al. (2000) on human cadaveric specimens, rim lesions were more pronounced at the human spinal level T12/L1. However, radial tears and concentric tears were reported to occur in equal frequency at level L4/L5 of the spine.
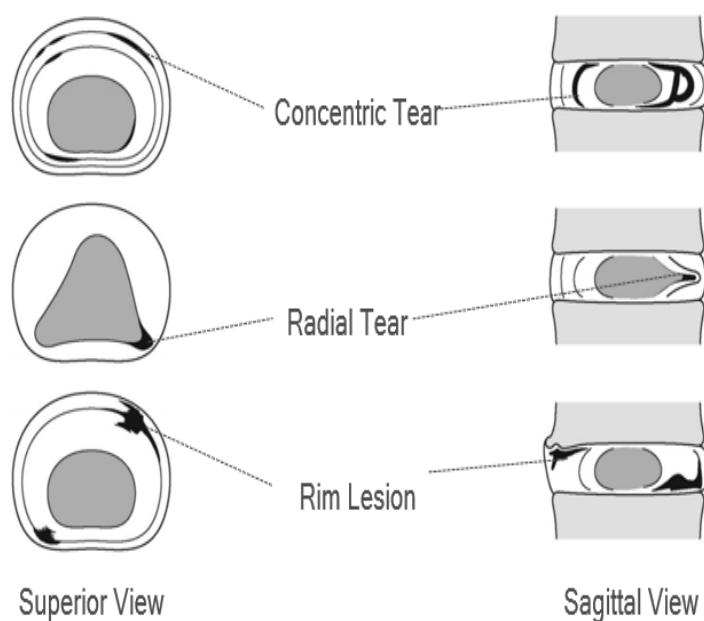
Figure 2.1: Common Types of Annular Tears: (A) Circumferential Tear, (B) Radial Tear and (C) Rim Lesion

Note: The black coloured area shows the disrupted tissue, while the shaded region indicates NP. Source: Adams and Roughley (2006).

2.1.1 Rim lesions

This type of annular lesion was described for the first time by Schmorl et al. (1959). Such lesions originate on the periphery of the disc, usually at the ends of bony epiphyseal plates. They are present at the conjunction of the disc with the vertebral bone and separate the attached vertebral rim from the anterior of the annulus (Schmorl 1959; Osti et al. 1990; Hilton et al. 1976). Rim lesions generally occur as a consequence of traumatic injury (Adams & Roughley 2006) and might be associated with bony spurs.

2.1.2 Radial tears

Radial tears spread across the NP and AF regions of the disc. This type of tear is irregular and initiates from the movement of nuclear material out towards the annular layers, either posteriorly or postero-laterally (Osti et al. 1990; Hirsch & Schajowicz 1952). In cadaveric discs, radial tears might be introduced via cyclic loading in compression and bending (Raj 2008). The severity of radial tears is a measure of the extent to which the NP moves outwards through the annular fibre layers. The severity of radial tears is graded on a scale of 0 to 5 (Raj 2008).

2.1.3 Concentric tears

Circumferential or concentric tears occur between the lamellae of the annulus as a result of injury or trauma to the disc. Concentric tears can be described as crescentic-shaped separations in the layers of the annulus. It has been reported that this type of lesion is more frequent in the lumbar region of the human spine, specifically at the L2/L3 vertebrae Osti et al. (1990).

Annular tears are associated with the presence of disc degeneration (Osti et al. 1992b; Boos et al. 2002). From 27 cadaveric spines aged 17 to 50 years, 135 lumbar discs were characterised based on the three types of annular tears (Osti et al. 1992a). The occurrence of annular tears was found to correlate with the ages of the specimens. For instance, 90 specimens aged 17 to 35 years exhibited a 50% chance of annular tears, while 45 specimens aged 35 to 50 years showed a 73% chance. Further, variation was reported between the different tears in terms of their locations on the discs. 69% of rim lesions were in the anterior annular fibres, whereas 91% of radial tears were observed in the posterior portion of the discs. Concentric tears showed a nearly equal distribution

throughout the anterior and posterior annular fibres with 44% and 56% occurrences respectively. The annular tears were assessed by a histochemical technique and seemed likely to have been produced by mechanical trauma. Moreover, the study indicated that annular tears resulted in the degeneration of NP and could potentially accelerate the process of disc degeneration.

Annular tears were related to Thompson Grading Scale which is a clinical method used to classify FSUs based on the severity of disc degeneration defined by its gross morphology. The method consists of five grades; grade I indicates normal, grades II and III, moderate, and grades IV and V, severe, respectively (Thompson et al. 1990). Rim lesions are often perceived in Thompson Grades II and III, whereas radial tears are regularly found in Thompson Grade IV; however, concentric tears are associated with both types of tears (Liebenberg et al.n.d).

2.2 The Biomechanical Influence of Annular Tears

There are limited studies investigating the mechanism through which annular tears affect FSU biomechanics, particularly kinematics and stress distribution, leading to further degeneration of the disc. The presence of annular tears in the mild stages of disc degeneration was first hypothesised to influence clinical instability by Kirkaldy-Willis and Farfan (1982) and the biomechanical influence of annular tears has been of interest to researchers since then. Instability is caused by an abnormal increase in the range of motion and occurs in response to applied load. It is a phase of the disc degeneration process, in addition to the dysfunction and the stabilisation phases, as identified and classified by Kirkaldy-Willis and Farfan (1982).

Using in vitro cadaveric specimens, the biomechanical changes resulting from the occurrence of annular lesions were studied in different papers. Schmidt et al. (1998) measured a significant decrease in FSU stiffness associated with the presence of radial tears in the disc under axial rotation (71%) as well as less severe decreases in flexion/extension (40%) and lateral bending (38%). They used MRI imaging of the disc tears to compare with corresponding FSU stiffness.

In a later study, by applying an axial rotation torque alone, Haughton et al. (1999; 2000) conducted a similar protocol on FSUs, including rim lesions and concentric tears, in

addition to the radial tears. They reported a decrease in axial rotational stiffness where rim lesions, concentric tears and radial tears were present in the discs: a 73% decrease for concentric or rim lesions and a greater decrease of 76% for radial tears. These decreases in stiffness caused by radial tears are consistent with the results obtained by Schmidt et al. (1998). Both Schmidt et al. (1998) and Haughton et al. (1999; 2000) studied the effects of disc tears by relating MRI images to measured stiffness.

In another study using also cadaveric specimens, the biomechanical responses of annular lesions were studied according to type and size (Thompson et al. 2000). This study provided a view of the mechanical effects of severe tears in combination with other tears, rather than considering their individual effects in isolation. The specimens were grouped into three levels—T12/L1, L2/L3 and L4/L5—and stiffness was measured under three loading modes: flexion, extension and torsion. Following the mechanical testing, each disc was cut transversely into three sections to map and quantify the severity of the rim lesions, concentric tears and radial tears, which could then be linked to their corresponding levels of stiffness. The findings showed that stiffness became greater in proportion to the increasing severity of concentric tears and rim lesions in flexion and to concentric tears and radial tears in extension; however, stiffness decreased along with the severity of the concentric tears and rim lesions in axial rotation. The effects of tear type and size were considered in relation to other tears incurred under uncontrolled degrees of disc degeneration (e.g. chemical factors). In conclusion, the effects could not be attributed to individual tears in isolation, but were rather incurred in combination with other tears and degenerative factors; thus, the mechanical effects of individual tears in isolation could not be determined (Thompson et al. 2004).

Tanaka et al. (2001) studied the effects of disc degeneration on FSU flexibility in cadaveric specimens under flexion/extension, right/left lateral bending and right/left axial rotation. They found that flexibility increased with Thompson Grades III and IV—the grades at which rim lesions and radial tears are respectively expected to appear and at which the instance of concentric tears is common (Liebenberg et al.). However, changes in flexibility cannot solely be attributed to the presence of annular tears, which normally exist in association with other degenerative properties such as reduced disc height, degeneration of the facet joints, osteophytes and a fibrotic nucleus. These

combined factors provide an example of the limitations of cadaveric specimens with pre-existing degeneration levels for interpreting the biomechanical effects of different annular tears.

The influence of disc degeneration on shear loading was viewed for the first time in a six degrees of freedom (6DOF) mechanical testing of cadaveric FSUs by Amin et al. (2016). The cadaveric FSUs were grouped according to different grades of disc degeneration: mild, moderate and severe. 6DOF mechanical testing was performed under different strain rates with loadings of 1 Hz, 0.1 Hz and 0.01 Hz (Costi et al. 2008) and, along with the measurement for stiffness, the phase angle, which yields an insight into the viscoelasticity of specimens, was also measured. As opposed to mild degeneration, moderate degeneration exhibited significantly less stiffness under lateral shear loading and axial rotation by approximately 58% and 62% respectively; however, it showed a significant increase in phase angle by around 62% under anterior shear loading and by 123% under axial rotation. The study concluded that the influence of degeneration on the 6DOF mechanical response of specimens produced the greatest levels of stiffness under flexion, lateral shear loading and axial rotation and the most significant phase angle under anterior shear loading and axial rotation.

Osti et al. (1990) have opened new avenues by creating annular lesions in healthy animal discs to recognise and investigate their potential roles in disc degeneration. Using an in vivo ovine model, they produced rim lesions in the left antero-lateral annulus of the discs and, after periods of between one and 18 months, post mortem evaluations of the morphological changes in the discs were carried out. The evaluation showed progressive degenerative changes that appeared as concentric and radial tears in the nucleus and inner annulus of the discs. Further mechanical investigation by Latham et al. (1994) was undertaken to determine the effects of rim lesions by means of an in vivo ovine model previously proposed by Osti et al. (1990). Six months later, the lumbar spine was dissected post mortem for mechanical testing by flexion, extension and axial rotation. A decrease in stiffness for axial rotation was seen along with the consequent progressive degeneration of the disc, which provided similar results to those discussed above by Osti et al. (1990). The conclusion of the study attributed these mechanical effects to the consequent degeneration of the disc instead of to the rim

lesion. It is worth indicating that stiffnesses of intact sheep specimens were measured in a later study by Latham et al. (1994) (Table 2.1).

Table 2.1: Stiffnesses of Intact Sheep Specimens

Testing Mode	In-vitro stiffness	In-vivo stiffness
Flexion (N/mm)	375	380
Extension (N/mm)	90	100
Right Axial rotation (Nm/degree)	3.5	5
Left Axial rotation (Nm/degree)	3.25	5.6

In another study by Kaigle et al. (1997), rim lesions were examined using an in vivo model, but in porcine rather than ovine specimens. Kaigle et al. (1997) created a rim lesion in the mid part of the anterior AF of the disc and, three months after the injury, the influence was quantified. An alteration in joint kinematics was reported; for example, when measuring the ranges of motion during flexion–extension, the axial translation and anteroposterior shear translation revealed the most significant changes in rim lesions. In addition, as for the in vivo ovine lesion model presented by Osti et al (1990), the progressive degeneration of the disc was observed as a disruption in the inner annulus and fibrous nucleus of the disc. Similar to Latham et al (1994), the study ascribed a kinematic alteration, rather than the rim lesion, to the degeneration of the FSU (Thompson et al. 2004).

The concentric tear was introduced by Fazzalari et al. (2001) in the in vivo ovine model. In a time, interval of 18 months, post mortem mechanical testing followed by morphological assessment was performed. This found neither a measurable mechanical influence nor subsequent degenerative changes in the disc structure. Concentric tears were induced in previous studies (Fazzalari et al., 2001, Thompson et al., 2004) via an injection of saline solution or Indian ink which also served in marking the injury. However, this type of injury could not be included in the experimental testing due to lack of apparatus for creating it.

In a remarkable study using in vitro healthy ovine specimens, Thompson et al. (2004) implemented a protocol to examine the immediate effects of induced rim lesions, radial tears and concentric tears in isolation. Based on the prevalence of lesions in the levels of specimens, the lesions were induced in a sequence (Table 2.2).

Table 2.2: Sequence Followed in Introducing the Injuries

Level	Injury 1	Injury 2	Injury 3
L1/L2	Rim	Concentric	Radial
L3/L4	Concentric	Radial	Rim
L5/L6	Radial	Concentric	Rim

Note: Adapted from Thompson et al. (2004).

The mechanical measurements were obtained before and after creating each injury of a pre-determined size. Different lesions were inflicted at each level so that conclusions on the individual effect of lesions could be made. Successively, two more tears were then applied to illuminate the effects of new tears with pre-existing ones. The findings were consistent with those of previous studies in that the rim lesions decreased the stiffness in axial rotation—as in the study by Latham et al. (1994)—and the concentric tear did not change the stiffness of the disc—as reported by Fazzalri et al. (2001), it exhibited no mechanical influence. Further, the anterior rim lesions in this study also decreased the disc stiffness in extension and via lateral bending; however, no effect was observed to arise from the concentric and radial tears. The study by Thompson et al. (2004) exposed the effect of tears in combination, whereby their mechanical effects on joint stiffness appeared to vary. For example, similar to their effects under lateral bending and axial rotation, when considered in combination, the concentric and radial tears did not affect stiffness, while introducing a concentric tear negated the decrease in stiffness caused by the rim lesion. However, this study did not cover all possible combinations. For instance, the introduction of the radial tear in combination with a pre-existing rim lesion was not applied and, therefore, its effect remains unknown. Nonetheless, further insight into the effects of tears on mechanical properties was revealed by this study (Thompson et al. 2004). The hysteresis and the neutral zone were measured, and the hysteresis was found to decrease with radial tears in flexion/extension and under lateral bending, whereas the neutral zone was not affected by any type of lesions. This indicated that the change in hysteresis loss arose from a change in stress distribution inside the disc,

which, in turn, worked to overload and damage the surrounding ligaments, muscles and zygapophysial joint.

A similar and consistent result was found in a later study by Przybyla et al. (2006) where rim lesions exhibited a negligible effect on the stress inside cadaveric discs in contrast to the endplate fracture effect.

Despite the advantage of animal models in revealing the biomechanical effects of annular lesions, the conclusions that may be drawn are limited, as it is difficult to definitively relate the animal model to the corresponding changes in human FSU. A further difficulty accompanies the creation of annular lesions, such as concentric tears and radial tears, without damaging the endplate or the outer annulus of the disc.

An additional study was conducted by de Visser et al. (2007) to evaluate the mechanical effects of rim lesions on in vitro sheep FSUs at two speeds of loading. The stiffness was measured in flexion and extension after the removal of the posterior element followed by the creation of the rim lesion. As a result, the FSUs stiffness showed a 9% and a 23% reduction in flexion and extension respectively. This study also revealed a significant effect arising from the posterior element, whereby stiffness dropped by 72% in flexion and by 38% in extension upon its removal. This emphasises the importance of keeping specimens intact when testing their mechanical properties.

Because of their greatest reduction to disc stiffness (Thompson et al. 2004), rim lesions were nominated to simulate annular lesions in the early stages of disc degeneration in a finite element method (FEM) study by Little et al. (2007). Opposing two different types of degenerative changes observed in the disc, this simulation made it possible to predict the extent of the mechanical effect of annular lesions on copies of healthy discs and to compare it with the simulated NP pressure loss. Moreover, a new approach towards investigating the mechanics of extreme degeneration of the disc (Thompson Grade V) was developed by generating another model incorporating the pressure loss of the NP with the individual presence of a rim lesion, a radial tear and a concentric tear and the simultaneous presence of a rim and a radial tear. Care was taken by this study to closely resemble the structural geometry and mechanical behaviour of a normal disc. For example, the ground substance in the disc's AF was represented as a nonlinear, incompressible material, as previously reported by Shirazi-Adl et al. (1986) with the use

of polynomial equations to fit experimental data from ovine discs (Little 2004; Reid et al. 2002). In addition, the loading conditions were defined to simulate the in vivo deformation of the disc (Pearcy 1985). As a result, preceding the nucleus degeneration in the disc, the annular lesions, represented by rim lesions, were reported to cause fewer mechanical effects than those under the NP pressure loss. Examining the effects of individual tears in this study, rim lesions only had the chance to act alone without occurring alongside the loss of NP or in the presence of other lesions. Proving inconsistent with the results of previous studies (Latham et al. 1994; Thompson et al. 2004), low variations in stiffness were found between the healthy disc and the disc that only had a rim lesion. For instance, a minor decrease in stiffness was reported in flexion, left lateral bending and left/right axial rotation, whereas a mild increase occurred in extension and in right lateral bending. Conversely, under all loading conditions, there was a significant reduction in stiffness exhibited by all types of annular lesions when in combination with reduced NP pressure. This reduction was revealed by rim lesions in flexion and under right/left axial rotation, by concentric tears in extension and by radial tears undergoing right/left lateral bending. However, the combined effects of annular lesions with the loss of NP pressure either made the stiffness remain the same or reduced it slightly more than under the NP pressure loss alone. There were two exceptions to this: in right lateral bending, a 2% increase in stiffness was caused by the loss of NP pressure in combination with rim lesions and rim lesions and radial tears together while in flexion, a 7% decrease in stiffness was caused by NP pressure loss in combination with rim lesions and a 4% decrease was produced by its combination with concentric tears. One limitation of this study is that the observations were made on the mechanical effects of the disc alone, without considering the vertebral bones and joints which comprise the FSU.

In a similar study to the one conducted by Thompson et al. (2004), Michalek and Iatridis (2012) evaluated the mechanical effects before and after the introduction of different types and sizes of annular tears to an in vitro bovine model. The tests were applied under multiple mechanical modes: flexion–extension, compression, axial rotation and lateral bending. The effects of three types of disc injuries were measured: needle punctures, radial tears and rim lesions. The specimens used were randomly assigned into three groups; A served as control and B and C as injuries. Mechanical tests were applied before and after each type of injury. A needle puncture was applied

first using a 21-gauge needle on the anterior side of the disc for groups B and C, followed by a 22-gauge scalpel-produced radial tear and rim lesion in Group B and a 22-gauge scalpel-produced rim lesion and radial tear in Group C. The results revealed that large sized injuries significantly decreased the axial rotational stiffness by approximately 73% for the radial tear and 63% for the rim lesion, while the phase angle decreased by around 6% in both the radial tears and the rim lesions. Further, insignificant effects were noticed in both parameters.

Previous studies showed the three types of tears to cause stiffness reduction to the FSU except for concentric tears, which sometimes showed no effect. Some studies measured the hysteresis which was found to decrease as result of annular tears. The studies meant to evaluate the mechanical effects of annular tears; however, the evaluation was performed in the presence of other affecting factors. These factors were sometimes apparent in the forms of testing at different levels of disc degeneration or a pre-existence of other tears. Moreover, the studies' experiments were carried out under different mechanical and physiological conditions. For instance, the effects of annular tears were sometimes quantified under various loading modes (static/cyclic) or/and under the application of compressive preload (recovery preload/follower preload). Further, the specimens used were even variant in the tissues comprising the FSU. For example, some studies tested the mechanical impact of the disc alone, without considering the articulated vertebral bones and joints. The present study aims to evaluate the mechanical effects of disc tears under simulated physiological conditions and a minimum presence of other affecting factors.

Chapter 3: Aim, Objectives and Hypotheses

3.1 Aim

Previous studies have investigated the effects of disc injuries on the mechanical behaviour of the FSUs in degrees of freedom (DOF) (e.g. flexion–extension, bending and axial rotation). However, to the author's knowledge, no studies have examined the 6DOF behaviour of the FSU as a function of disc injuries. Therefore, the aim of this thesis has been to evaluate the effects of disc injuries, particularly rim lesions and radial tears, on the mechanical and viscoelastic properties of the ovine lumbar FSUs. These properties are evaluated under 6DOF dynamic testing, mimicking three physiological disc conditions that occur during walking and through office work (Costi et al. 2008).

The dynamic testing utilises three different frequencies: 1 Hz, 0.1 Hz and 0.01 Hz. The specimens are then subjected to failure by traumatic overload to evaluate their failure peak loads when exhibiting two types of injuries.

3.2 Objectives

To accomplish the above stated aim of the project, specific objectives were determined as follows:

1. To design precise blades with proper dimensions for the creation of radial tears and rim lesions with constant insertion depths and widths, as determined for each type of injury.
2. To develop and validate a reliable protocol for the creation of injuries and to test its reliability via the creation of pilot injuries and the analysis of their results.
3. To test the specimens under 6DOF dynamic cyclic loading and to measure FSU stiffness— as a mechanical parameter and phase angle—as a viscoelastic indicator of energy absorption. Dynamic testing is to be applied at three frequencies: (1 Hz, 0.1 Hz and 0.01 Hz) before the injuries (intact FSUs) and after the injuries.

4. To compare the failure peak loads of radial tear and rim lesion specimens under a sudden compressive overload.

3.3 Hypotheses

The hypotheses tested in this project are as follows:

1. The radial tear and the rim lesion will both significantly decrease the 6DOF stiffnesses of the FSUs and increase the phase angle.
2. Radial tears will cause significant changes of a greater magnitude in the 6DOF stiffnesses and the phase angles of each FSU.
3. There will be no significant differences between the ultimate failure loads of both injuries.

Chapter 4: Methods

The methodology of this project included the preparation of specimens, the creation of annular injuries, mechanical testing and data analysis (Figure 4.1).

```
                    ┌─────────────────────────┐
                    │     FSUs Dissection     │
                    └─────────────────────────┘
                                 │
                    ┌─────────────────────────┐
                    │ FSU Potting & Measurement│
                    └─────────────────────────┘
                                 │
                    ┌─────────────────────────────┐
                    │ Overnight Hydration and Preloading │
                    └─────────────────────────────┘

              Specimens assigned randomly into Two groups

   Group 1:                                        Group 2:
   For Radial Tear                                 For Rim Lesion

                    a-  6 DOF Dynamic Testing
                    b-  Injury Creation
                    c-  6 DOF Dynamic Testing

                    FSU Failure (Sudden Overload)

                    Data Analysis
```
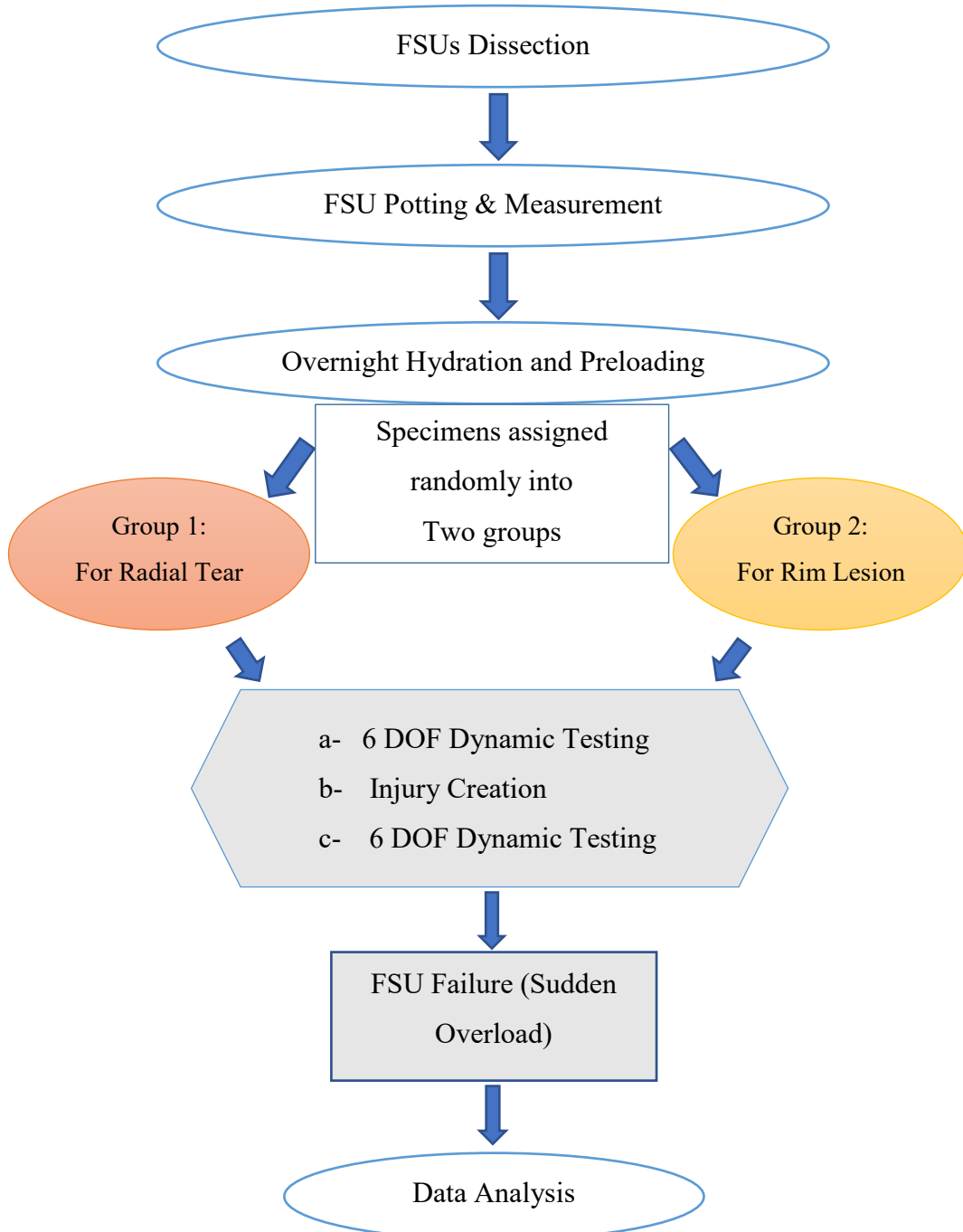
Figure 4.1: An Overall Illustration of the Project Methodology.

Prior to the mechanical testing, the FSUs were randomly assigned into two groups: Group 1 for radial tears and Group 2 for rim lesions. 6DOF dynamic testing was then

applied at three frequencies to each group of specimens before and after the creation of injuries to evaluate the effects of the injuries under dynamic testing. Each group of specimens were then subject to a traumatic failure under a sudden overload. All methodological procedures were performed under conditions that carefully mimicked those of the in vivo environment to minimise any potential consequences for the study's validity. More details related to the methods are included in sections (5.1–5.4).

4.1 Preparation of Specimens

The preparation of the specimens entailed the dissection and extraction of the FSUs from their sheep lumbar spines, the measuring and potting of the FSUs in polymethyl methacrylate (PMMA) and their alignment using a custom-built rig before they were finally placed in overnight hydration bath under recovery preload. Twenty lumbar spines of healthy sheep (aged one to three years old), sourced from Austral Meat (716 Main N Rd, Gepps Cross, South Australia (SA) 5094), were obtained frozen and were immediately stored at a temperature below minus 20°C in the freezer cabinet of the biomechanics and implants laboratory. Four of the specimens were dedicated to the pilot creation of injuries and the remaining ones were utilised intact for the project.

4.1.1 Dissection and extraction of the lumbar FSUs

Over a one-week period, the dissections and the extractions of the L4/L5 FSUs from their lumbar spines were carried out. The procedures commenced with the removal of the spines from the freezer to be thawed at room temperature for approximately three hours, at which point a semi-frozen state was reached. It is worth ensuring that such repeated-freeze-thaw cycles were found to show no effects on the specimens' mechanical properties (Tan and Uppuganti, 2012). Dissection was then conducted using scalpel and forceps, by which all of the soft tissues were carefully removed from each L4/L5 spine section, leaving the vertebra–disc–vertebra with the posterior longitudinal ligament intact (see Figure 4.2). Throughout the dissection process, any spines with visible damage to their discs were immediately excluded.

(a)   (b)

Figure 4.2: Anterior (a) and Lateral (b) View of a Sheep Lumbar Spine After the Dissection of All Surrounding Tissues Except the Posterior Elements and the Ligament Between the Vertebrae

During and after the dissection process, the effects of dehydration were minimised by the moistening of each FSU with saline-soaked paper towels; the samples were then sealed in plastic bags before being restored to the freezer. Another day was allocated for the extraction of the L4/L5 FSUs (the vertebra–disc–vertebra segments including posterior element) from their lumbar spines. This process also commenced with the removal of the spines from the freezer to thaw for three hours at room temperature. The L4/L5 FSUs were then bisected in the transversal plane using a band saw, with care to preserve the discs and posterior elements from any damage (see Figure 4.3). Finally, the FSUs were moistened with saline-soaked paper towels, sealed in their plastic bags and stored inside the freezer until the day of testing.

(a)   (b)

Figure 4.3: Extracted Lateral (a) and Anterior (b) Views of the L4/L5 FSU (Vertebra–Disc–Vertebra Segment) After Transversal Bisection Using a Band Saw

21

4.1.2 Measuring the heights and disc areas of the FSUs

The day prior to mechanical testing, the FSUs were allowed to thaw for three hours at room temperature in readiness for the measuring of their dimensions. Using a Vernier calliper, the heights of the disc and vertebrae as well as the widths of the lateral (LAT) and the anterior–posterior (AP) sides of the discs—both superior and inferior—were measured three times for each specimen; the mean values were used. The FSU disc area was calculated for each specimen based on the following formula: disc area = 0.84 x AP x LAT (Nachemson & Morris 1964). These area measurements— along with the reported estimation of the intradiscal pressure as equivalent to 1.5 times of the external applied stress (force/area) (Nachemson & Morris 1964)—made it possible to later calculate the required load to apply to each FSU for the production of a target level of intradiscal pressure. The calculations were carried out as follows:

$$P = 1.5\ \sigma_{ext}$$

$$P = 1.5\ (A/F)$$

$$F = 1.5\ A/P$$

Here, P is the intradiscal pressure, σ_{ext} is the external applied stress on the disc, A is the disc area and F is the force or load (with a negative sign, in case of compression).

4.1.3 FSU potting and offset measurements

Once the FSU measurements were complete, each FSU underwent a potting procedure to provide effective mounting to the hexapod with precise alignment and stable fixtures. That is, the inferior and superior vertebrae were sequentially fixed between the bottom and the top cups respectively, in such a way that the centre of the canal was aligned with the centre of the cup. The two stainless steel/aluminium cups were, in turn, positioned using a custom-built rig and filled with a consistently mixed combination of polymethyl methacrylate (PMMA) powder and PMMA monomer liquid in a respective ratio of 1.7 mL to 1 mL (see Figure 4.4). This process resulted in the formation of solid cement that fixed the vertebrae and aligned the FSUs within the horizontally and vertically parallel cups.

Potting the inferior vertebra

Preparing to pot the superior vertebra

(a)   (b)
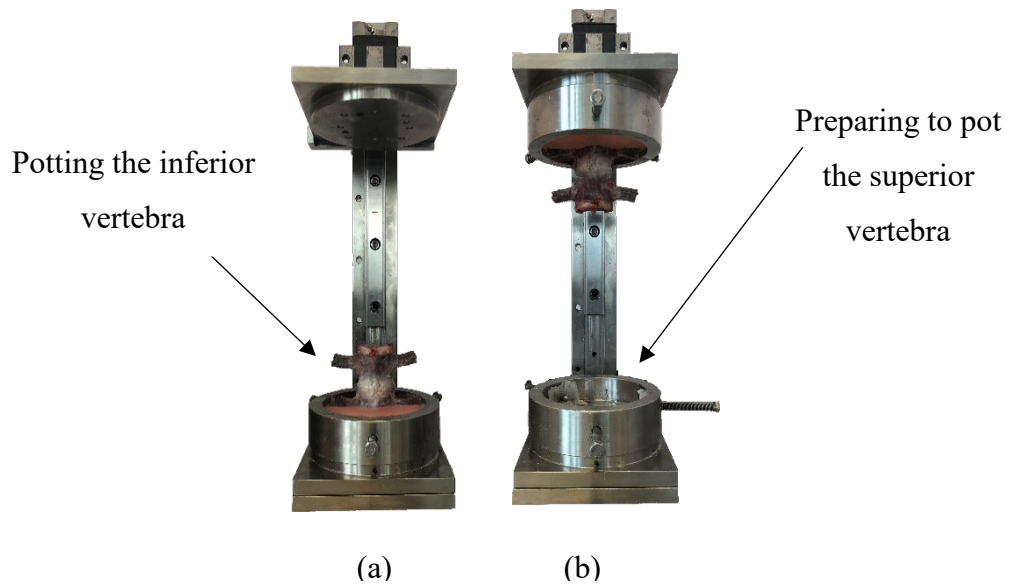
Figure 4.4: The Custom-built Alignment Rig and the Main Stages of Potting the FSU; the Inferior Vertebra Potted (a) in the First Instance and the Potting of the Superior Vertebra (b) in the Second

Note: Full details of the potting protocol are included in Appendix B.

The X, Y and Z offsets for the disc's axis of rotation (AoR), relative to the centre of the hexapod's global coordinate system (GCS), were measured after the potting of the inferior vertebra. The X and Y offsets were determined as the distances from the centre of the disc to the lateral and anterior edges of the cup respectively, whereas the measured Z offset was defined as the superior distance from the mid height of the disc to the load cell of the hexapod robot.

4.1.4 Overnight disc hydration and preloading

Because of its viscoelastic characteristics, in a diurnal cycle the disc shows fluid reduction accompanied by a decrease in height. During various daily activities, it exhibits high levels of varying intradiscal pressure. Under the influence of sleep at night, it exhibits fluid absorption accompanied by an increase in height along with minimum intradiscal pressure. These variations are synchronously caused by the variations in external loading on the disc: intense during the day as opposed to minimal at night. Thus, the day before mechanical testing, the physiological hydration and the intradiscal pressure were simulated by keeping the disc of the potted FSU fully immersed overnight in a 0.15 M PBS bath at room temperature and under a compressive

load that was vertically applied at the centre of the top cup (see Figure 4.5) (Costi et al. 2008). Based on the disc measurements previously recorded and the formulae relating the intradiscal pressure to the external load (see Section 5.1.2), the compressive load was calculated to produce an equivalent intradiscal pressure of 0.1 MPa, mimicking that of the unloaded disc at rest (Wilke et al. 1999). This was the recovery preload and it was used as the protocol for mechanical testing.
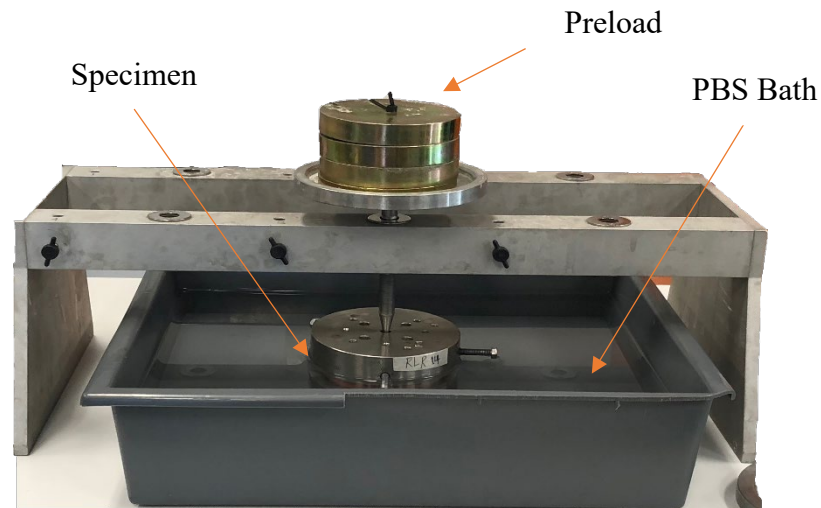
Figure 4.5: Overnight Hydration and Recovery Preloading of Specimen

4.2 The Creation of Annular Injuries

4.2.1 Blades and the Dimensions of the injuries

For the creation of injuries, two prepared craft blades (Celco brand) were obtained, each of which had been cut to smaller dimensions at a sharpening store (50 Dunorlan Road, Edwardstown, SA 5039). The blades' dimensions were 5 mm (width) x 8 mm (depth) and 2 mm (width) x 12 mm (depth) for the creation of rim lesions and radial tears respectively (see Figure 4.6). These dimensions had previously been used by Thompson et al. (2004) and Michalek and Iatridis (2012). However, the depth of the radial tears was 12 mm: 2 mm deeper than that used by Michalek and Iatridis (2012). This increase in depth was implemented in this project to ensure the blade's penetration into the disc's NP.

(a)

(b)
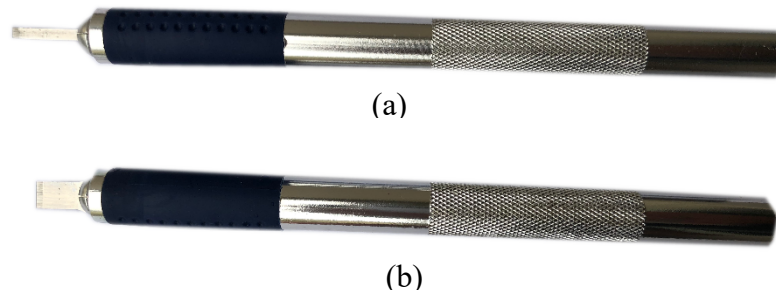
Figure 4.6: Blades Used for the Creation of the Injuries: Blade of Radial Tears (a) and Blade of Rim Lesions (b)

The blades were fully inserted to generate the injuries and the depth of each blade was limited by the edge of its holder in such a way as to control the depth of the injuries.

4.2.2 The creation of pilot injuries

The creation of pilot injuries was required to produce an acceptable methodology to achieve the aim and objectives of this project. The objectives for the creation of pilot injuries were to:

- Develop a protocol for the creation of injuries.
- Test the feasibility of simulating the injuries at their common locations using custom-made blades.
- Ensure the repeatability of injury creation.
- Become accustomed to applying the protocol.

For the pilot study, four sheep L4/5 FSUs (not included in the experiments of this project) were dissected and extracted from their lumbar spines (see Section 5.1.1). The locations of the injuries were selected to simulate the most common locations of wounds as reported in the literature (see Section 3.4). A rim lesion was induced at the right anterior portion of the disc for all four specimens, while a radial tear was attempted on the left lateral side of the disc with an oblique towards the posterior side cut (Thompson et al. 2004) in two specimens and the left lateral side of the disc with straight cut (Michalek and Iatridis 2012) in the other two specimens. The reason for testing for radial tears in two locations was to assess at which location the blade repeatedly seemed to better penetrate the NP. In the pilot study only, a radial tear and rim lesion were created on the same specimen as a consequence of a scarcity of samples. To track the extent of injuries, the blades were immersed into India ink before

being inserted into the discs, which were then transversely cut at the level of the injuries (see Figure 4.7).
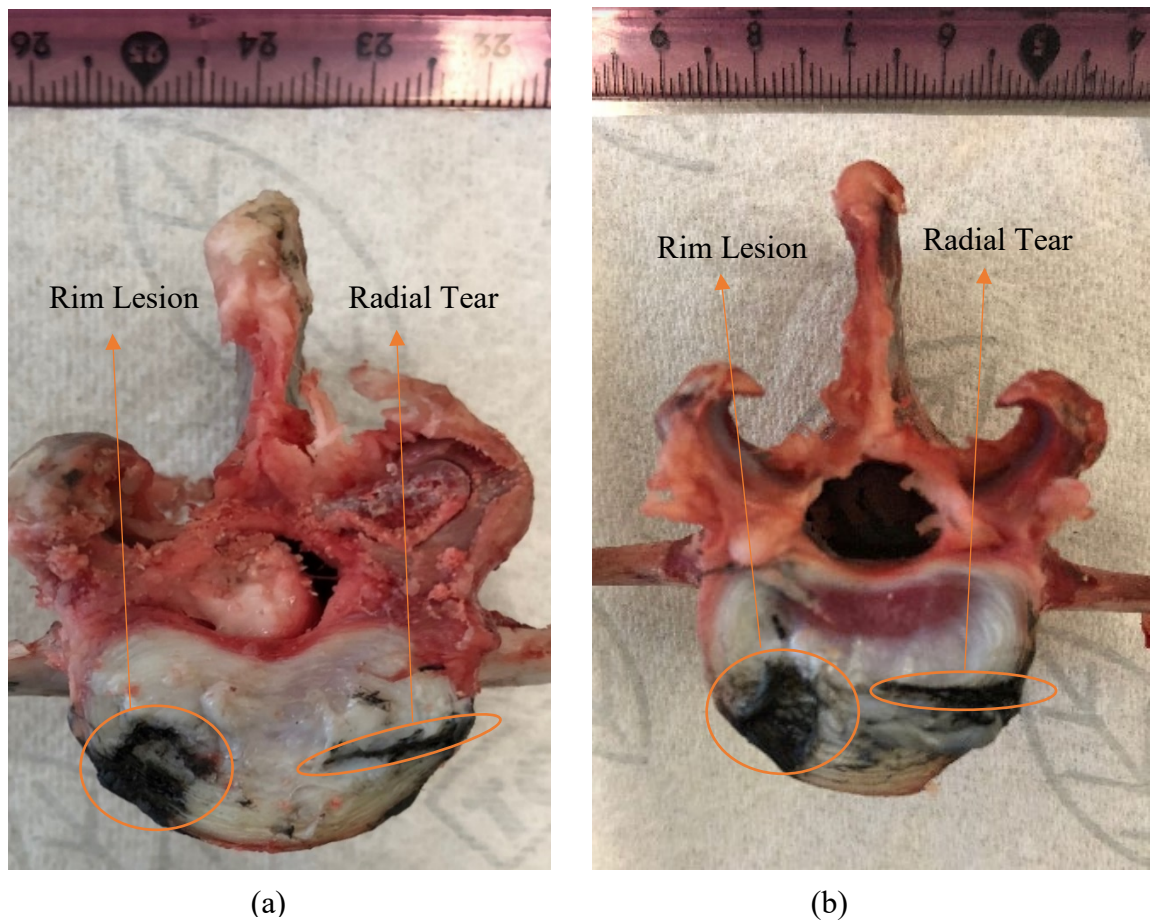
Figure 4.7 View of Pilot (a) Specimen 1 and (b) specimens 3 with Rim Lesions Created into both at the Right Anterolateral Portion of the Disc and Radial Tears (a) oblique and (b) straight Produced at the Left lateral Side of the Disc

Each injury was photographed using an Apple iPhone X camera (Dual 12- Megapixel) and analysed with ImageJ software (Version 1.52a, Wayne Rasband, National Institutes of Health, USA) to ascertain the depth and width of the injuries. There were some difficulties in controlling the transverse cut for each injury and the random spread of ink made tracking the injuries solely by their stained appearance inconsistent. However, the tracking of the injuries was still achievable by the notable symmetrical contrast that was present in the roughness of the surface at the injuries' boundaries. This contrast in surface that resulted from the blade insertion was visible to the naked eye. Therefore, at three intervals (each an hour apart), the specimens were photographed; the boundaries of each injury were determined by macroscopic inspection, whereby lines were drawn

across the depth and width of the boundaries using ImageJ software (see Figure 4.8). To further analyse the measurements for assessing any variation among and the capacity for repetition of the injuries, the interclass correlation coefficient (ICC) was then calculated using SPSS software (IBM SPSS Statistics 25). An ICC value ranging between 0 to 1 gives an indication on the differences between repeated measurements. As the value approaches 0, variation between the measurements increase; however as the value approaches 1, the variation decreases and turns out to be more negligible (Fleiss, 2011).

(a)   (b)
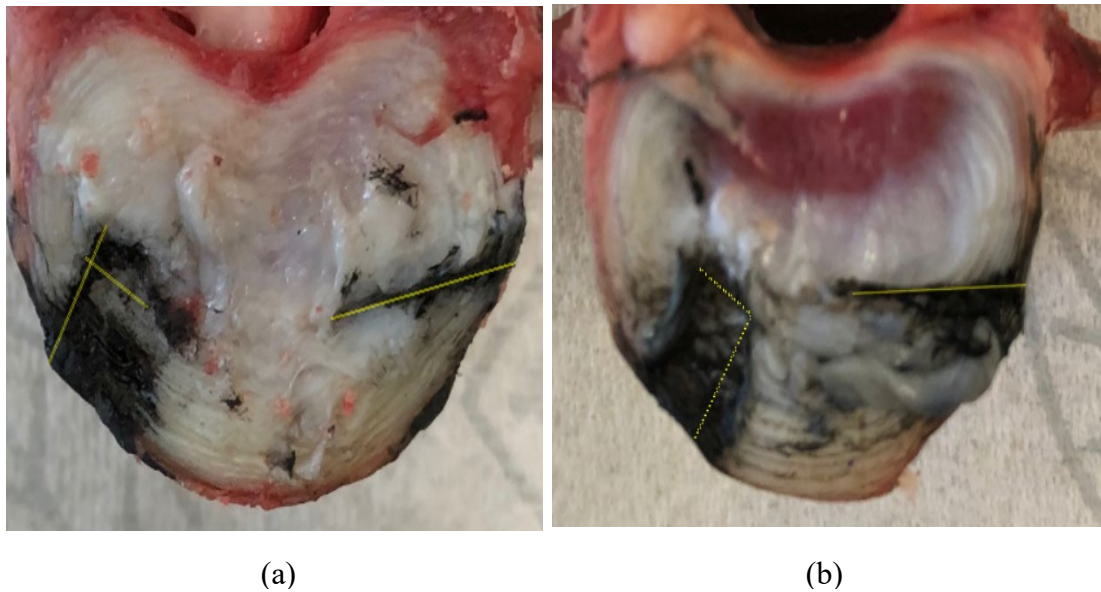
Figure 4.8: Images of the Transversely Cut (a) Specimens 1 and (b) specimen 3 with Lines Drawn Across the Boundaries Using ImageJ Software According to the Surface Contrast Resulting from the Injuries

Note: Larger size images and full measurements of all pilot specimens are shown in Appendix C.

4.2.2.1 Results of the creation of pilot injuries

The overall results of the measurement of the depth and width of the injuries for all specimens are as follows:

Table 4.1: The Mean and Standard Deviation of the Injury Measurements for All Specimens

Type	Dimension	Specimen (Intervals Mean)				Mean	SD
		1	**2**	**3**	**4**		
Radial tear	Depth	12.83	12.71	13.58	13.09	13.05	0.39
Rim Lesion	Depth	8.01	8.07	8.27	8	8.09	0.12
	Width	4.99	5.2	4.98	5.25	5.10	0.14
	Area	39.99	41.95	41.14	42	41.28	0.94

The ICC value for the depth of the radial tears was 0.763, whereas, for the area of the rim lesions, it was 0.886. These two ICC values are considered to indicate excellent reliable measurements (Fleiss, 2011). The ICC value from the measurements of radial tears was slightly smaller than that measured for rim lesions. This could be resulting from the relatively larger depth of radial tears (13.58) seen in specimen 3 resulting due to a difference in direction (oblique cut vs straight cut). Analysing the images of radial tears obtained from the pilot study, it was possible to ascertain that blade penetration of the NP in the creation of radial tears was more achievable and repeatable from the left lateral side of the disc with straight cut, as attempted by Michalek and Iatridis (2012), than from the left lateral side with oblique cut, as used by Thompson et al. (2004). Moreover, as ICC values were still with acceptable ranges of reliability of injury creation, in this project, it was decided that radial tears would be created on the left lateral side of the disc in straight cut to ensure less variation in injury depth, while the rim lesions remained into the right anterior side of the disc.

4.2.3 The creation of injuries

On the day of mechanical testing, radial tears and rim lesions were created individually in the discs after the intact specimens had been mechanically tested. Two custom-built blades with specific dimensions (see Section 5.2.1) were used on different specimens for the generation of radial tears and rim lesions. For the radial tears, a 2 mm wide blade was vertically inserted into the left lateral side of the disc at mid height to a depth of 12 mm. For the rim lesions, a 5 mm wide blade was horizontally inserted into the right anterior portion of the disc at the distal vertebral rim (see Figure 4.9).
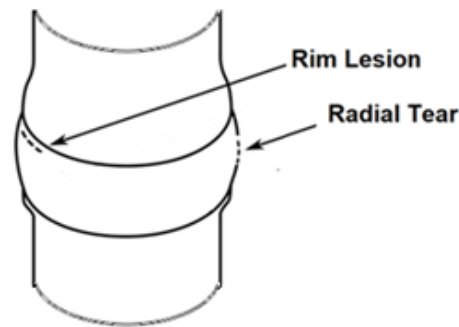
Figure 4.9: Anterior View of an FSU with the Locations of the Two Different Types of Injuries: Radial Tear on the Left Lateral Side of the Disc and Rim Lesion on the Right Anterior Side

The locations of the blade insertions into the discs were as near as possible to the most common locations of injuries reported in the literature (see Section 3.4) and observed in the pilot study (see Section 5.2.2.1). To minimise any possible variations, a protocol for creating the injuries was developed, including detailed steps to ensure the repeatability of each injury at the same location (see Appendix D).

4.3 Mechanical Testing

The previously prepared 16 specimens (eight for each injury group) (see Section 5.1) were now ready for mechanical testing. The estimated time to complete the mechanical testing of a single specimen was approximately seven hours (one specimen per day). The specimens were kept hydrated throughout the process by wrapping in saline-soaked paper towels. Further details of these methods are included under the subheadings that follow (5.3.1–5.3.3).

4.3.1 The six degrees of freedom (6DOF) testing hexapod robot

The custom-developed Stewart Platform-based hexapod is a 6DOF mechanical testing system consisting of a top plate positioned relative to a fixed base plate in such a prepared specimen can be bolted in between. The hexapod is driven in single or multi-axis directions and is capable of applying complex 6DOF testing to different biological tissues, simulating their physiological kinematics and conditions. These tissues include bones, muscles and joints, such as the intervertebral disc, on which measurements of loading and displacement are possible. (see Figure 4.10).

29
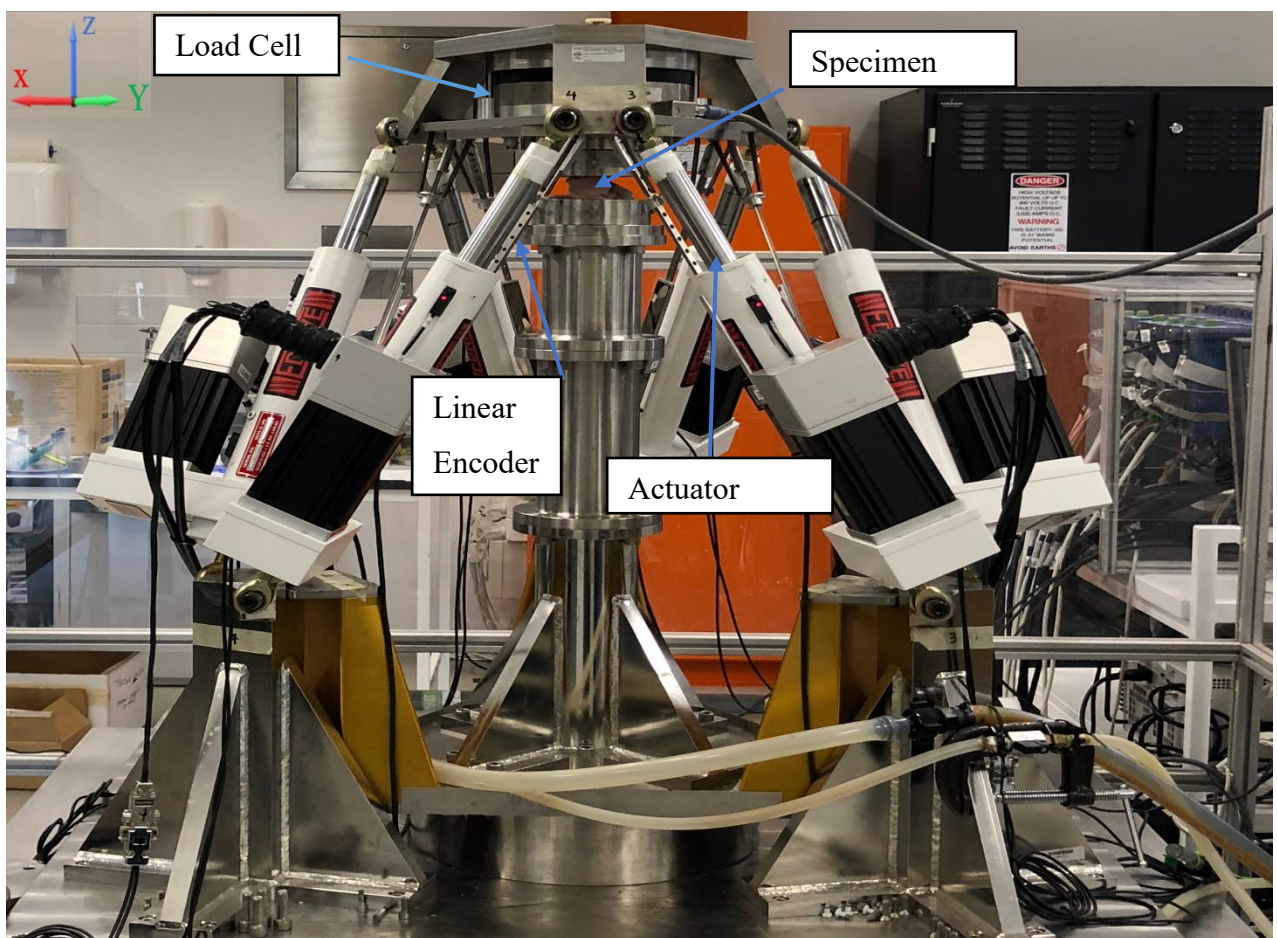
Figure 4.10: The Flinders Hexapod Robot with Sheep FSU Mounted for Mechanical Testing

Using screw bolts, the prepared specimen (see Section 5.1) is secured between the fixed base plate and the specimen coupling plate, which, in turn, is fixed to the movable top plate of the hexapod. The top plate is driven by six servo-controlled ball screw actuators that position it precisely with respect to the base plate. The actuators have accuracy in

displacement and have angles of rotation of 0.01 m and $\pm 0.2°$m respectively, as validated previously by the National Association of Testing Authorities (NATA). Parallel to the actuators, six linear optical linear encoders (B366784180185, LDM54, MicroE Systems Inc., Brillerica, MA) are seated to control and measure the actuator lengths at a resolution of 0.5μm. The hexapod also consists of a six-axis load cell (MC3A-6-1000, AMTI, Watertown, MA) mounted above the top plate with maximum measurement capacities of 4,400 N and 110 Nm and with NATA validated accuracies of ± 9 N and ± 0.2 N for axial compression and axial torque respectively (Ding et al. 2011). There are three control modes to drive the hexapod: 'load', 'position' and 'hybrid'. The capabilities of these modes differ in terms of what is being controlled (the load or position) and the number of DOF that are simultaneously controlled. For instance, the load control mode drives all six DOF simultaneously, whereas only one DOF may be driven in position control mode at a given. However, in hybrid control mode, which functions by enabling the other two modes at the same time, the instantaneous control drives six DOF: one DOF functions in position control, applied at the primary axis of the test, while the other five DOF operate in load control to reduce the loads of the off-axes to zero. The hexapod also has the capacity to test ramp and cyclic loading.

4.3.2 Six degree of freedom (6DOF) dynamic testing under simulated physiological conditions

To evaluate the mechanical behaviour of the disc, which is dependent on the orientation of its anisotropic structure, dynamic testing was applied in six DOF. The dynamic testing was applied at different frequencies since the disc exhibits viscoelasticity makes its mechanical behaviour to be strain rate dependent. During the 6DOF dynamic testing, in vivo physiological conditions were simulated via the application of the recovery preload and follower preload, equivalent to 0.1 MPa and 0.5 MPa respectively and corresponding to their in vivo estimated values (see Section 5.1.2). By reducing the biphasic behaviour of the disc in areas where its fluid flow was expected to be greater—for example, at lower frequency, rather than higher and/or at axial loading, rather than shear—it was decided that the dynamic testing would follow pre-determined sequences of loading and direction (Costi et al. 2008; Amin et al. 2016; see Figure 4.11).
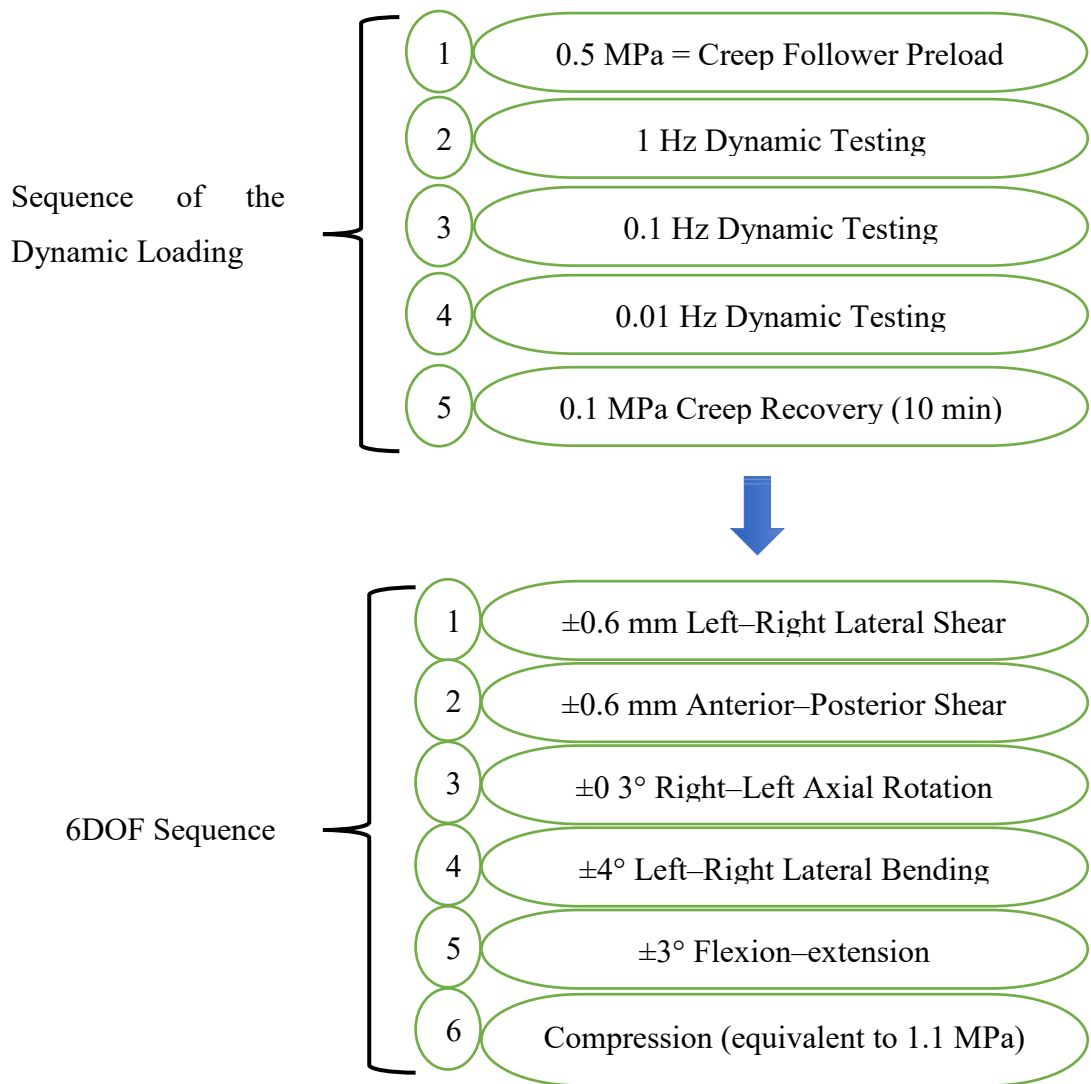
Figure 4.11: Illustration of the Sequence of Dynamic Loading Applied in Each DOF Following the 6DOF Sequence Outlined.

A follower preload equivalent to 0.5 MPa of intradiscal pressure, mimicking the physiological upper body weight, was first applied to the specimen. Dynamic testing was conducted for five cycles of sinusoidal displacement (translation/rotation) for each DOF, except compression, where the waveform was haversine and driven in load control. The frequencies of the 6DOF dynamic testing were 1 Hz, 0.1 Hz and 0.01 Hz to approximate the frequencies of the disc at two speeds of walking and when sitting, such as during office work, respectively. After applying dynamic testing at 1 Hz, 0.1 Hz and 0.01 Hz, successively, each specimen was allowed 10 minutes creep recovery. The 6DOF sequence and displacement amplitudes started with ±0.6 mm for lateral and AP shear, ±3° for axial rotation, ±4° for lateral bending and ±3° for flexion–extension and ended with an axial compressive load amplitude equivalent to 0.6 MPa of intradiscal

pressure. The displacement amplitudes were selected within the physiological range of motion (Costi et al. 2008; Lu et al. 2005; Pearcy & Tibrewal 1984; Stokes & Frymoyer 1987), while the compressive load amplitude was determined so that when it was added to the follower preload (equivalent to 0.5 MPa of intradiscal pressure), the total compressive load would produce 1.1 MPa of intradiscal pressure, mimicking the pressure experienced when standing (Wilke et al. 1999).

4.3.3 The traumatic failure of specimens under sudden overload

To ensure complete position control in failure tests, the specimens were secured on a custom-built X–Y table, previously used in other studies (Callaghan & McGill 2001; Skrzypiec et al. 2013; Skrzypiec et al. 2012). The table comprised a platform fixed on double linear motion rail tracks that slid to allow for transition on the X–Y planes with minimum shear forces (see Figure 4.12).
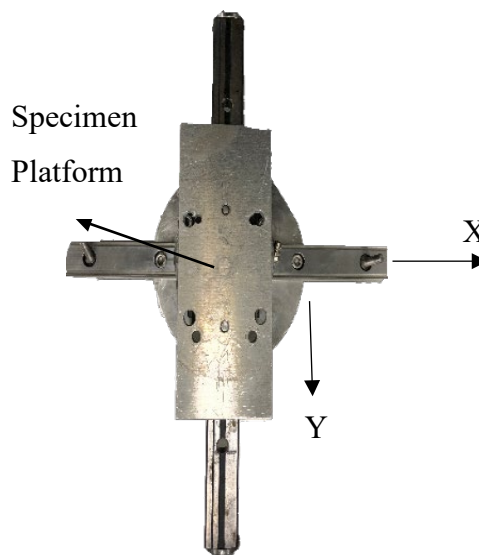
Figure 4.12: Top View of the X–Y Table Showing the Specimen Platform and the X–Y Axes Motion Rail Tracks

Once the specimen with the attached the X- Y table had been mounted, the hexapod controlling screens were set up for load cell limits of 6,000 N for shear forces, 17,000 N for the compression and 1,000 Nm for moments. This was to avoid the generation of load cell faults when failing the specimen. The rotations about the X and Y axes were constrained to prevent any flexion–extension and lateral bending from occurring respectively. Next, under position control, 13-degree flexion was applied to simulating the normal physiological position; this was followed by a sudden overload of ramp

velocity at 6.67 mm/s and a 3 mm compressive displacement. The failure data collection frequency was set to 250 Hz for a period of 20 seconds.

4.4 Data Analysis

The 6DOF data collected by the hexapod were received in two text files for each specimen: one for the 6DOF translations and rotations of the hexapod actuators and another for the 6DOF forces and moments recorded by the hexapod load cell. Using the specimens' measured offsets on the X and Y axes (see Section 5.1.3), the displacement data relative to the axes of the hexapod actuators were transformed via the LabVIEW program into data representing the specimen displacement. The specimen data were then imported into MATLAB software (Matlab R2016b) for analysis. In the last dynamic cycle (the fifth cycle) for each DOF and frequency, stiffness as the linear regression slope of the curve of the loading/unloading portions was calculated by implementing MATLAB's built-in functions, polyfit and polyval (Figure 4.13).
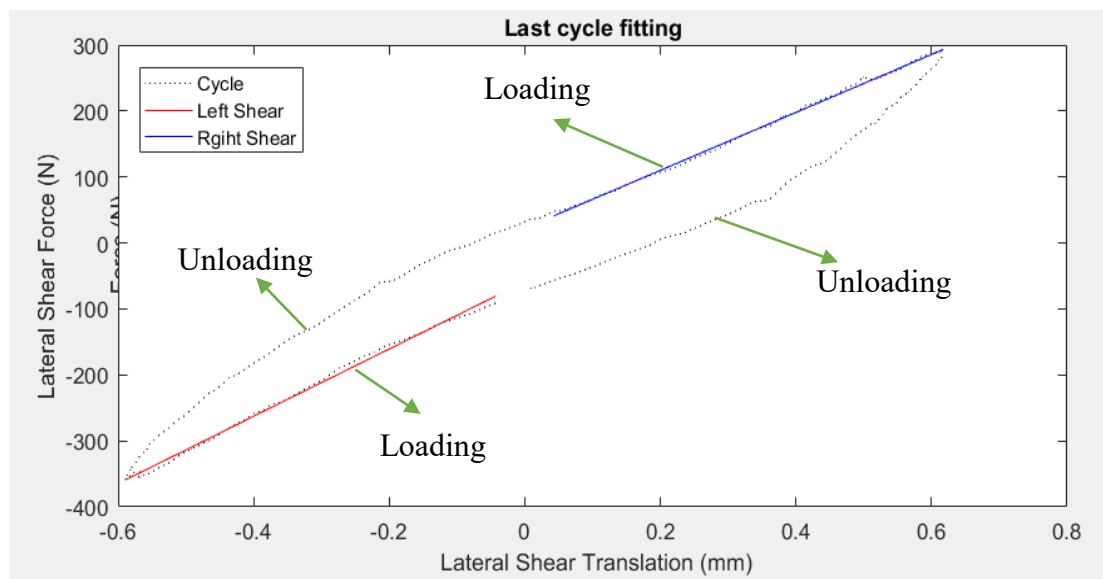
Figure 4.13: An Example Plot of the Last Cycle Showing the Pattern of Dynamic Testing in Lateral Shear at 0.1 Hz with the Loading Portions (Red and Blue) Wherein Stiffnesses Were Calculated

The viscoelastic parameter of the phase angle, representing the temporal shift between the synchronised loading and the displacement signals, was measured over the five cycles using the MATLAB estimate functions' cross power spectral density (CPSD.m). Furthermore, it was calculated as the distance between the peak of displacement and

load. The ultimate failure load of the FSU, as the peak load under which the failure of the specimen occurred, was measured in both groups for comparison.

The data were analysed using SPSS to test the hypotheses of this project (see Section 3.3). A separate repeated measures ANOVA test for each direction was conducted on the data for each group at the two frequencies. The analyses sought to evaluate data from the 6DOF dynamic tests before and after applying each injury (e.g. differences in the means of stiffnesses before and after each injury type at 0.1 Hz and 0.01 Hz). Further analysis was applied using a two-way univariate test with Bonferroni and post-hoc analyses of multiple comparisons to assess the level of variance in the post-injury data from the two groups (the data for intact specimens were excluded). An independent sample T-test was also performed on the failure-inducing peak load data for the specimens in the two groups. The differences in the means for each statistical test were determined to be significant when the *p-* value was in the range of 0 to 0.05.

Chapter 5: Results

The results obtained from the hexapod at a frequency of 1 Hz have been omitted since the hexapod control at 1 Hz became unstable. This issue could be due to unsuitable setting of the compressive load gain when testing at 1 Hz causing the target 1.1 MPa intradiscal pressure to be unachievable. For each specimen, the recorded data of the 6DOF dynamic testing and failure were plotted and calculations for stiffness, phase angle and ultimate loads of failure were obtained (see Section 5.4) and checked to ensure they were acceptable.

Note: The calculations and plots of all specimens can be found in Appendix E.

The mean load-displacement curves for the 6DOF dynamic testing of all specimens—before injury (intact) in the two groups (n = 16) and after the creation of radial tears in Group 1 (n = 8) and rim lesions in Group 2 (n =8)—were plotted for each frequency: 0.1 Hz (see Figure 5.1) and 0.01 Hz (see Figure 5.2).
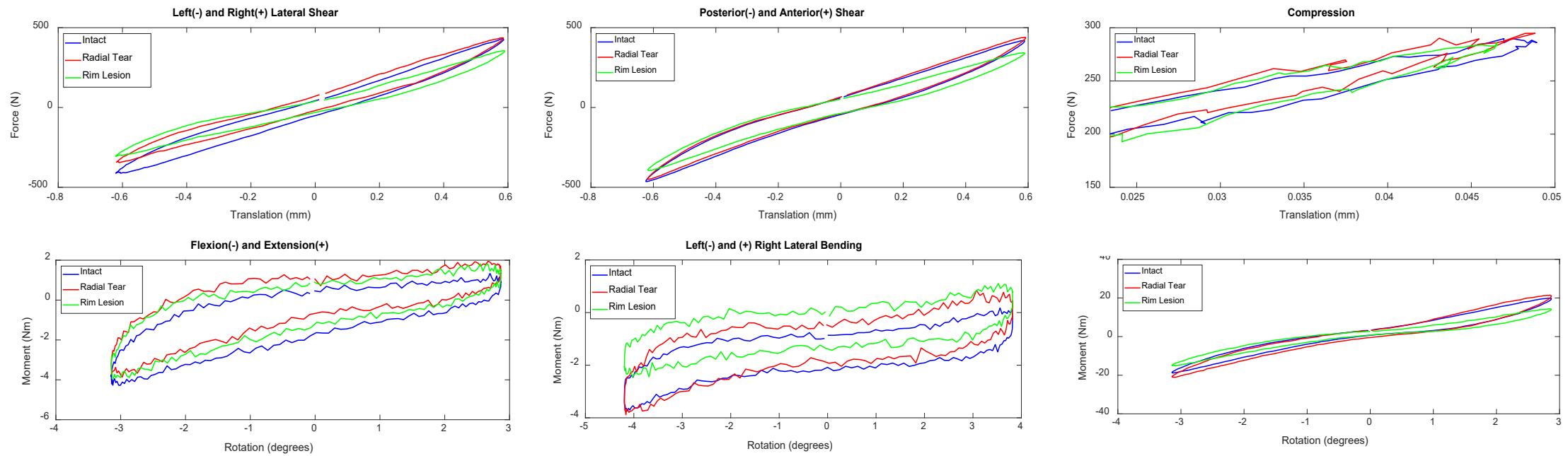
Figure 5.1 The Recorded Data Averages from the 6DOF Dynamic Tests at a Frequency of 0.1 Hz Showing All Intact (Blue) Specimens from Both Groups (N = 16), the Specimens in Group 1 (N = 8) after the Creation of Radial Tears (Red) and Those in Group 2 (N = 8) after the Creation of Rim Lesions (Green)
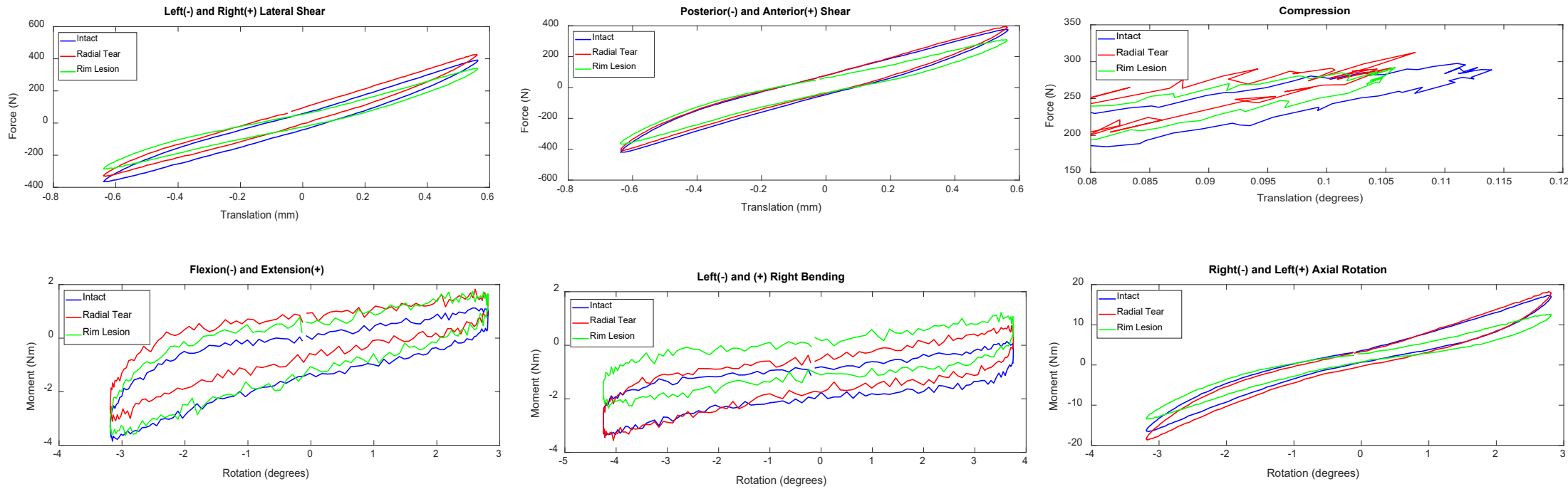
Figure 5.2 The Recorded Data Averages from the 6DOF Dynamic Tests at a Frequency of 0.01 Hz Showing All Intact (Blue) Specimens from Both Groups (N = 16), the Specimens in Group 1 (N = 8) after the Creation of Radial Tears (Red) and Those in Group 2 (N = 8) after the Creation of Rim Lesions (Green)

5.1 Repeated Measures ANOVA Tests of Hypotheses 1:

For testing whether radial tears and rim lesions significantly decreased 6DOF stiffness of the FSUs and increased the phase angle (hypothesis 1, Section 3.3), a separate repeated measures ANOVA for each DOF was performed on each group. This analysis was to display if there was significant differences in measurements before and after introducing each tear.

5.1.1 Stiffness

Averages stiffness and standard deviation before and after each injury were also calculated for comparison (Table 5.1)

Table 5.1: Average stiffness and standard deviation (SD) of each group by specimens before (intact) and after each injury type and at 0.1 Hz and 0.01 Hz.

Group	Specimen of	Left lateral. Shear	Right Lateral Shear	Posterior Shear	Anterior Shear	Compression	Flexion	Extension	Left Lat. Bending	Right Lat. Bending	Right. Axial Rotation	Left. Axial Rotation
1. Radial tear	Intact at 0.1HZ	715 (224)	629 (235)	675 (183)	770 (245)	2795 (748)	0.415 (0.851)	0.881 (0.808)	0.295 (0.275)	0.562 (0.269)	7.02 (3.30)	7.84 (7.83)
	Radial tear at 0.1HZ	629 (170)	511 (242)	633 (182)	705 (218)	3184 (1259)	0.442 (0.885)	0.971 (1.11)	0.286 (0.289)	0.523 (0.225)	6.73 (3.42)	7.12 (2.78)
	Change (%)	12.2	18.7	6.30	8.45	-13.9	-6.51	-10.2	3.05	6.94	4.23	9.16
	Intact at 0.01HZ	667 (217)	542 (181)	591 (173)	662 (211)	225 (661)	0.380 (0.690)	0.835 (0.704)	0.255 (0.223)	0.435 (0.218)	5.88 (2.94)	6.67 (2.25)
	Radial tear at 0.01HZ	601 (168)	500 (220)	572 (174)	607 (180)	2503 (984)	0.302 (0.600)	0.774 (0.631)	0.305 (0.273)	0.424 (0.186)	5.45 (3.09)	6.20 (2.28)
	Change (%)	10.92	8.54	3.40	9.18	-9.98	25.83	7.88	-16.4	2.59	7.87	7.58
2. Rim lesion	Intact at 0.1HZ	630 (179)	544 (158)	558 (182)	642 (250)	3027 (1367)	0.183 (0.230)	0.658 (0.217)	0.284 (0.347)	0.318 (0.242)	5.18 (1.86)	5.69 (2.31)
	Rim lesion at 0.1HZ	556 (168)	443 (124)	514 (142)	622 (242)	2678 (1020)	0.342 (0.649)	0.830 (0.416)	0.303 (0.327)	0.325 (0.287)	4.34 (1.47)	5.51 (2.24)
	Change (%)	11.8	18.5	7.90	3.15	11.5	-86.9	-26.1	-6.69	-2.20	16.1	3.09
	Intact at 0.01HZ	537 (169)	479 (143)	487 (157)	551 (215)	2457 (1183)	0.362 (0.464)	0.708 (0.270)	0.222 (0.221)	0.262 (0.180)	4.10 (1.70)	5.04 (2.15)
	Rim lesion at 0.01HZ	520 (184)	421 (102)	448 (136)	552 (221)	2125 (932)	0.388 (0.597)	0.724 (0.380)	0.243 (0.227)	0.272 (0.165)	3.68 (1.50)	4.84 (1.97)
	Change (%)	3.05	12.1	8.02	-0.268	13.5	-7.18	-2.25	-9.45	-3.82	10.36	3.97

Overall effect of the radial tear group showed significant differences in stiffness in right lateral shear ($p = 0.030$), in posterior shear ($p = 0.010$), in right axial rotation ($p = 0.013$) and in left axial rotation ($p = 0.003$). However, the frequency level showed main effect in by radial tear that was significant in left lateral shear ($p = 0.003$), compression ($p = 0.002$), right lateral bending ($p = 0.025$) and left axial

rotation (p =0.001). The interactions between radial tear and frequency illustrated further significant differences in right lateral shear (p =0.006) and posterior shear (p = 0.006) while the pairwise comparisons revealed significant differences by radial tears at 0.1 Hz in left lateral shear (p =0.044), right lateral shear (p =0.003), posterior shear (p =0.002) and left axial rotation (p =0.007), as well as at 0.01 Hz in right axial rotation (p = 0.007) and left axial rotation (p =0.012). The repeated measures ANOVA conducted on data of the rim lesion group displayed main effects with significant differences produced by rim lesions in right lateral shear (p = 0.033), posterior shear (p = 0.077) and right axial rotation (p = 0.004), as well as overall difference by frequency in left lateral shear (p = 0.005), compression (p = 0.029) and flexion (p = 0.041). There were also significant differences arising from the interactions of injury and frequency in right lateral shear (p = 0.042) and right axial rotation (p =0.008). Pairwise comparisons showed that a significant difference was caused by the rim lesion at 0.1 Hz in left lateral shear (p = 0.016), in right lateral shear (p =0.012) and in right axial rotation (p =0.001), and at 0.01 Hz in right axial rotation (p = 0.032). See Figure 5.2 for average stiffnesses (Table 5.1) with the significance indicated on the figure representing differences before and after injury within each group, based on the analysis of repeated measures ANOVA (Table 5.2).
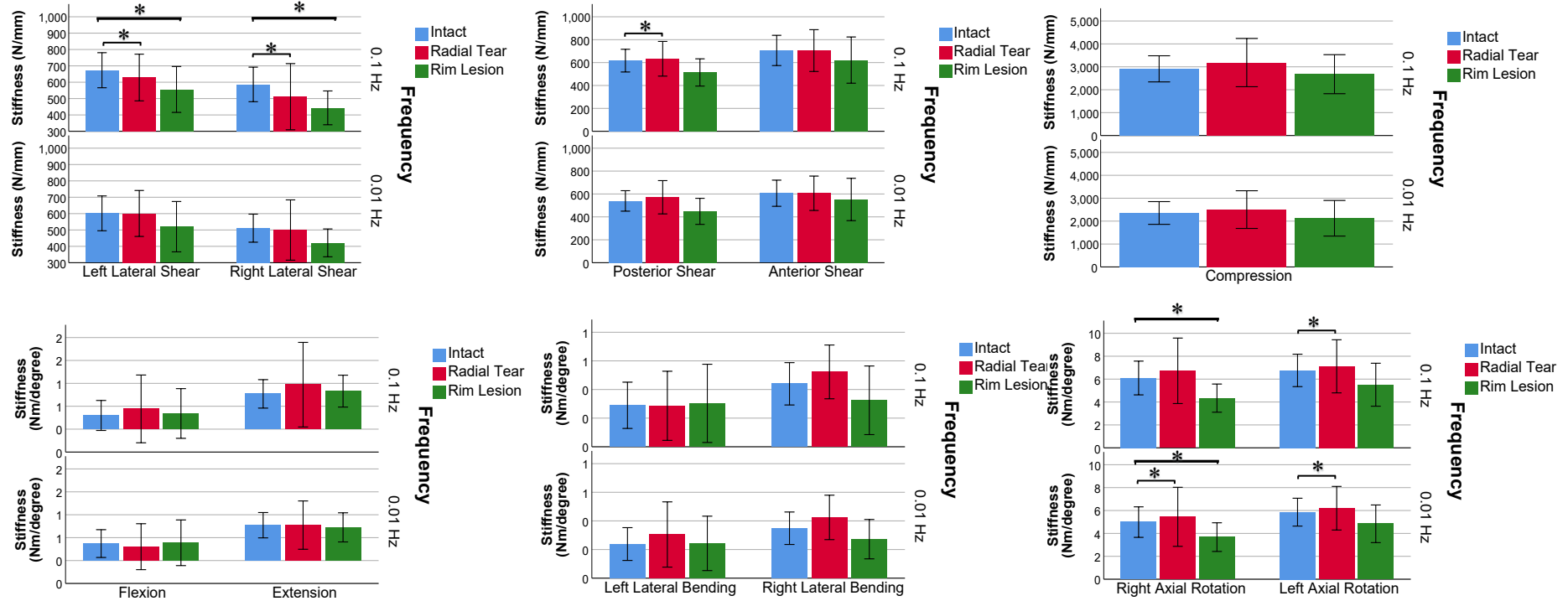
Figure 5.2: Bar Graph Showing the Average Stiffnesses at 0.1 Hz and 0.01 Hz for All Intact (Blue) Specimens from Both Groups (N = 16, pooled only for simplifying the bar graph plots – refer to Table 5.1 for actual intact group values), for the Specimens in Group 1 (N = 8) after the Creation of Radial Tears (Red) and for Those in Group 2 (N = 8) after the Creation of Rim Lesions (Green). Error Bars: 95% Confidence Interval Asterisk: p < 0.05

Analysis	Effect	Left lateral. Shear	Right Lateral Shear	Posterior Shear	Anterior Shear	Compression	Flexion	Extension	Left Lat. Bending	Right Lat. Bending	Right. Axial Rotation	Left. Axial Rotation
Repeated Measures ANOVA (N = 8) (Group 1 Pre-& Post radial tear data)	Radial tear		0.030	0.01							0.013	0.003
	Frequency	0.003		0		0.002				0.025	0	0.001
	Radial tear*Frequency		0.006	0.006								
	Radial tear at 0.1 Hz	0.044	0.003	0.002								0.007
	Radial tear at 0.01 Hz										0.007	0.012
Repeated Measures ANOVA (N = 8) (Group 2 Pre-& Post Rim lesion data))	Rim lesion		0.033	0.077							0.004	
	Frequency	0.005				0.029	0.041				0	0
	Rim lesion*Frequency		0.042								0.008	
	Rim lesion at 0.1 Hz	0.016	0.012								0.001	
	Rim lesion at 0.01 Hz										0.032	

Table 5.2: Significant effects on FSUs stiffnesses of the repeated measures, including the p-values and directions where significant differences in means were found (empty cell means not significant)

5.1.2 Phase angle

Averages phase angle and standard deviation (SD) before and after each injury were calculated for comparing the magnitude of effects (Table 5.3)

Table 5.3: Average phase angle and standard deviation (SD) of each group by specimens before (intact) and after each injury type and at 0.1 Hz and 0.01 Hz.

Group		Left-Right Lateral Shear	Posterior–Anterior Shear	Compression	Flexion-Extension	Left-Right Lateral Bending	Right–Left Axial Rotation
Radial tear	Intact at 0.1HZ	9.070 (2.031)	9.233 (1.592)	10.550 (4.362)	38.217(15.884)	38.241(15.860)	9.616 (3.012)
	Radial tear at 0.1HZ	10.200 (2.704)	9.193 (1.596)	10.300(2.419)	42.347 (20.830)	42.128 (14.283)	10.035 (3.211)
	Change (%)	-12.45	0.43	2.36	-10.8	-10.1	-4.35
	Intact at 0.01HZ	8.784 (1.586)	10.902 (1.617)	13.335(4.064)	34.680 (14.890)	39.943 (18.886)	9.272 (1.048)
	Radial tear at 0.01HZ	8.90 (2.297)	10.275 (1.938)	12.432(3.466)	38.918(16.823)	37.265 (9.139)	9.349 (1.275)
	Change (%)	-1.41165756	5.75124	6.77165	-12.22	6.70455	-0.8305
Rim lesion	Intact at 0.1HZ	9.138 (1.510)	9.079(2.019)	10.680 (5.801)	37.079 (9.472)	53.003 (27.726)	8.417(2.475)
	Rim lesion at 0.1HZ	9.905(2.306)	8.977(1.391)	12.804 (7.609)	40.706(15.964)	51.429 (22.449)	8.447 (1.870)
	Change (%)	39.83112623	1.12347	-19.888	-9.7818	2.96964	-0.3564
	Intact at 0.01HZ	9.010 (1.860)	11.299 (2.244)	14.266 (4.783)	35.158 (8.849)	46.436 (18.557)	9.066 (2.014024)
	Rim lesion at 0.01HZ	9.168(2.139)	10.831(1.651)	15.282 (6.129)	35.525(10.726)	47.271(16.462)	9.048 (1.317)
	Change (%)	-1.753607103	4.141959	-7.12183	-1.04386	-1.79817	0.198544

The analysis of repeated measures ANOVAs was also conducted in each group of injury on the output measure of phase angle. In radial tear group, the main effects showed significant differences on phase angle by radial tear in flexion–extension (p = 0.037) and by frequency level in left–right lateral shear (p =0.027), posterior–anterior shear (p = 0.014) and compression (p = 0.019). The interactions between radial tears and frequency indicated further significant differences on phase angle in left–right lateral shear (p =0.002), posterior– anterior shear (p = 0.007) and left–right lateral bending (p = 0.025). Pairwise comparisons showed significant differences by radial tear at 0.1 Hz in left–right lateral shear (p = 0.044)

only and at 0.01 Hz in posterior–anterior shear (p = 0.021) and flexion–extension (p = 0.009). The main effects also showed significant differences in phase angle by rim lesions under compression (p =0.045) and according to frequency in posterior–anterior shear (p = 0.001), compression (p = 0.048) and right–left axial rotation (p = 0.031) where interactions between rim lesions and frequency showed no significant differences in all directions. However, pairwise comparisons showed significant differences according to rim lesion at 0.1 Hz in compression (p = 0.045) only, while no significant differences were revealed in any direction at 0.01 Hz. See Figure 5.4 for average phase angles (Table 5.3) with the significance indicated on the figure representing the differences before and after injury within each group, based on the analysis of repeated measures ANOVA (Table 5.4).
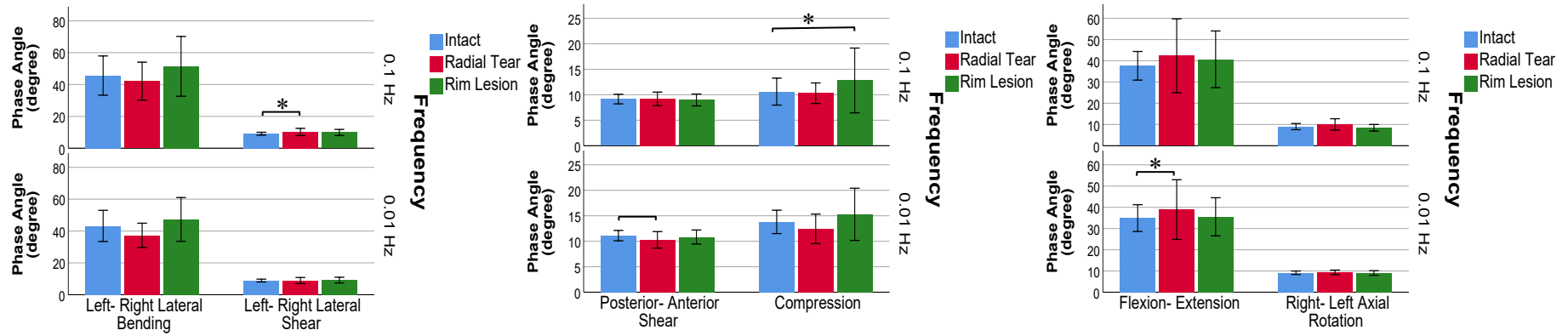
Figure 5.3: Bar Graph Showing the Average Phase Angles at 0.1 Hz and 0.01 Hz for All Intact (Blue) Specimens from Both Groups (N = 16, pooled only for simplifying the bar graph plots – refer to Table 5.3 for actual intact group values), for the Specimens in Group 1 (N = 8) after the Creation of Radial Tears (Red) and for Those in Group 2 (N = 8) after the Creation of Rim Lesions (Green). Error Bars: 95% Confidence Interval Asterisk: p < 0.05

Table 5.4: Phase angle significant results of the repeated measures including the p-values for the effects and directions where significant differences in means were found (empty cell means not significant)

Analysis	Effect	Left-Right Lateral Shear	Posterior–Anterior Shear	Compression	Flexion- Extension	Left-Right Lateral Bending	Right–Left Axial Rotation
Repeated Measures ANOVA (N = 8) (Group 1 Pre-& Post radial tear data)	Radial tear				0.037		
	Frequency	0.027	0.014	0.019			
	Radial tear*Frequency	0.002	0.007			0.025	
	Radial tear at 0.1 Hz	0.009					
	Radial tear at 0.01 Hz		0.021		0.009		
Repeated Measures ANOVA (N = 8) (Group 2 Pre-& Post Rim lesion data))	Rim lesion			0.045			
	Frequency		0.001	0.048			0.031
	Rim lesion*Frequency						
	Rim lesion at 0.1 Hz			0.045			
	Rim lesion at 0.01 Hz						

5.2 Two-way Univariate ANOVA Test of Hypothesis 2

For testing whether radial tears will cause significant changes of a greater magnitude in the 6DOF stiffnesses and the phase angles of each FSU (Hypothesis 2, 3.3 section), two-way univariate ANOVAs were conducted on each group. Overall, results showed significant differences in the means of stiffness according to injury in posterior shear (p = 0.040), right lateral bending (p = 0.033) and right axial rotation (p =0.028. As for phase angle main effect of significant differences, resulting from frequency, in the phase angle means between the two groups in posterior–anterior shear (p =0.018).

5.2.1 Stiffness

The significant effects on FSUs stiffness (Table 5.5) were obtained in all directions to compare the difference in effects between the two injuries.

Table 5.5: Effects on FSUs stiffness by the two-way univariate ANOVA tests, including the p-values for the effects and directions where significant differences in means were found (empty cell means not significant)

Analysis	Effect	Left lateral. Shear	Right Lateral Shear	Posterior Shear	Anterior Shear	Compression	Flexion	Extension	Left Lat. Bending	Right Lat. Bending	Right. Axial Rotation	Left. Axial Rotation
Two- way univariate ANOVA: Post radial tear & Post rim lesion	Injury			0.040						0.033	0.028	
	Frequency											
	Injury *Frequency											
	0.1 Hz											
	0.01 Hz											

5.2.2 Phase angle

The Two-way ANOVA analysis was also performed for comparing the effects of injuries on the phase angle (Table 5.6) where main effect of frequency in posterior-anterior shear was found (0.018).

Table 5.6: Effects on FSUs phase angle by the two-way univariate ANOVA tests, including the p-values for the effects and directions where significant differences in means were found (empty cell means not significant)

Analysis	Effect	Left-Right Lateral Shear		Posterior–Anterior Shear	Compression	Flexion-Extension	Left-Right Lateral Bending	Right–Left Axial Rotation
Two-way univariate ANOVA forPost radial tear & post rim lesion Data of group 1 & 2	Injury							
	Frequency			0.018				
	Injury*Frequency							
	0.1 Hz							
	0.01 Hz							

5.3 Independent Sample T- test of Hypothesis 3

5.3.1 Failure

Independent sample t-test was conducted on the data of ultimate failure loads from the two groups to ascertain that there will be no significant difference in means of the two groups of injuries (Hypothesis 3, 3.3 section). The obtained means and standard deviations (SD) from radial tears and rim lesions groups were 13518N (3381) and 12346N (2838) respectively. The result showed no significant difference (p = 0.532) (Figure 5.5)
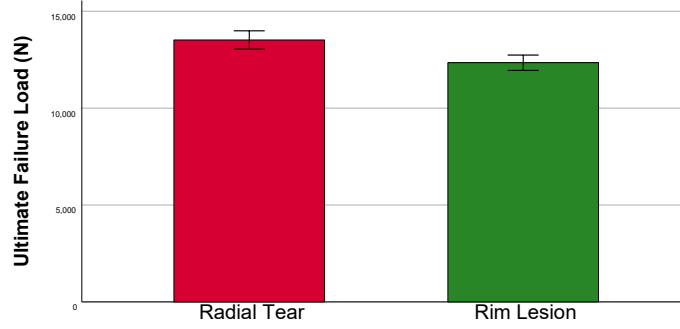
Figure5.5: Bar Graph Showing the Ultimate Failure Load Averaged Across all Specimens from the Radial Tear Group and the Rim Lesion Group. Error Bars: 95% Confidence Interval Asterisk: p < 0.05

Chapter 6: Discussion

This project mainly evaluated the mechanical implications of annular tears; radial tears and rim lesions, on the six principle degrees of freedom of sheep spinal segments. This animal model is becoming more popular due to its ready availability and its structural and chemical relevance to human specimens. As this project shed light on the mechanical influence of disc annular tears on spinal segments, the findings introduced here remain irrelevant to human spinal segments until such study is implemented in human specimens. The mechanical testing and data analysis of six-teen specimens were successfully achieved. Similar to any other study, some limitations existed and should be acknowledged.

6.1 Limitations

Indian ink raised a limitation when it was attempted for marking and tracking the depth of injuries in the pilot study of this project. When discs were transversely cut, the ink appeared to randomly spread and extend across the annulus fibrosus and nucleus pulposus. Nevertheless, this could result from the cutting process of discs as it was difficult to control due to the injuries being applied on different transverse levels into the same specimen. However, this could have been avoided if injuries had been created into individual specimens which was not possible because of the limitation in the number of sheep specimens collected. It is worth pointing out that the tracking of injures boundaries was effectively reached since the symmetrical contrast could be clearly distinguished by the naked eye when looking carefully at the surface roughness. The 6DOF mechanical testing results of specimens at 1 Hz frequency were omitted due to being unsatisfactory. Furthermore, the required compressive amplitude of 1.1 MPa could not be accomplished. This could be related to the settings of compressive gain knowing that such dynamic testing at this frequency level had been achieved by the hexapod in previous studies (Amin et al., 2016, Costi et al., 2008).

6.2 Effects of radial tears and rim lesions

Overall, radial tears and rim lesions seemed to decrease FSU stiffness as it was hypothesised (Section 3.3). The results obtained from the 6DOF mechanical testing at 0.1 Hz showed FSU stiffness with significant decrease by radial tears in posterior shear and by both types of tears in left and right lateral shear and in axial rotation (towards the direction of injury). At 0.01 Hz testing, the significant decrease from both tears were narrowed in direction to the axial rotation – right and left– by radial tears and right– by rim lesion. However, FSU phase angles seemed to significantly differ by only radial tears at both frequency levels. At 0.1 Hz, it decreased in left-right lateral shear whereas at 0.01 Hz it increased in flexion-extension and decreased in posterior- anterior shear. The decrease was significant by radial tears at 0.1 Hz in left axial rotation (9.16%), posterior shear (6.30%) and left (12.17%) and right (18.74%) lateral shears. However, at 0.01 Hz, the decrease in stiffness was contracted to be only in axial rotation-left (7.58%) and right (7.87%) directions. The radial tears effects on the FSU stiffness were consistent to previous studies (Michalek and Iatridis, 2012, Thompson et al., 2004) in which specimens tested in axial rotation, flexion-extension, compression and lateral bending showed no significant changes except a significant decrease in axial rotation (Michalek and Iatridis, 2012). This decrease in axial rotation was estimated to be 65.42-65.13% higher than that of the present study. As expected in the hypotheses, radial tears were found to increase FSU phase angle in left-right lateral shear (12.46%) at 0.1 Hz and in flexion-extension (12.22%) at 0.01 Hz. However, a decrease in phase angle was exhibited in posterior- anterior shear (5.75%). These results were different from those of the hysteresis (a measure of viscoelasticity) reported in the literature in that hysteresis was thought to decrease (~ 6%) by radial tears in flexion-extension and lateral bending (Thompson et al., 2004) and in axial rotation (73%) (Michalek and Iatridis, 2012).Similar to radial tears and in consistence with earlier findings, rim lesions seemed to cause significant stiffness decrease in left (11.81%) and right (18.53%) lateral shear at 0.1 Hz and in right axial rotation at both frequencies, (16.13%) and (10.37%) respectively. Nevertheless, rim lesions were found to cause no significant effects on the FSU phase angle in all directions and at both frequency levels which appeared to be inconsistent with the study of Michalek and Iatridis (2012) where it caused hysteresis decrease (~6%) in axial rotation. The significant difference between the two frequency levels (p=0.001) from the radial tear group was found in left axial rotation where 37.7%

stiffness reduction drop (12.17% at 0.1 Hz to 7.58% at 0.01 Hz) was noticed in the presence of radial tears. Similarly, in the rim lesion group, another significant difference between the two frequency levels (p=0) was found in right axial rotation (towards the location of rim lesion) where stiffness reduction drop (16.13% at 0.1 Hz to 10.37% at 0.01 Hz) was also measured after the creation of rim lesions. This intersection of significant differences from both types of injuries could be an indication of a direct correlation between the level of frequency and FSU stiffness reduction in axial rotation in the direction of injury location and this was consistent with previous findings (Costi et al., 2008). This correlation was notable as the FSU stiffness reduced in magnitude by both tears from high to low frequency levels.

Specimens from both groups of injuries were subjected to 13-degree flexion before they were failed by sudden overload under compressive translation of 3 mm magnitude and 6.67 mm/s rate. The means of the ultimate failure loads from the specimens of the two groups were compared to see if there was any significant difference in the effects of the two types of tears. The results showed no significant difference, however, such approach with annular tears was not preceded by other studies, to the author knowledge. The results could be compared with those of degenerative human specimens which were failed under different physiological conditions (e.g. radial tears and rim lesions were often present in conjunction in one specimen) and also different testing conditions (e.g. failure displacement was 0.2 mm with 0.167 mm/s rate) (Thompson et al., 2000). This comparison may establish a ground for further studies in future to investigate if these conditions could make variations in result. The ultimate failure loads of the human degenerative specimens revealed variation between radial tears and rim lesions in that its decrease was of a very strong correlation with the size of radial tears only. This finding was obviously different from the present study's as the significant different conditions could play a major role.

For clinical relevance, the project considered the importance of testing specimens within their intact physiological conditions such leaving the posterior element intact. Furthermore, intradiscal pressure was simulated by maintaining proper preload on the disc before and throughout the experiments, exceeding any differences in conditions found in previous studies. For example, one study found preload to increase the FSU

stiffness (Stokes et al., 2002) while another suggested it made no difference and hence it was applied in that study (Thompson et al., 2004). Such difference in protocols could lead to unpredictable results from different studies. The significant reduction found in radial tears and rim lesions compared to the study of Michalek and Iatridis (2012) could be justified by the pre-needle puncture applied on specimen prior to the creation of radial tears in that study. Interestingly, although of the common radial tears effects in decreasing axial rotational stiffness, the different animal models (bovine vs sheep) of the two studies could also contribute to the reduction magnitude in stiffness. Potential variation between different animal models are consolidated knowing that differences in the animal models' structures and mechanical properties (e.g. bovine disc lamellae being stiffer in tension than Ovine) (Monaco et al., 2016) could exist. On the other hand, the inconsistency in results of the current study with the sheep model study of (Thompson et al., 2004) where radial tears had shown no effect on axial rotational stiffness, could be explained by the different testing conditions (e.g. no compressive preload applied in that testing) and/or the different spine levels of specimen (L4/L5 vs L5/L6) used in that study. Here the importance of physiological conditions effect is reflected since it could potentially lead to different mechanical response of specimen.

6.3 Radial tears and rim lesions effects in degenerative discs

The two injuries tend to be present in degenerative human discs (Hilton et al., 1976) and as structural changes, they could alter the biomechanical behaviour of the disc at the presence of other potentially contributing factors such (e.g. chemical) (Adams and Roughley, 2006, Galbusera et al., 2014). The findings of this study were compared to the study by Amin et al. (2016). Remarkably, it was found that difference in mechanical stiffness between such acute injuries induced on healthy sheep discs, in the absence of other degenerative/degeneration changes, revealed similarities to those of different levels of disc degeneration. This comparison seemed to be logical as each injury effects was compared to the degeneration level where it was evident to be present. For instance, radial tears were frequently noticed in the moderate level of disc degeneration (Thompson 4) while rim lesions were common in the mild level (Thompson grade 3) (Liebenberg et al.n.d). The comparison was also encouraged by the common use of hexapod robot and testing under similar protocols and physiological conditions. Further, the results were compared at the same frequency level of mechanical testing (0.1 Hz)

where in the current study a significant difference (p = 0.028) was found in stiffness between radial tears and rim lesions in right axial rotation. This was consistent to the findings of Amin et al. (2016) in which moderate degenerative specimens, whereby radial tears exist, were significantly different in axial rotation stiffness (p=0.001) than the mild degenerated ones (rim lesions were expected). If this similarity was confirmed in further studies this could lead to a conclusion relating disc correlation more in relation or even cause to structural changes than other changes (e.g. chemical changes).

Chapter 7: Conclusions

The mechanical effects of radial tears and rim lesions were successfully evaluated under 6DOF Dynamic testing simulating two different frequency levels such as during in-vivo walking or office sitting. Injury creation protocol was developed and pilot testing of creating injury showed an acceptable level of repeatability from the pilot testing results. The effects of radial tears and rim lesions on FSU stiffness were similar in the directions of 6DOF dynamic testing at each level. At the high frequency they caused decrease in stiffness in axial rotation (towards the location of injury), left and right lateral shear with extension of effect in posterior shear by radial tears. However, at the low frequency, the stiffness decrease was limited to axial rotation only (left and right by radial tears and right by rim lesions). Furthermore, in axial rotation, frequency level seemed to affect stiffness magnitude by both injury types. This effect was demonstrated by the lessened reduction in stiffness at the low frequency relative to the high frequency level. However, FSU phase angle displayed significant variation by radial tears and no changes by rim lesions. At high frequency it decreased in left-right lateral shear while at the low frequency level it increased in flexion-extension and decreased in posterior-anterior shear. There was not significant difference in ultimate failure load between radial tears and rim lesions specimens when they were traumatically failed.

7.1 Future Work

Future work is needed to extend our understanding of the mechanical effects of annular tears. One important direction for future work is the mechanical evaluation of the concentric tears since it was a limitation of the present study because of lack of apparatus. Concentric tears are common structural changes occur into the disc and the assessment of its structural change could lead to a better understanding to the correlation between disc changes in structure and mechanics. Further, its mechanical effects are still not clear and, to the author knowledge, haven't been measured under shear mechanical testing (e.g. anterior-posterior shear and lateral bending) or related to the effects of different frequency levels under 6DOF dynamic testing. Another area of future work will be expansion the influence investigation of all three annular tears; radial tears, rim lesions and concentric tears on the viscoelastic properties of the disc

under creep and stress relaxation. These tests will provide an insight into the deformation and resistance of disc tissues exhibiting a form of annular tear during steady load or displacement applied. The relation between annular tears and disc herniation under sudden overload will also be an important aspect for future work as annular such as rim lesions have thought to be the consequence of sudden overload to the disc (Hilton et al., 1980)

These findings can be clinically beneficial for example to people diagnosed with radial tears or rim lesions in their discs. It raises their awareness and better understanding on the effects of directions they need to avoid where FSU stiffness can be most affected. Fields such as tissue engineering can benefit from understating a viscoelastic property of disc under dynamic movement simulating that of the in-vivo condition.

References

ADAMS, M. A. & ROUGHLEY, P. J. 2006. What is intervertebral disc degeneration, and what causes it? *Spine (Phila Pa 1976),* 31**,** 2151-61.

AMIN, D. B., SOMMERFELD, D., LAWLESS, I. M., STANLEY, R. M., DING, B. & COSTI, J. J. 2016. Effect of degeneration on the six degree of freedom mechanical properties of human lumbar spine segments. *Journal of Orthopaedic Research,* 34**,** 1399-1409.

ANDERSON, D. G., IZZO, M. W., HALL, D. J., VACCARO, A. R., HILIBRAND, A., ARNOLD, W., TUAN, R. S. & ALBERT, T. J. 2002. Comparative gene expression profiling of normal and degenerative discs: analysis of a rabbit annular laceration model. Spine, 27, 1291-1296

ANDERSSON, G. B. 1999. Epidemiological features of chronic low-back pain. *The lancet,* 354**,** 581-585.

BOGDUK, N. 1997. International Spinal Injection Society guidelines for the performance of spinal injection procedures. Part 1: Zygapophysial joint blocks. *Clin J Pain,* 13**,** 285-302.

BOOS, N., WEISSBACH, S., ROHRBACH, H., WEILER, C., SPRATT, K. F. & NERLICH, A. G. 2002. Classification of age-related changes in lumbar intervertebral discs: 2002 Volvo Award in basic science. *Spine,* 27**,** 2631-2644.

BUCKWALTER, J. A. 1995. Aging and degeneration of the human intervertebral disc. *Spine (Phila Pa 1976),* 20**,** 1307-14.

CALLAGHAN, J. P. & MCGILL, S. M. 2001. Intervertebral disc herniation: studies on a porcine model exposed to highly repetitive flexion/extension motion with compressive force. *Clinical Biomechanics,* 16**,** 28-37.

COSTI, J. J., STOKES, I. A., GARDNER-MORSE, M. G. & IATRIDIS, J. C. 2008. Frequency-dependent behavior of the intervertebral disc in response to each of six degree of freedom dynamic loading: solid phase and fluid phase contributions. *Spine,* 33**,** 1731.

DE VISSER, H., ROWE, C. & PEARCY, M. 2007. A robotic testing facility for the measurement of the mechanics of spinal joints. *Proceedings of the Institution of Mechanical Engineers, Part H: Journal of Engineering in Medicine,* 221**,** 221-227.

DING, B., STANLEY, R. M., CAZZOLATO, B. S. & COSTI, J. J. Real-time FPGA control of a hexapod robot for 6-DOF biomechanical testing. IECON 2011-37th Annual Conference on IEEE Industrial Electronics Society, 2011. IEEE, 252-257.

FAZZALARI, L. N., COSTI, J. J., HEARN, C. T., FRASER, D. R., VERNON-ROBERTS, A. B., HUTCHINSON, H. J., MANTHEY, H. B., PARKINSON, H. I. & SINCLAIR, H. C. 2001. Mechanical and Pathologic Consequences of Induced Concentric Anular Tears in an Ovine Model. *Spine,* 26**,** 2575-2581.

FERGUSON, S. J. & STEFFEN, T. 2003. Biomechanics of the aging spine. *European Spine Journal,* 12**,** S97-S103.

FLEISS, J. L. 2011. *Design and analysis of clinical experiments*, John Wiley & Sons.

HAUGHTON, V. M., LIM, T. H. & AN, H. 1999. Intervertebral Disk Appearance Correlated with Stiffness of Lumbar Spinal Motion Segments. *American journal of neuroradiology,* 20**,** 1161-1165.

HAUGHTON, V. M., SCHMIDT, T. A., KEELE, K., AN, H. S. & LIM, T.-H. 2000. Flexibility of lumbar spinal motion segments correlated to type of tears in the annulus fibrosus. *Journal of Neurosurgery: Spine,* 92**,** 81-86.

HILTON, R. C., BALL, J. & BENN, R. T. 1976. Vertebral end-plate lesions (Schmorl's nodes) in the dorsolumbar spine. *Annals of the Rheumatic Diseases,* 35**,** 127-132.

HIRSCH, C. & SCHAJOWICZ, F. 1952. Studies on Structural Changes in the Lumbar Annulus Fibrosus. *Acta Orthopaedica Scandinavica,* 22**,** 184-231.

KAIGLE, M. A., HOLM, H. S. & HANSSON, H. T. 1997. 1997 Volvo Award Winner in Biomechanical Studies: Kinematic Behavior of the Porcine Lumbar Spine: A Chronic Lesion Model. *Spine,* 22**,** 2796-2806.

KIRKALDY-WILLIS, W. H. & FARFAN, H. F. 1982. Instability of the lumbar spine. *Clin Orthop Relat Res***,** 110-23.

LATHAM, J. M., PEARCY, M. J., COSTI, J. J., MOORE, R., FRASER, R. D. & VERNON-ROBERTS, B. 1994. Mechanical consequences of annular tears and subsequent intervertebral disc degeneration. *Clinical Biomechanics,* 9**,** 211-219.

LIEBENBERG, E., GIAMPAOLI, A. & LOTZ, J. Cross-talk between Discs and Adjacent Bone, Implication for Vertebrogenic Pain.

LITTLE, J. P. 2004. *Finite element modelling of anular lesions in the lumbar intervertebral disc.* Queensland University of Technology.

LU, W. W., LUK, K. D., HOLMES, A. D., CHEUNG, K. M. & LEONG, J. C. 2005. Pure shear properties of lumbar spinal joints and the effect of tissue sectioning on load sharing. *Spine,* 30**,** E204-E209.

MICHALEK, A. J. & IATRIDIS, J. C. 2012. Height and torsional stiffness are most sensitive to annular injury in large animal intervertebral discs. *The Spine Journal,* 12**,** 425-432.

MONACO, L. A., DEWITTE-ORR, S. J. & GREGORY, D. E. 2016. A comparison between porcine, ovine, and bovine intervertebral disc anatomy and single lamella annulus fibrosus tensile properties. Journal of morphology, 277, 244-251.

MOORE, R. J. 2006. The vertebral endplate: disc degeneration, disc regeneration. *European Spine Journal,* 15**,** 333-337.

NACHEMSON, A. & MORRIS, J. M. 1964. In vivo measurements of intradiscal pressure: discometry, a method for the determination of pressure in the lower lumbar discs. *JBJS,* 46**,** 1077-1092.

NEWELL, N., LITTLE, J. P., CHRISTOU, A., ADAMS, M. A., ADAM, C. J. & MASOUROS, S. D. 2017. Biomechanics of the human intervertebral disc: A review of testing techniques and results. *Journal of the Mechanical Behavior of Biomedical Materials,* 69**,** 420-434.

OSTI, O., VERNON-ROBERTS, B., MOORE, R. & D FRASER, R. 1992a. *Annular tears and disc degeneration in the lumbar spine. A post-mortem study of 135 discs*.

OSTI, O., VERNON-ROBERTS, B., MOORE, R. & FRASER, R. 1992b. Annular tears and disc degeneration in the lumbar spine. A post-mortem study of 135 discs. *The Journal of bone and joint surgery. British volume,* 74**,** 678-682.

OSTI, O. L., VERNON-ROBERTS, B. & FRASER, R. D. 1990. 1990 Volvo Award in experimental studies. Anulus tears and intervertebral disc degeneration. An experimental study using an animal model. *Spine (Phila Pa 1976),* 15**,** 762-7.

PEARCY, M. & TIBREWAL, S. 1984. Axial rotation and lateral bending in the normal lumbar spine measured by three-dimensional radiography. *Spine,* 9**,** 582-587.

PEARCY, M. J. 1985. Stereo radiography of lumbar spine motion. *Acta Orthopaedica Scandinavica,* 56**,** 1-45.

PRZYBYLA, A., POLLINTINE, P., BEDZINSKI, R. & ADAMS, M. A. 2006. Outer annulus tears have less effect than endplate fracture on stress distributions inside intervertebral discs: Relevance to disc degeneration. *Clinical Biomechanics,* 21**,** 1013-1019.

RAJ, P. P. 2008. Intervertebral disc: anatomy-physiology-pathophysiology-treatment. *Pain Pract,* 8**,** 18-44.

REID, J. E., MEAKIN, J. R., ROBINS, S., SKAKLE, J. M. S. & HUKINS, D. W. L. 2002. Sheep lumbar intervertebral discs as models for human discs. *Clinical Biomechanics,* 17**,** 312-314.

SCHMIDT, A. T., AN, S. H., LIM, H. T.-H., NOWICKI, M. B. & HAUGHTON, M. V. 1998. The Stiffness of Lumbar Spinal Motion Segments With a High-Intensity Zone in the Anulus Fibrosus. *Spine,* 23**,** 2167-2173.

SCHMORL, G., GOIN, L.S., JUNGHANNS, H. AND WILK, S.P., 1959. The human spine in health and disease: anatomicopathologic studies. . *Grune& Stratton*.

SENGUPTA, D. K. 2017. Clinical Biomechanics of the Spine. *Spine (Phila Pa 1976),* 42 Suppl 7**,** S3.

SHIRAZI-ADL, M. A., AHMED, C. A. & SHRIVASTAVA, C. S. 1986. Mechanical Response of a Lumbar Motion Segment in Axial Torque Alone and Combined with Compression. *Spine,* 11**,** 914-927.

SKRZYPIEC, D. M., BISHOP, N. E., KLEIN, A., PÜSCHEL, K., MORLOCK, M. M. & HUBER, G. 2013. Estimation of shear load sharing in moderately degenerated human lumbar spine. *Journal of biomechanics,* 46**,** 651-657.

SKRZYPIEC, D. M., KLEIN, A., BISHOP, N. E., STAHMER, F., PÜSCHEL, K., SEIDEL, H., MORLOCK, M. M. & HUBER, G. 2012. Shear strength of the human lumbar spine. *Clinical Biomechanics,* 27**,** 646-651.

STOKES, I. & FRYMOYER, J. W. 1987. Segmental motion and instability. *Spine,* 12**,** 688-691.

STOKES, I. A., GARDNER-MORSE, M., CHURCHILL, D. & LAIBLE, J. P. 2002. Measurement of a spinal motion segment stiffness matrix. Journal of biomechanics, 35, 517-521.

TANAKA, N., AN, H. S., LIM, T.-H., FUJIWARA, A., JEON, C.-H. & HAUGHTON, V. M. 2001. The relationship between disc degeneration and flexibility of the lumbar spine. *The Spine Journal,* 1**,** 47-56.

TAN, J. S. & UPPUGANTI, S. 2012. Cumulative multiple freeze-thaw cycles and testing does not affect subsequent within-day variation in intervertebral flexibility of human cadaveric lumbosacral spine. Spine, 37, E1238-E1242.

THOMPSON, J. P., PEARCE, R. H., SCHECHTER, M., ADAMS, M. E., TSANG, I. & BISHOP, P. B. 1990. *Preliminary Evaluation of a Scheme for Grading the Gross Morphology of the Human Intervertebral Disc.*

THOMPSON, R. E., PEARCY, M. J. & BARKER, T. M. 2004. The mechanical effects of intervertebral disc lesions. *Clinical Biomechanics,* 19**,** 448-455.

THOMPSON, R. E., PEARCY, M. J., DOWNING, K. J., MANTHEY, B. A., PARKINSON, I. H. & FAZZALARI, N. L. 2000. Disc lesions and the mechanics of the intervertebral joint complex. *Spine (Phila Pa 1976),* 25**,** 3026-35.

URBAN, J. P. G. & ROBERTS, S. 2003. Degeneration of the intervertebral disc. *Arthritis Research & Therapy,* 5**,** 120-130.

WHITE, A. A. 1990. *Clinical biomechanics of the spine, Philadelphia, Philadelphia : Lippincott.*

WILKE, H. J., NEEF, P., CAIMI, M., HOOGLAND, T. & E. CLAES, L. 1999. *New In Vivo Measurements of Pressures in the Intervertebral Disc in Daily Life.*

Appendices

Appendix A: FSU Measurements and overall steps

		FSU Measurment Protocol 2018				
1						
2						
3		**Specimen Prep Date**		**Testing Date**		**Testing Conditions**
4						
5		**Specimen ID**		**Specimen Number**		**Disc Level**
6						
7						
8						
9						
10	**Day 1**			Specimen Preparation		
11						
12		**Prepping FSUs**				
13		1. Clean Spines (~3hrs)				
14		2. Cut two FSUs from each spine using bandsaw				
15		3. Ensure vertebral body surfaces are parallel				
16		4. Specimen height should be >60mm to ensure hexapod is at mid-stroke when testing				
17		5. Clean soft tissue off superior and inferior vertebra, keeping ligaments intact				
18		6. Keep facets on				
19						
20		**Storing FSUs**				
21		1. Wrap FSUs in saline soaked gauze				
22		2. Seal in ziplock plastic bags				
23		3. Make and place specimen label (specimen ID, date, FSU level in bag)				
24		4. Place specimen in walk-in freezer in cadaver prep room				
25						
26						

	Day 2	Specimen Preloading & Hydration				
27	**Day 2**	**Specimen Preloading & Hydration**				
28						
29		**Prepping for overnight preload**				
30		1. Remove specimen from freezer				
31		2. Thaw on bench for 2hrs				
32		3. Take geometric centre measurements to calculate offsets				
33						
34						
35		**1. Measure the total height of the FSU**				
36						
37		1. FSU height	1	2	3	Average
38		Height (mm)				0.00
39						
40		**2. Measure the height of the superior (top) vertebra**				
41						
42		Superior	1	2	3	Average
43		Height (mm)				0.00
44						
45		**3. Measure the height of the inferior (bottom) vertebra**				
46						
47		Inferior	1	2	3	Average
48		Height (mm)				0.00
49						
50		**4. Measure the height of the disc**				
51		Take three measuments at left lateral, right lateral and the center of the disc				
52						
53						
54		Disc	1	2	3	Average
55		Height (mm)				0.00
56						
57		**5. Calculate Z offset from the sum of specimen coupling plate, height of the top cup, superior vertebra and half the disc**				

58							
59	Height of specimen Coupling plate (mm)			24			
60							
61	Height of Top Cup (mm)			29			
62	Base top cup thickness	5					
63	Z-Offset (mm)	29.00			60.00		
64							
65	**6. Measure endplate dimensions using caliper**						
66							
67	**Superior**	**1**	**2**	**3**	**Average**		
68	AP_S (mm)				#DIV/0!	19.00	
69	LAT_S (mm)				#DIV/0!	26.00	
70							
71	**Inferior**	**1**	**2**	**3**	**Average**		
72	AP_I (mm)				#DIV/0!	19.00	
73	LAT _I (mm)				#DIV/0!	36.00	
74							
75	**Combined Superior/Inferior Avge Dimensions**			**Disc Area**		**mm²**	
76		**Avgerage (mm)**		0.84 x Avge_AP x Avge_ LAT		#DIV/0!	405.00
77	Avge_AP =	#DIV/0!					
78	Avge_LAT =	#DIV/0!					
79							
80							

81	
82	
83	**After Potting Base Cup**
84	
85	**7. Measure the X offset**
86	take this measurment once the specime has been potted in the bottom cup
87	measure from the center of the disc to the inside left edge of the cup
88	or the outside of the cup and subtract the width of the cup wall
89	
90	
91	
92	FRONT
93	
94	
95	
96	
97	

98	Cup edge thickness	12				
99	X-Offset	1	2	3	Average inner radius	
100	Outer radius (mm)				-12.00	44.00
101						
102	Inner Radius of Cup (mm)		45			
103						
104	X-Offset	-57.00	-0.50			
105						
106	**8. Measure the Y offset**					
107	take this measurment once the specime has been potted in the bottom cup					
108	measure from the center of the disc to the inside front edge of the cup or the outside of the cup and subtract the width of the cup wall					
109						
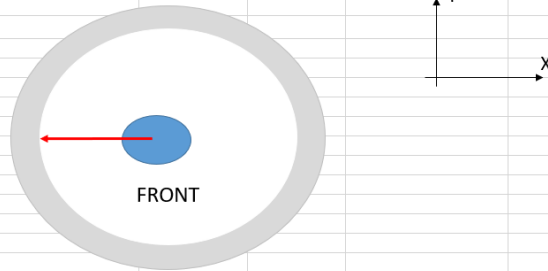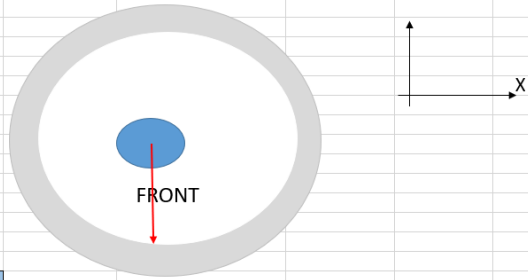
Cup edge thickness	12				
Y-Offset	1	2	3	Average	
Length (mm)				-12.00	33.00
Inner Radius of Cup (mm)		45			
Y-Offset (mm)	-57.00	-11.00			

9. Once potted, measure the height of the potted assembly

take one measurment and then rotate the assembly 90 degress, repeat anouther three times

	1	2	3	4
height (mm)				

10. Calculate testing parameters:

	Preload (N)	Follower (N)	Compression (N)
	0.1MPa	0.5MPa	0.6MPa
	(Area*0.1)/1.5	(Area*-0.5)/1.5	(Area*-0.6)/1.6
Compressive Loads	#DIV/0!	#DIV/0!	#DIV/0!

11. Take specimen photos

12. Preload outside of hexapod using weights

Preload weights	Start height	Start Time	End Height	End Time

13. Leave specimens in rig outside hexapod overnight

	Hexapod Setup						
USE HEXAPOD PROTOCOL							
6DOF TESTING							
File Names:				Tz (Start)			
				Tz (End)			
6DOF	Start Time	End Time					
SET POSTURE							
File Names:							
Offsets	X	Y	Z				
	-57.00	-57.00	29.00				
Load cell limits	Fx (N)	Fy(N)	Fz(N)	Mx(Nm)	My(Nm)	Mz(Nm)	
	6000	6000	17000	1000	1000	1000	
Angle							
Collecting Data							
Sample Rate	100						
Time	75						
FAIL BY SUDDEN OVERLOAD							
File Names:							
Ramp Velocity	6.67	mm/s					
Ramp Displacement	-3	mm					
Collecting Data							
Sample Rate	250	Hz					
Time	20	s					

	Hexapod Setup						
USE HEXAPOD PROTOCOL							
6DOF TESTING							
File Names:				Tz (Start)			
				Tz (End)			
6DOF	Start Time	End Time					
SET POSTURE							
File Names:							
Offsets	X	Y	Z				
	-57.00	-57.00	29.00				
Load cell limits	Fx (N)	Fy(N)	Fz(N)	Mx(Nm)	My(Nm)	Mz(Nm)	
	6000	6000	17000	1000	1000	1000	
Angle							
Collecting Data							
Sample Rate	100						
Time	75						
FAIL BY SUDDEN OVERLOAD							
File Names:							
Ramp Velocity	6.67	mm/s					
Ramp Displacement	-3	mm					
Collecting Data							
Sample Rate	250	Hz					
Time	20	s	The excel sheet adopted from prevouse students and emailed by Bethany Kamitakahara				

Figure A.1: FSU Measurements using Excel

Appendix B: Potting Protocol

Potting protocol

Preparing cups:

1   Clean the cups using alcohol (70% ethanol)

Figure B.1: Two Potting Cups

2   Clear tape to cover up the holes in the base of the cups.

3   Use clear tape to cover up the holes in the base of the cups.

Figure B.2: Two Bolts Screws into the Cups

4   Use masking tape for to cover the holes of the side screws.

5   Secure the three bolts so that they penetrate the masking tape and fixate the specimen.

6   Grease the side screws with Molybond.

Potting the two cups:

Figure B.3: Alignment Rig Used for Potting Specimen

1   Secure one cup to the alignment rig in such that rig and cup are aligned.

2   Screw in the bolts of the rig into the cup.

3   Place the specimen into the cup in such that the inferior vertebra in contact with the cup and the canal is at the centre of the cup.

4   Bolt the fixation screws and ensure they grip the vertebra and the specimen is positioned correctly.

5   Mix 100 ml of PMMA powder with 60 ml PMMA liquid (ratio of 1.7 powder to 1.0 liquid) in a container using utensil.

6   Stir until proper consistency is reached.

7   Pour the mixture into the cup.

8   Wait 15 to 20 minutes.

9   Measure the x and y offsets as outlined in Appendix A.

10 Unscrew the base plate of the rig from the alignment rig.

11 Unscrew the bottom cup from the base plate of the alignment rig.

12 Secure the prepared potting cup to the upper plate of the rig so that the superior vertebra is facing down.

13 Screw the base plate in the alignment rig.

14 Move the top cup down (sliding within the rig) until the superior vertebra facing down is in contact with the bottom cup.

15 Repeat steps d-h.

Appendix C: Results of Pilot Creation of Injuries

Specimen 1

Figure C.1: Superior View of Transversely Sectioned Specimen 1

Note: Radial tear into the left posterior portion and rim lesion into the right anterior of the disc.
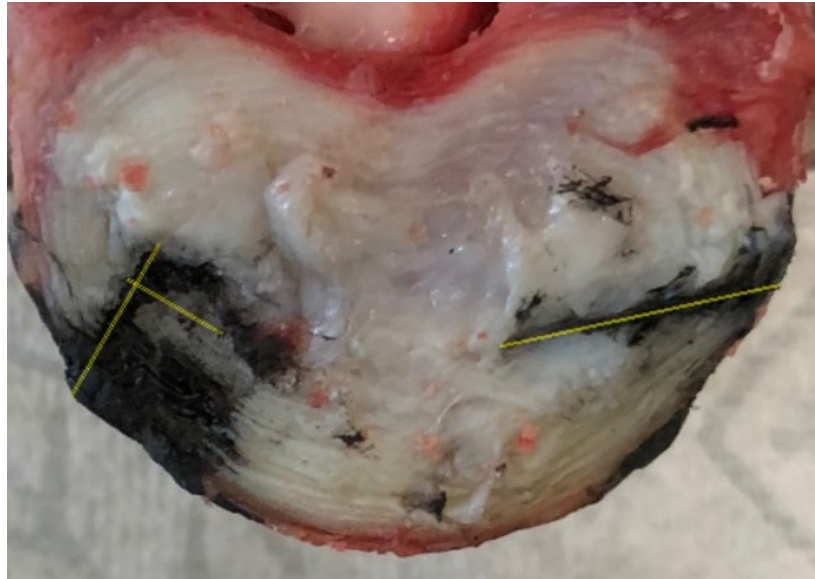
Figure C.2: The Outlined Depth and Width of Specimen 1 Injuries

Table C.1: Measurements of Specimen 1 Injuries

ID	Dimension	Interval 1	Interval 2	Interval 3	Mean	SD
Radial tear	depth	12.89	12.84	12.76	12.83	0.06557439
Rim Lesion	depth	8.05	7.98	8.01	8.0133	0.03511885
	width	4.97	4.99	5.01	4.99	0.02
	Area	40.009	39.82	40.13	39.987	0.15614174

Figure C.3: Superior View of Transversely Sectioned Specimen 2

Figure C.4: The Outlined Depth and Width of Specimen 2 Injuries

Table C.2: Measurements of Specimen 2 Injuries

Type	Dimension	Interval 1	Interval 2	Interval 3	Mean	SD
Radial tear	depth	12.28	13.07	12.78	12.71	0.39962482
Rim Lesion	depth	8.07	8.11	8.02	8.06666667	0.0450925
	width	5.24	5.15	5.21	5.2	0.04582576
	Area	42.287	41.767	41.784	41.9466667	0.29541839

S4

Figure C.5: Superior View of Transversely Sectioned Specimen 3

Figure C.6: The Outlined Depth and Width of Specimen 3 Injuries

Table C.3: Measurements of Specimen 3 Injuries

Type	Dimension	Interval 1	Interval 2	Interval 3	Mean	SD
Radial tear	depth	13.59	13.6	13.55	13.58	0.02645751
Rim Lesion	depth	8.3	8.33	8.17	8.26666667	0.08504901
	width	4.98	4.91	5.04	4.97666667	0.06506407
	Area	41.334	40.9	41.177	41.1404444	0.21956767

Figure C.7: Superior View of Transversely Sectioned Specimen 4
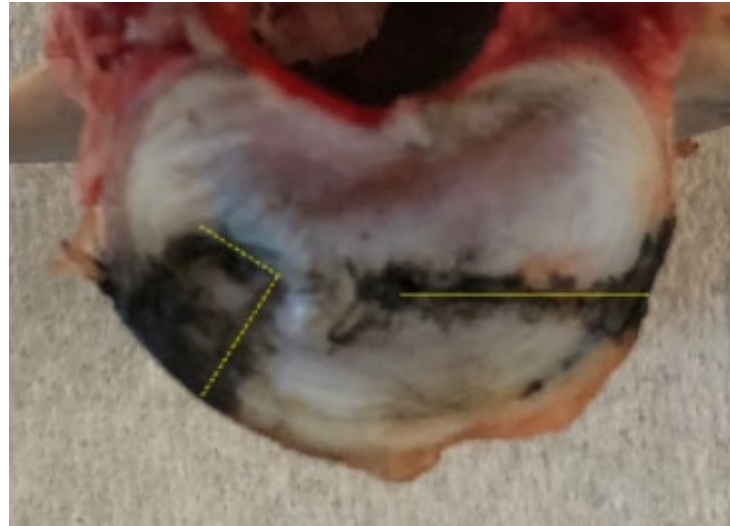
Figure C.8: The Outlined Depth and Width of Specimen 4 Injuries

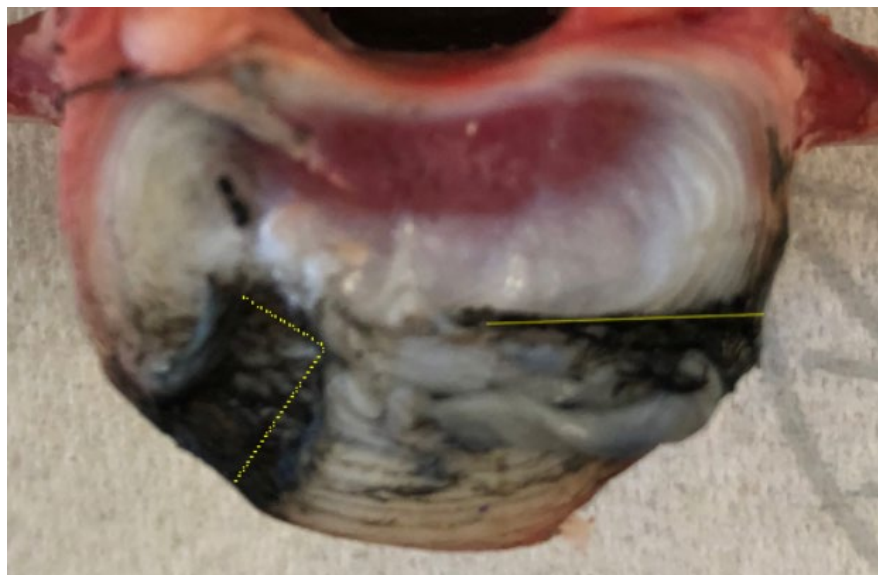**Table C.4: Measurements of Specimen 4 Injuries**

Type	Dimension	Interval 1	Interval 2	Interval 3	Mean	SD
Radial tear	depth	13.07	13.15	13.04	13.0866667	0.05686241
Rim Lesion	depth	7.97	8.01	8.02	8	0.02645751
	width	5.34	5.18	5.23	5.25	0.08185353
	Area	42.56	41.492	41.945	42	0.53605393

Table C.5: The Mean and Standard Deviation of All Specimens' Injuries

Type	Dimension	Specimen (Intervals Mean)				Mean	SD
		1	2	3	4		
Radial tear	depth	12.83	12.71	13.58	13.087	13.0516667	0.38567401
Rim Lesion	depth	8.0133	8.06666667	8.26666667	8	8.08665834	0.12341499
	width	4.99	5.2	4.97666667	5.25	5.10416667	0.14111658
	Area	39.98637	41.9466667	41.1404445	42	41.2756519	0.94079142

Appendix D: Protocol of the Creation of Injuries

For the creation of radial tear on the left lateral side of the disc

- While the FSU is set in the alignment rig determine the left lateral side of the disc and draw a line for it on the flat surface side of the bottom cup so that the line is parallel to the x axis and in a straight line with the centre of the disc.
- Measure and determine the disc midheight and set a ruler vertically and perpendicular to the disc and in alignment with the line drawn on the edge of the bottom cup.
- Position the blade holder horizontally on the levelled ruler.
- Hold the ruler still while constantly sliding the blade holder on the ruler towards the disc until full immersion of the radial tear blade is reached.

For the creation of rim lesion on the right anterior portion of the disc

- Using a protractor draw a line 45° from the y-axis of the disc on the flat surface side of the bottom cup towards the right anterior of the disc.
- Determine the edge between the superior vertebral rim and the disc and set a ruler vertically and perpendicular to it and in alignment with the line drawn on the edge of the bottom cup.
- Position the blade holder horizontally on the levelled ruler.
- Hold the ruler still while constantly sliding the blade holder on it towards the disc until full immersion of rim lesion blade is reached.
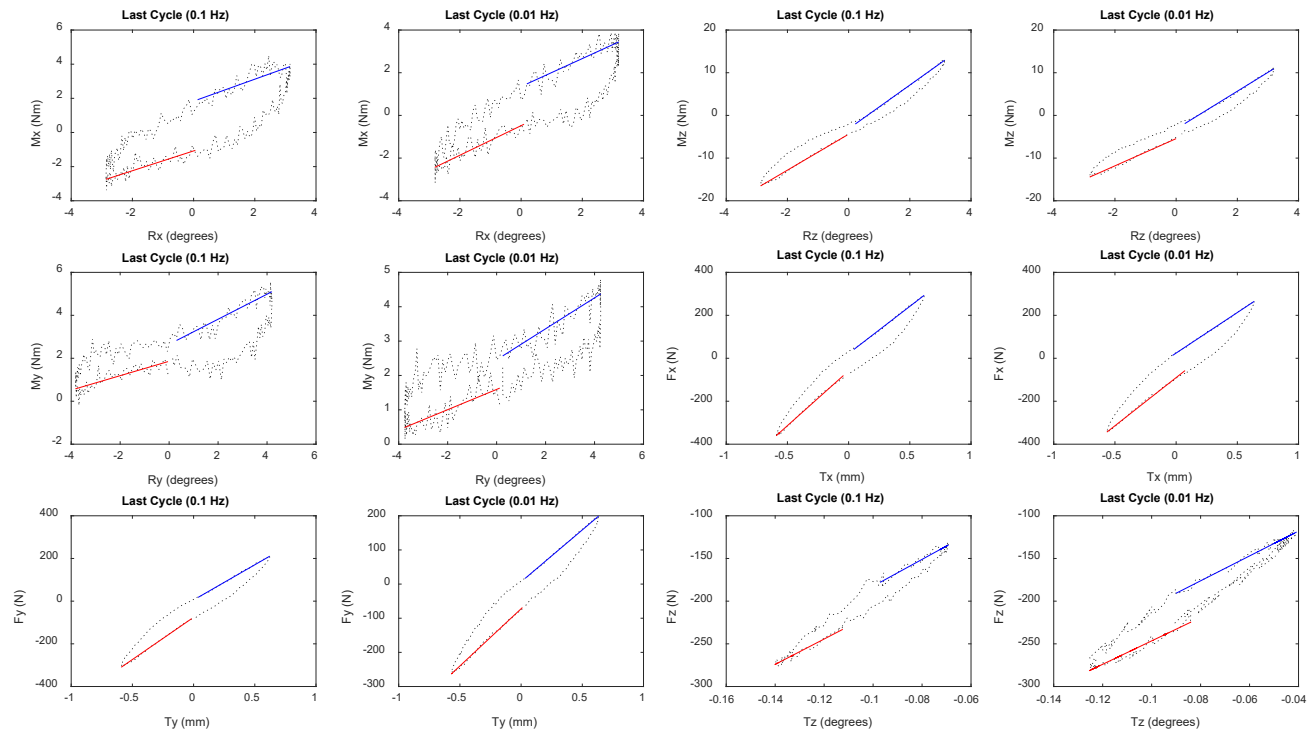
Appendix E: Specimen Results

Specimen 2 (Before Rim Lesion): T for translation, R for rotation, F for force, M for moment in/relative to x,y,z-axes

Last Cycles of the 6DOF Dynamic Test at 0.1 Hz and 0.01 Hz of

Specimen 2 (Before Rim Lesion): T for translation, R for rotation, F for force, M for moment in/relative to x,y,z-axes

Calculations of Stiffness and Phase Angle:

FileName	Test	Frequency	Stiffness_Positive_Direction	Stiffness_Negative_Direction	Phase
RLR02COB003Rx5E2	Rx	0.1	0.58083 Nm/degree	0.64294 Nm/degree	29.45625408
RLR02COB003Rx5E3	Rx	0.01	0.69262 Nm/degree	0.65489 Nm/degree	25.86914081
RLR02COB003Rz5E2	Rz	0.1	4.2133 Nm/degree	5.1194 Nm/degree	7.817216413
RLR02COB003Rz5E3	Rz	0.01	3.1896 Nm/degree	4.419 Nm/degree	8.759515879
RLR02COB004Ry5E2	Ry	0.1	0.33542 Nm/degree	0.5829 Nm/degree	33.57016821
RLR02COB004Ry5E3	Ry	0.01	0.29477 Nm/degree	0.45058 Nm/degree	31.31573751
RLR02COB6E1Tx5E2	Tx	0.1	510.1134 N/mm	438.9374 N/mm	10.32135594
RLR02COB6E1Tx5E3	Tx	0.01	448.6499 N/mm	377.4934 N/mm	12.32287843
RLR02COB6E1Ty5E2	Ty	0.1	395.9175 N/mm	329.8929 N/mm	11.07891251
RLR02COB6E1Ty5E3	Ty	0.01	335.1295 N/mm	303.9171 N/mm	11.55420964
RLR02CON153Tz1E1M	Tz	0.1	1485.7228 N/mm	1570.4896 N/mm	11.40513601
RLR02CON153Tz1E2M	Tz	0.01	1370.9133 N/mm	1457.3348 N/mm	14.09314677

Specimen 2 (After Rim Lesion): T for translation, R for rotation, F for force, M for moment in/relative to x,y,z-axes
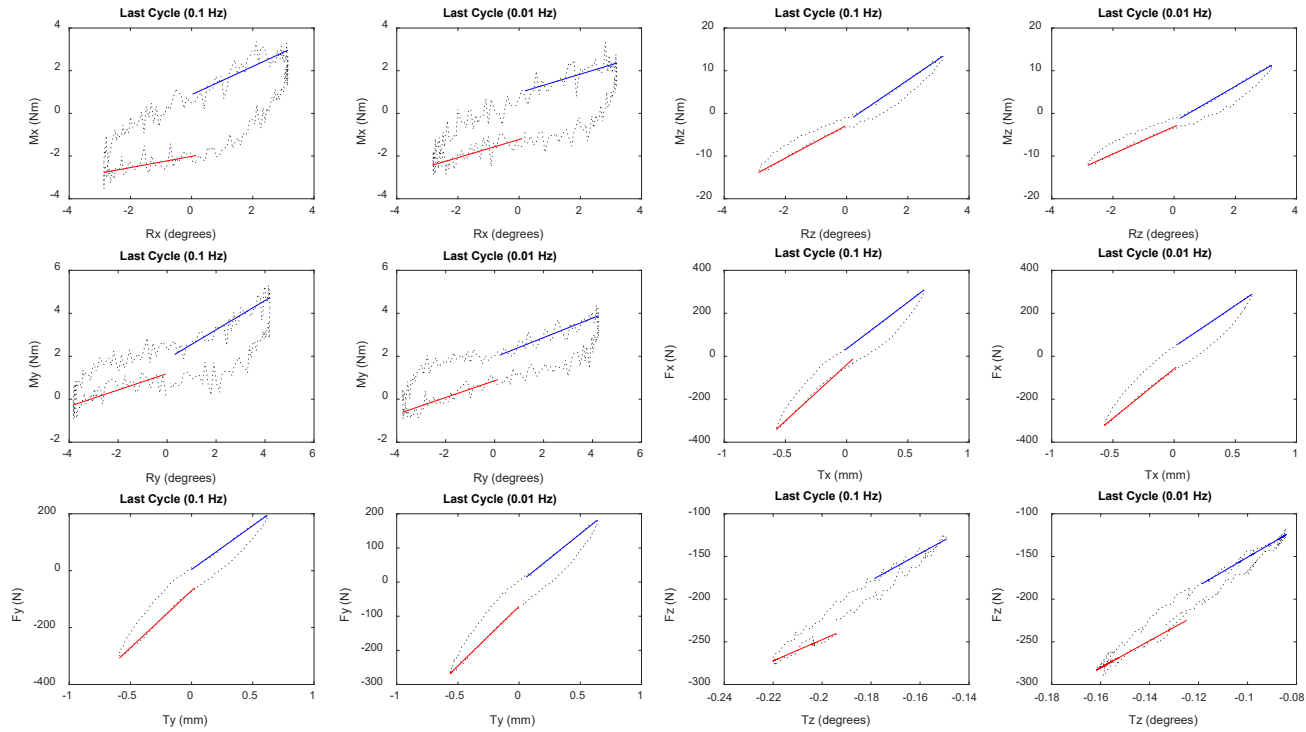
Last Cycles of the 6DOF Dynamic Test at 0.1 Hz and 0.01 Hz:

Specimen 2 (After Rim Lesion): T for translation, R for rotation, F for force, M for moment in/relative to x,y,z-axes

Calculations of Stiffness and Phase Angle

FileName	Test	Frequency	Stiffness_Positive_Direction	Stiffness_Negative_Direction	Phase
RLR02INB003Rx5E2	Rx	0.1	0.26385 Nm/degree	0.66155 Nm/degree	37.59500019
RLR02INB003Rx5E3	Rx	0.01	0.42583 Nm/degree	0.43309 Nm/degree	34.27326789
RLR02INB003Rz5E2	Rz	0.1	3.8406 Nm/degree	4.8818 Nm/degree	7.977571744
RLR02INB003Rz5E3	Rz	0.01	3.2082 Nm/degree	4.1562 Nm/degree	9.115578529
RLR02INB004Ry5E2	Ry	0.1	0.38096 Nm/degree	0.68107 Nm/degree	30.62023098
RLR02INB004Ry5E3	Ry	0.01	0.3893 Nm/degree	0.45466 Nm/degree	30.88999094
RLR02INB6E1Tx5E2	Tx	0.1	522.9661 N/mm	432.6337 N/mm	9.880759499
RLR02INB6E1Tx5E3	Tx	0.01	461.0897 N/mm	385.0889 N/mm	11.48712724
RLR02INB6E1Ty5E2	Ty	0.1	401.4571 N/mm	308.1555 N/mm	10.80082495
RLR02INB6E1Ty5E3	Ty	0.01	349.1145 N/mm	287.6879 N/mm	10.87604755
RLR02INN153Tz1E1M	Tz	0.1	1241.7345 N/mm	1570.0745 N/mm	13.29909207
RLR02INN153Tz1E2M	Tz	0.01	1579.3251 N/mm	1672.0336 N/mm	13.2525355

Failure Under Sudden Overload

Fz at fail = 12435.699

Specimen 4 (Before Rim Lesion): T for translation, R for rotation, F for force, M for moment in/relative to x,y,z-axes

Last Cycles of the 6DOF Dynamic Test at 0.1 Hz and 0.01 Hz:

Specimen 4 (before Rim Lesion): T for translation, R for rotation, F for force, M for moment in/relative to x,y,z-axes
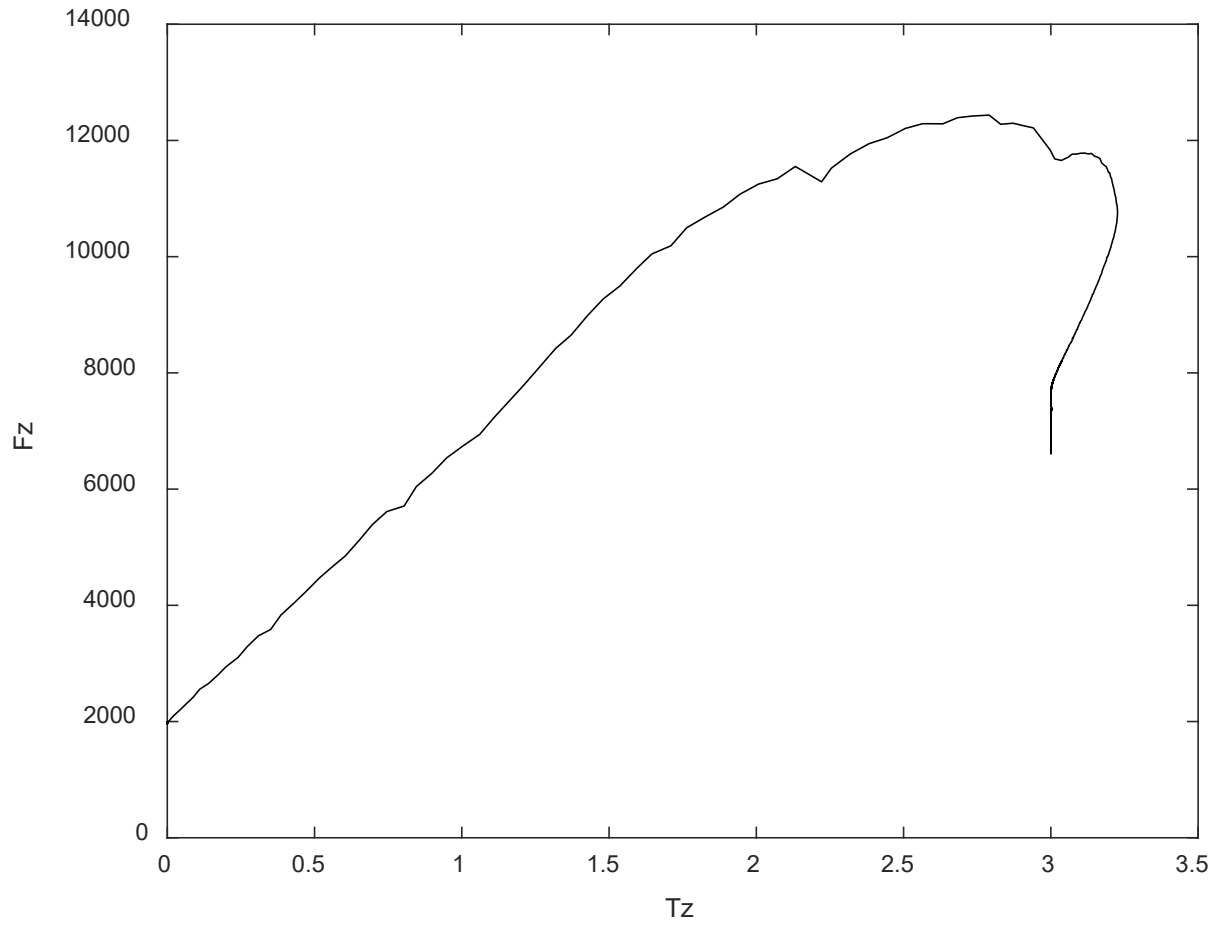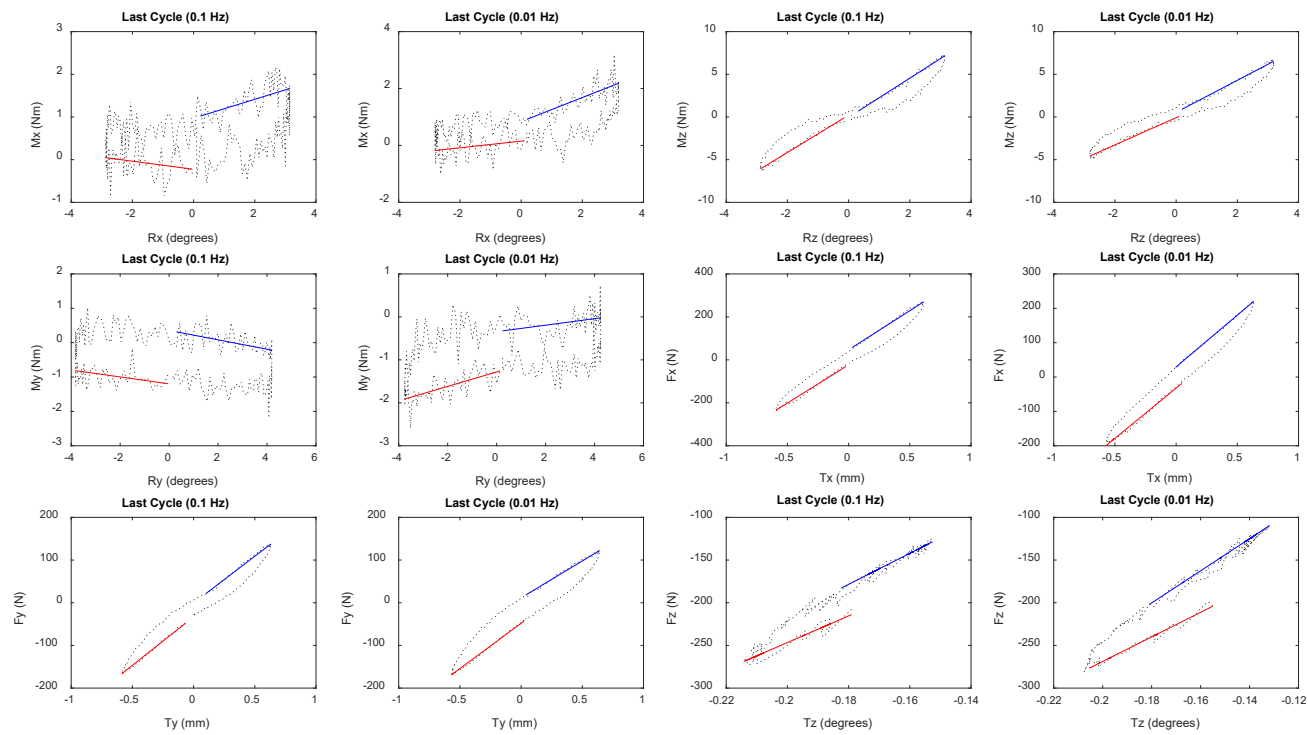
Calculations of Stiffness and Phase Angle:

FileName	Test	Frequency	Stiffness_Positive_Direction	Stiffness_Negative_Direction	Phase
RLR04COB003Rx5E2	Rx	0.1	-0.094723 Nm/degree	0.22169 Nm/degree	59.30222935
RLR04COB003Rx5E3	Rx	0.01	0.11719 Nm/degree	0.42295 Nm/degree	49.51870399
RLR04COB003Rz5E2	Rz	0.1	2.1871 Nm/degree	2.2918 Nm/degree	11.34435786
RLR04COB003Rz5E3	Rz	0.01	1.5962 Nm/degree	1.8768 Nm/degree	11.89037405
RLR04COB004Ry5E2	Ry	0.1	-0.1005 Nm/degree	-0.1365 Nm/degree	104.7044574
RLR04COB004Ry5E3	Ry	0.01	0.16808 Nm/degree	0.075502 Nm/degree	65.01658618
RLR04COB6E1Tx5E2	Tx	0.1	356.4106 N/mm	364.3585 N/mm	10.17327483
RLR04COB6E1Tx5E3	Tx	0.01	292.1861 N/mm	301.3394 N/mm	9.522172945
RLR04COB6E1Ty5E2	Ty	0.1	227.1367 N/mm	218.8102 N/mm	10.08433693
RLR04COB6E1Ty5E3	Ty	0.01	212.0878 N/mm	172.9153 N/mm	14.33298488
RLR04CON151Tz1E1M	Tz	0.1	1559.368 N/mm	1816.2417 N/mm	10.41625349
RLR04CON151Tz1E2M	Tz	0.01	1438.8234 N/mm	1882.0713 N/mm	11.17785551

Specimen 4 (After Rim Lesion): T for translation, R for rotation, F for force, M for moment in/relative to x,y,z-axes

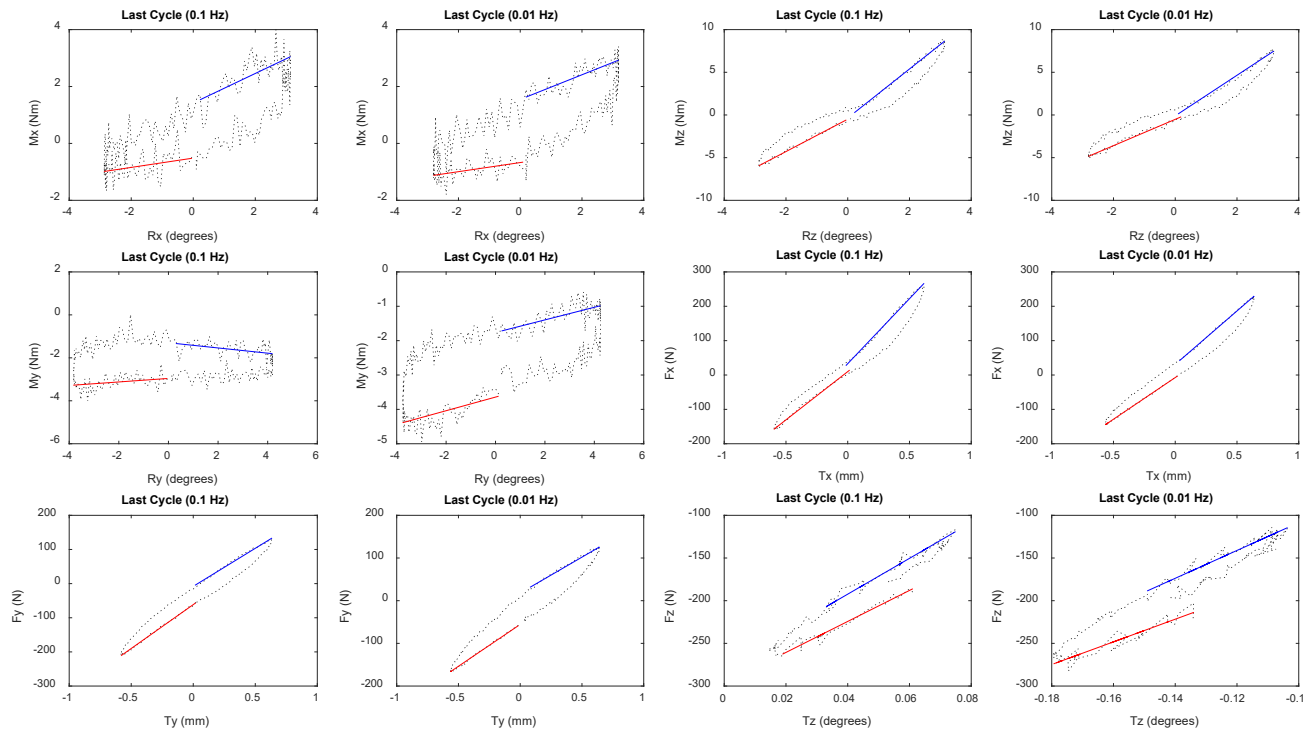Last Cycles of the 6DOF Dynamic Test at 0.1 Hz and 0.01 Hz:

Specimen 4 (After Rim Lesion): T for translation, R for rotation, F for force, M for moment in/relative to x,y,z-axes

Calculations of Stiffness and Phase Angle

FileName	Test	Frequency	Stiffness_Positive_Direction	Stiffness_Negative_Direction	Phase
RLR04INB003Rx5E2	Rx	0.1	0.16365 Nm/degree	0.51905 Nm/degree	32.96991536
RLR04INB003Rx5E3	Rx	0.01	0.16019 Nm/degree	0.43316 Nm/degree	34.39010871
RLR04INB003Rz5E2	Rz	0.1	1.8963 Nm/degree	2.8693 Nm/degree	9.15304418
RLR04INB003Rz5E3	Rz	0.01	1.541 Nm/degree	2.3767 Nm/degree	10.1548086
RLR04INB004Ry5E2	Ry	0.1	0.082224 Nm/degree	-0.12145 Nm/degree	83.92880487
RLR04INB004Ry5E3	Ry	0.01	0.19834 Nm/degree	0.18349 Nm/degree	59.10272362
RLR04INB6E1Tx5E2	Tx	0.1	280.7055 N/mm	378.2715 N/mm	10.43374956
RLR04INB6E1Tx5E3	Tx	0.01	242.5457 N/mm	311.064 N/mm	8.794871031
RLR04INB6E1Ty5E2	Ty	0.1	257.0262 N/mm	222.8289 N/mm	10.19087418
RLR04INB6E1Ty5E3	Ty	0.01	196.2221 N/mm	168.0671 N/mm	13.46342335
RLR04INN151Tz1E1M	Tz	0.1	1815.6521 N/mm	2096.8616 N/mm	10.88384505
RLR04INN151Tz1E2M	Tz	0.01	1327.385 N/mm	1631.1538 N/mm	15.88846624

Failure Under Sudden Overload:

Fz at fail = 7744.9369

Specimen 6 (Before Rim Lesion): T for translation, R for rotation, F for force, M for moment in/relative to x,y,z-axes

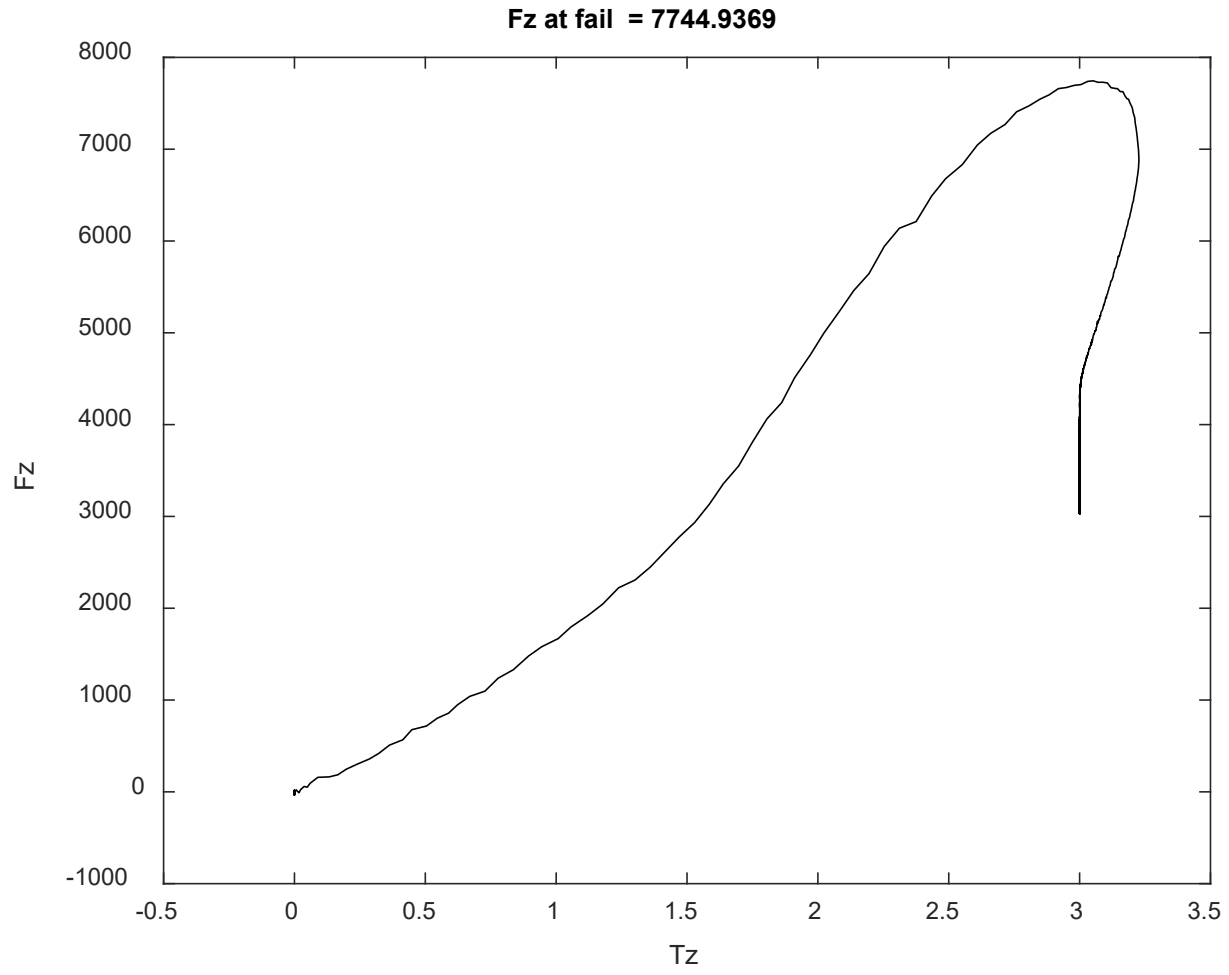Last Cycles of the 6DOF Dynamic Test at 0.1 Hz and 0.01 Hz:

Specimen 6 (Before Rim Lesion): T for translation, R for rotation, F for force, M for moment in/relative to x,y,z-axes
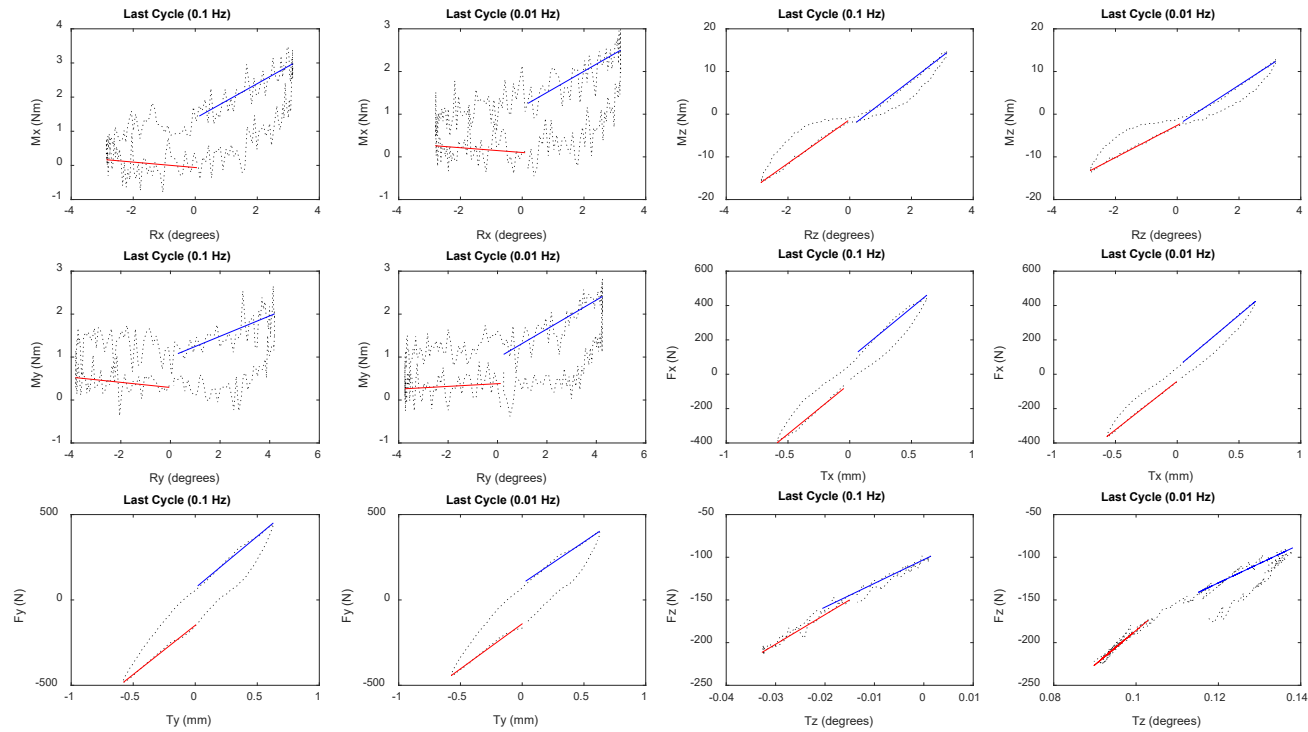
Calculations of Stiffness and Phase Angle:

FileName	Test	Frequency	Stiffness_Positive_Direction	Stiffness_Negative_Direction	Phase
RLR06COB003Rx5E2	Rx	0.1	-0.079646 Nm/degree	0.50781 Nm/degree	35.3144796
RLR06COB003Rx5E3	Rx	0.01	-0.055739 Nm/degree	0.41496 Nm/degree	45.37254848
RLR06COB003Rz5E2	Rz	0.1	5.1317 Nm/degree	5.5665 Nm/degree	8.733860819
RLR06COB003Rz5E3	Rz	0.01	3.7681 Nm/degree	4.694 Nm/degree	9.698866952
RLR06COB004Ry5E2	Ry	0.1	-0.06001 Nm/degree	0.23744 Nm/degree	60.00330805
RLR06COB004Ry5E3	Ry	0.01	0.031534 Nm/degree	0.33706 Nm/degree	49.35013701
RLR06COB6E1Tx5E2	Tx	0.1	586.3235 N/mm	591.3068 N/mm	10.80052163
RLR06COB6E1Tx5E3	Tx	0.01	565.6825 N/mm	604.5819 N/mm	8.449077584
RLR06COB6E1Ty5E2	Ty	0.1	576.1741 N/mm	604.8206 N/mm	12.53728234
RLR06COB6E1Ty5E3	Ty	0.01	527.6501 N/mm	488.234 N/mm	14.94183862
RLR06CON116Tz1E1M	Tz	0.1	3468.1677 N/mm	2786.4779 N/mm	5.219306378
RLR06CON116Tz1E2M	Tz	0.01	4031.9759 N/mm	2272.3071 N/mm	9.087765599

Specimen 6 (After Rim Lesion): T for translation, R for rotation, F for force, M for moment in/relative to x,y,z-axes

Last Cycles of the 6DOF Dynamic Test at 0.1 Hz and 0.01 Hz:

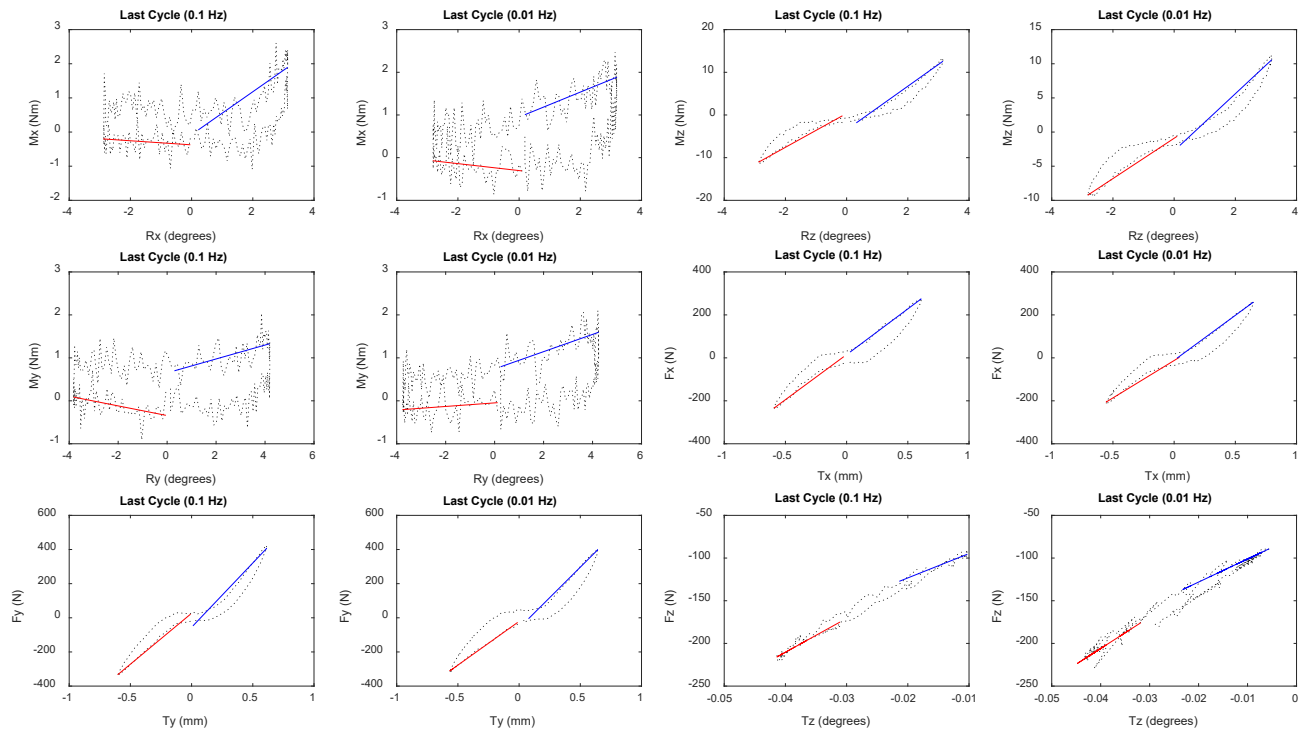Specimen 6 (After Rim Lesion): T for translation, R for rotation, F for force, M for moment in/relative to x,y,z-axes

Calculations of Stiffness and Phase Angle:

FileName	Test	Frequency	Stiffness_Positive_Direction	Stiffness_Negative_Direction	Phase
RLR06INB003Rx5E2	Rx	0.1	-0.059925 Nm/degree	0.62742 Nm/degree	46.35640085
RLR06INB003Rx5E3	Rx	0.01	-0.081429 Nm/degree	0.29258 Nm/degree	55.83437224
RLR06INB003Rz5E2	Rz	0.1	3.968 Nm/degree	5.1005 Nm/degree	7.815667487
RLR06INB003Rz5E3	Rz	0.01	2.9521 Nm/degree	4.1776 Nm/degree	8.874179165
RLR06INB004Ry5E2	Ry	0.1	-0.11262 Nm/degree	0.16194 Nm/degree	67.06995014
RLR06INB004Ry5E3	Ry	0.01	0.04157 Nm/degree	0.20075 Nm/degree	59.97982362
RLR06INB6E1Tx5E2	Tx	0.1	420.3307 N/mm	426.2483 N/mm	12.70653269
RLR06INB6E1Tx5E3	Tx	0.01	348.1856 N/mm	418.6372 N/mm	10.59777706
RLR06INB6E1Ty5E2	Ty	0.1	596.3947 N/mm	753.3363 N/mm	7.321145683
RLR06INB6E1Ty5E3	Ty	0.01	512.2175 N/mm	714.0755 N/mm	11.09301065
RLR06INN116Tz1E1M	Tz	0.1	3967.699 N/mm	2854.2822 N/mm	6.085494134
RLR06INN116Tz1E2M	Tz	0.01	3678.1385 N/mm	2705.7049 N/mm	6.606518902

Failure Under Sudden Overload:

Fz at fail = 13141.525

Specimen 8 (Before Rim Lesion): T for translation, R for rotation, F for force, M for moment in/relative to x,y,z-axes

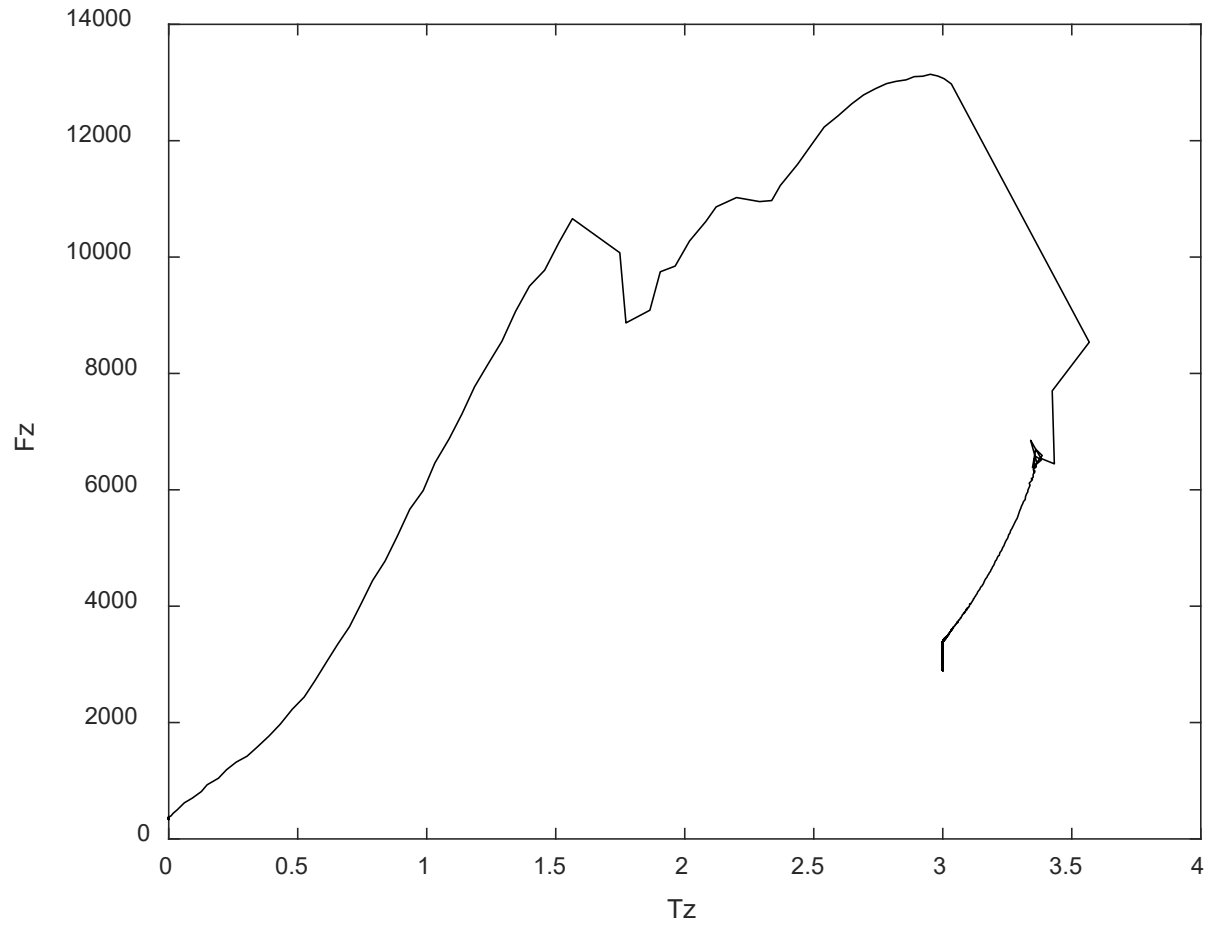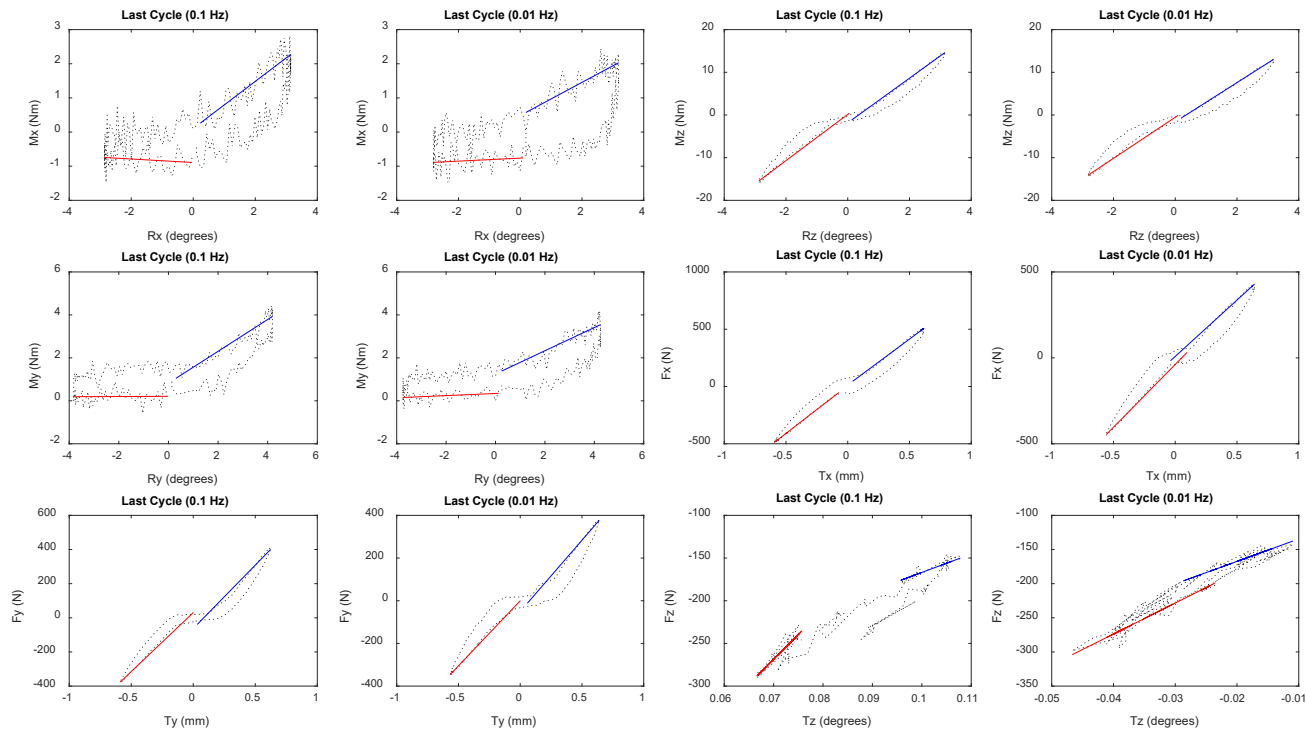Last Cycles of the 6DOF Dynamic Test at 0.1 Hz and 0.01 Hz:

Specimen 8 (Before Rim Lesion): T for translation, R for rotation, F for force, M for moment in/relative to x,y,z-axes

Calculations of Stiffness and Phase Angle:

FileName	Test	Frequency	Stiffness_Positive_Direction	Stiffness_Negative_Direction	Phase
RLR08COB003Rx5E2	Rx	0.1	-0.051635 Nm/degree	0.68911 Nm/degree	36.25119087
RLR08COB003Rx5E3	Rx	0.01	0.044597 Nm/degree	0.4852 Nm/degree	39.11801463
RLR08COB003Rz5E2	Rz	0.1	5.4174 Nm/degree	5.2316 Nm/degree	6.303918796
RLR08COB003Rz5E3	Rz	0.01	4.8094 Nm/degree	4.6003 Nm/degree	7.614618037
RLR08COB004Ry5E2	Ry	0.1	0.0040682 Nm/degree	0.74098 Nm/degree	30.69943942
RLR08COB004Ry5E3	Ry	0.01	0.050069 Nm/degree	0.54052 Nm/degree	32.91782209
RLR08COB6E1Tx5E2	Tx	0.1	832.9934 N/mm	801.7531 N/mm	8.96190212
RLR08COB6E1Tx5E3	Tx	0.01	730.7229 N/mm	655.5625 N/mm	8.766544579
RLR08COB6E1Ty5E2	Ty	0.1	690.9549 N/mm	742.8312 N/mm	6.746963617
RLR08COB6E1Ty5E3	Ty	0.01	608.8814 N/mm	667.9082 N/mm	9.340081322
RLR08CON120Tz1E1M	Tz	0.1	5805.2299 N/mm	2153.5926 N/mm	7.476592323
RLR08CON120Tz1E2M	Tz	0.01	4535.1589 N/mm	3291.4227 N/mm	8.830387385

Specimen 8 (After Rim Lesion): T for translation, R for rotation, F for force, M for moment in/relative to x,y,z-axes

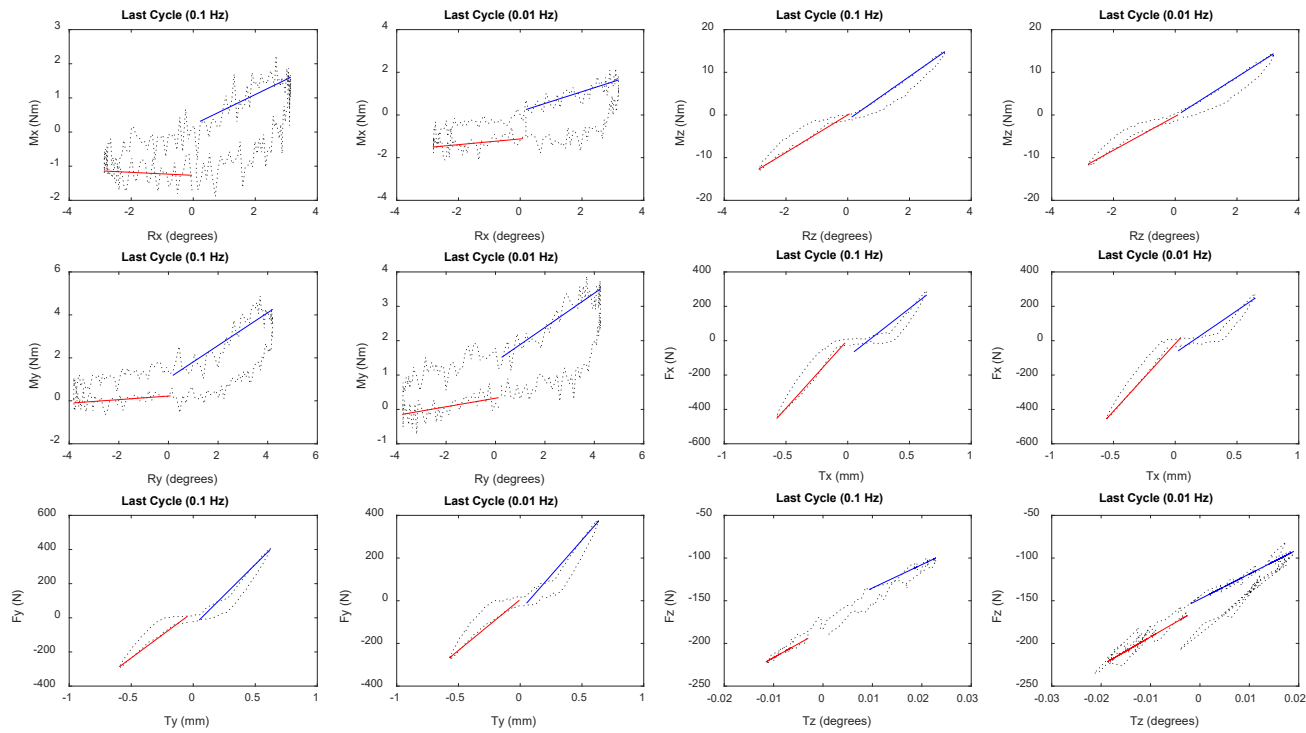Last Cycles of the 6DOF Dynamic Test at 0.1 Hz and 0.01 Hz:

Specimen 8 (After Rim Lesion): T for translation, R for rotation, F for force, M for moment in/relative to x,y,z-axes

Calculations of Stiffness and Phase Angle:

FileName	Test	Frequency	Stiffness_Positive_Direction	Stiffness_Negative_Direction	Phase
RLR08INB003Rx5E2	Rx	0.1	-0.043781 Nm/degree	0.44134 Nm/degree	75.41774164
RLR08INB003Rx5E3	Rx	0.01	0.13422 Nm/degree	0.46177 Nm/degree	41.41452241
RLR08INB003Rz5E2	Rz	0.1	4.4015 Nm/degree	5.0798 Nm/degree	7.595842491
RLR08INB003Rz5E3	Rz	0.01	3.9676 Nm/degree	4.6035 Nm/degree	8.088808586
RLR08INB004Ry5E2	Ry	0.1	0.083142 Nm/degree	0.76351 Nm/degree	35.74115504
RLR08INB004Ry5E3	Ry	0.01	0.12436 Nm/degree	0.49781 Nm/degree	36.68177008
RLR08INB6E1Tx5E2	Tx	0.1	796.1799 N/mm	561.7638 N/mm	7.607788693
RLR08INB6E1Tx5E3	Tx	0.01	786.5755 N/mm	492.6402 N/mm	6.553026291
RLR08INB6E1Ty5E2	Ty	0.1	538.4505 N/mm	721.8809 N/mm	8.262677033
RLR08INB6E1Ty5E3	Ty	0.01	476.6371 N/mm	659.269 N/mm	8.816119974
RLR08INN120Tz1E1M	Tz	0.1	3230.9798 N/mm	2735.3472 N/mm	5.415072708
RLR08INN120Tz1E2M	Tz	0.01	3342.6875 N/mm	2936.9667 N/mm	9.90675499

Failure Under Sudden Overload:

Fz at fail = 9111.9049

Specimen 10 (Before Rim Lesion): T for translation, R for rotation, F for force, M for moment in/relative to x,y,z-axes

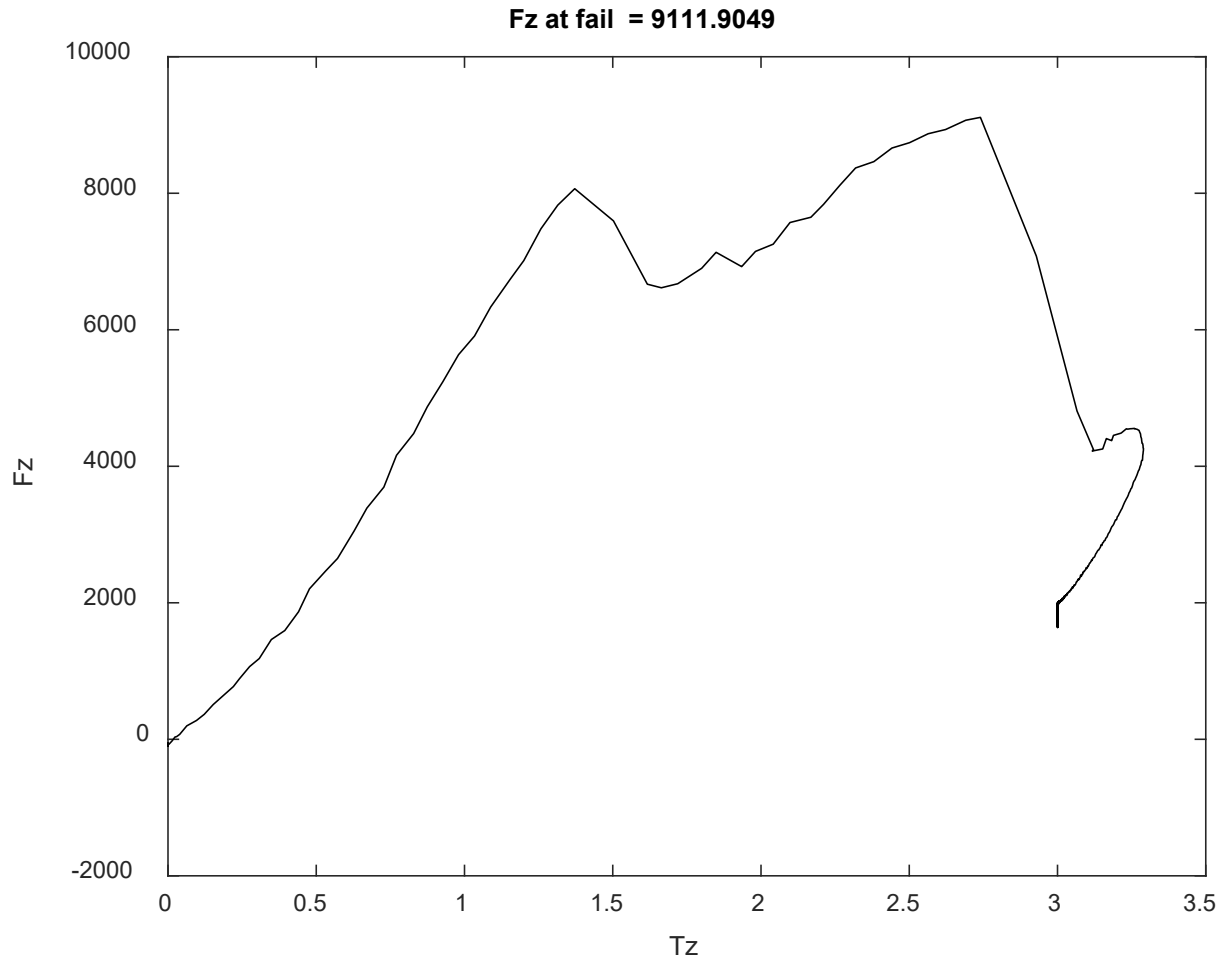Last Cycles of the 6DOF Dynamic Test at 0.1 Hz and 0.01 Hz:

Specimen 10 (Before Rim Lesion): T for translation, R for rotation, F for force, M for moment in/relative to x,y,z-axes

Calculations of Stiffness and Phase Angle:

FileName	Test	Frequency	Stiffness_Positive_Direction	Stiffness_Negative_Direction	Phase
RLR10COB003Rx5E2	Rx	0.1	-0.016819 Nm/degree	0.74429 Nm/degree	32.27447161
RLR10COB003Rx5E3	Rx	0.01	0.091186 Nm/degree	0.70383 Nm/degree	33.18658959
RLR10COB003Rz5E2	Rz	0.1	6.5872 Nm/degree	5.7016 Nm/degree	7.057554887
RLR10COB003Rz5E3	Rz	0.01	5.5254 Nm/degree	4.9891 Nm/degree	7.690731081
RLR10COB004Ry5E2	Ry	0.1	0.082287 Nm/degree	0.40756 Nm/degree	47.73592197
RLR10COB004Ry5E3	Ry	0.01	0.088986 Nm/degree	0.16397 Nm/degree	48.13071907
RLR10COB6E1Tx5E2	Tx	0.1	772.0027 N/mm	611.8778 N/mm	7.526848597
RLR10COB6E1Tx5E3	Tx	0.01	435.1135 N/mm	441.4843 N/mm	7.150385901
RLR10COB6E1Ty5E2	Ty	0.1	622.7963 N/mm	679.5931 N/mm	8.263192787
RLR10COB6E1Ty5E3	Ty	0.01	553.1518 N/mm	576.1927 N/mm	10.63419228
RLR10CON167Tz1E1M	Tz	0.1	3391.9778 N/mm	3086.6114 N/mm	11.73218227
RLR10CON167Tz1E2M	Tz	0.01	2034.5949 N/mm	1662.9931 N/mm	19.25641931

Specimen 10 (After Rim Lesion): T for translation, R for rotation, F for force, M for moment in/relative to x,y,z-axes

Last Cycles of the 6DOF Dynamic Test at 0.1 Hz and 0.01 Hz:
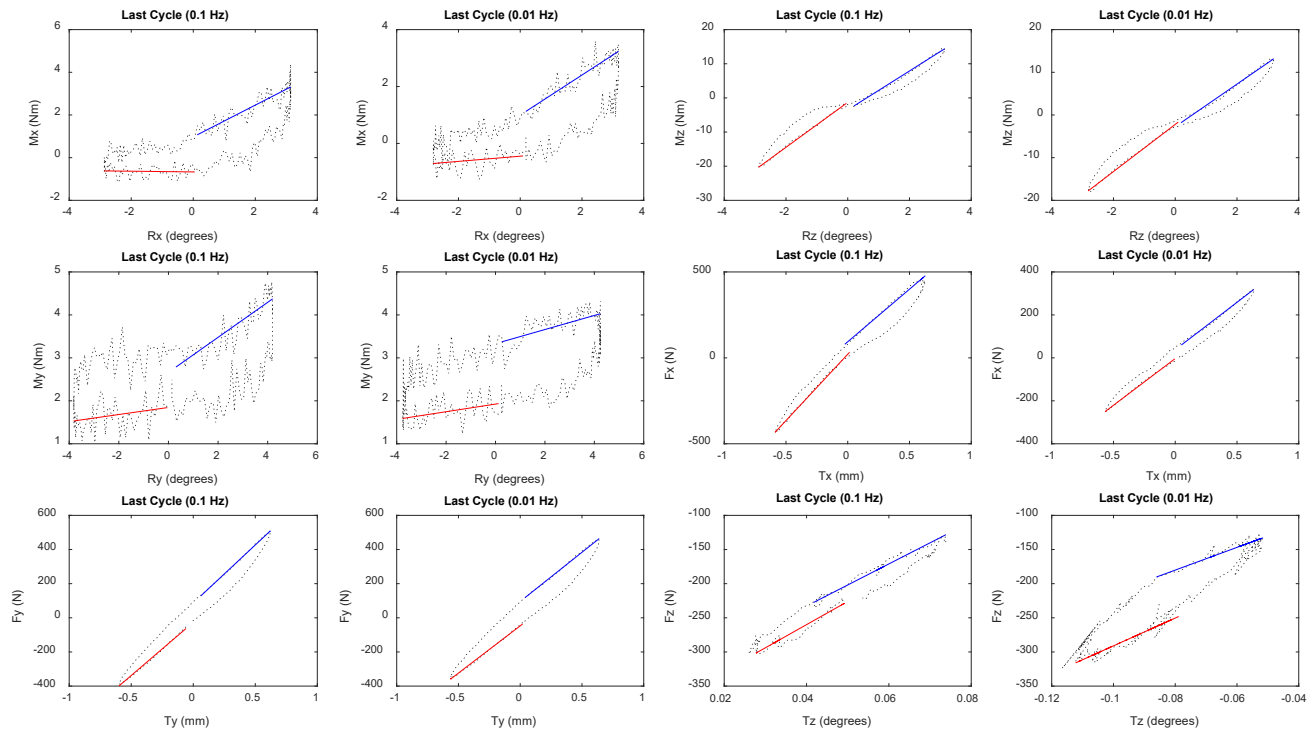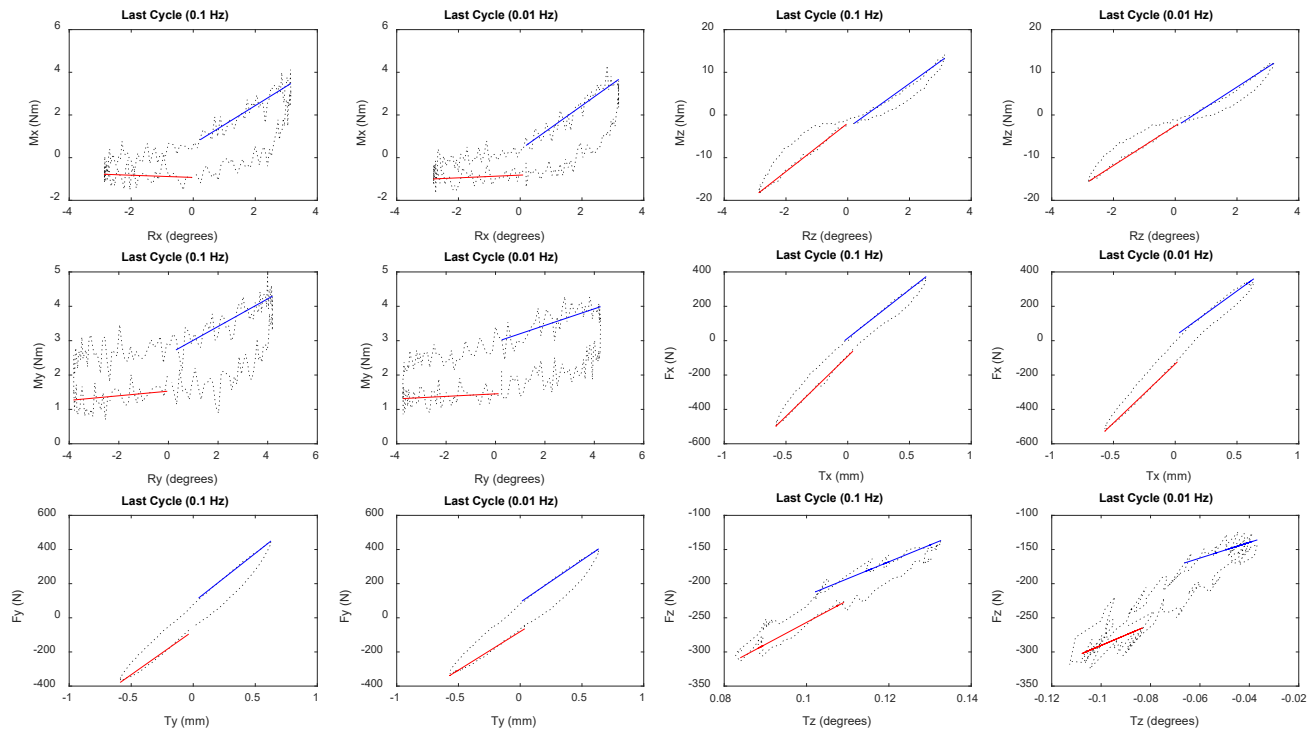
Specimen 10 (After Rim Lesion): T for translation, R for rotation, F for force, M for moment in/relative to x,y,z-axes

Calculations of Stiffness and Phase Angle:

FileName	Test	Frequency	Stiffness_Positive_Direction	Stiffness_Negative_Direction	Phase
RLR10INB003Rx5E2	Rx	0.1	-0.051763 Nm/degree	0.90057 Nm/degree	31.4248328
RLR10INB003Rx5E3	Rx	0.01	0.063438 Nm/degree	1.0321 Nm/degree	29.2996392
RLR10INB003Rz5E2	Rz	0.1	5.6643 Nm/degree	5.2058 Nm/degree	7.702672828
RLR10INB003Rz5E3	Rz	0.01	4.643 Nm/degree	4.6764 Nm/degree	7.815860301
RLR10INB004Ry5E2	Ry	0.1	0.066878 Nm/degree	0.40217 Nm/degree	45.45786513
RLR10INB004Ry5E3	Ry	0.01	0.036554 Nm/degree	0.24144 Nm/degree	50.1271815
RLR10INB6E1Tx5E2	Tx	0.1	699.9604 N/mm	564.3345 N/mm	8.18946407
RLR10INB6E1Tx5E3	Tx	0.01	687.0011 N/mm	521.1777 N/mm	8.241223421
RLR10INB6E1Ty5E2	Ty	0.1	512.8535 N/mm	572.9067 N/mm	10.5772406
RLR10INB6E1Ty5E3	Ty	0.01	450.8935 N/mm	493.049 N/mm	12.70966243
RLR10INN167Tz1E1M	Tz	0.1	3222.9394 N/mm	2465.8738 N/mm	16.64181615
RLR10INN167Tz1E2M	Tz	0.01	1532.0048 N/mm	1145.99 N/mm	22.43904869

Failure Under Sudden Overload:

Fz at fail = 15782.929

Specimen 12 (Before Rim Lesion): T for translation, R for rotation, F for force, M for moment in/relative to x,y,z-axes

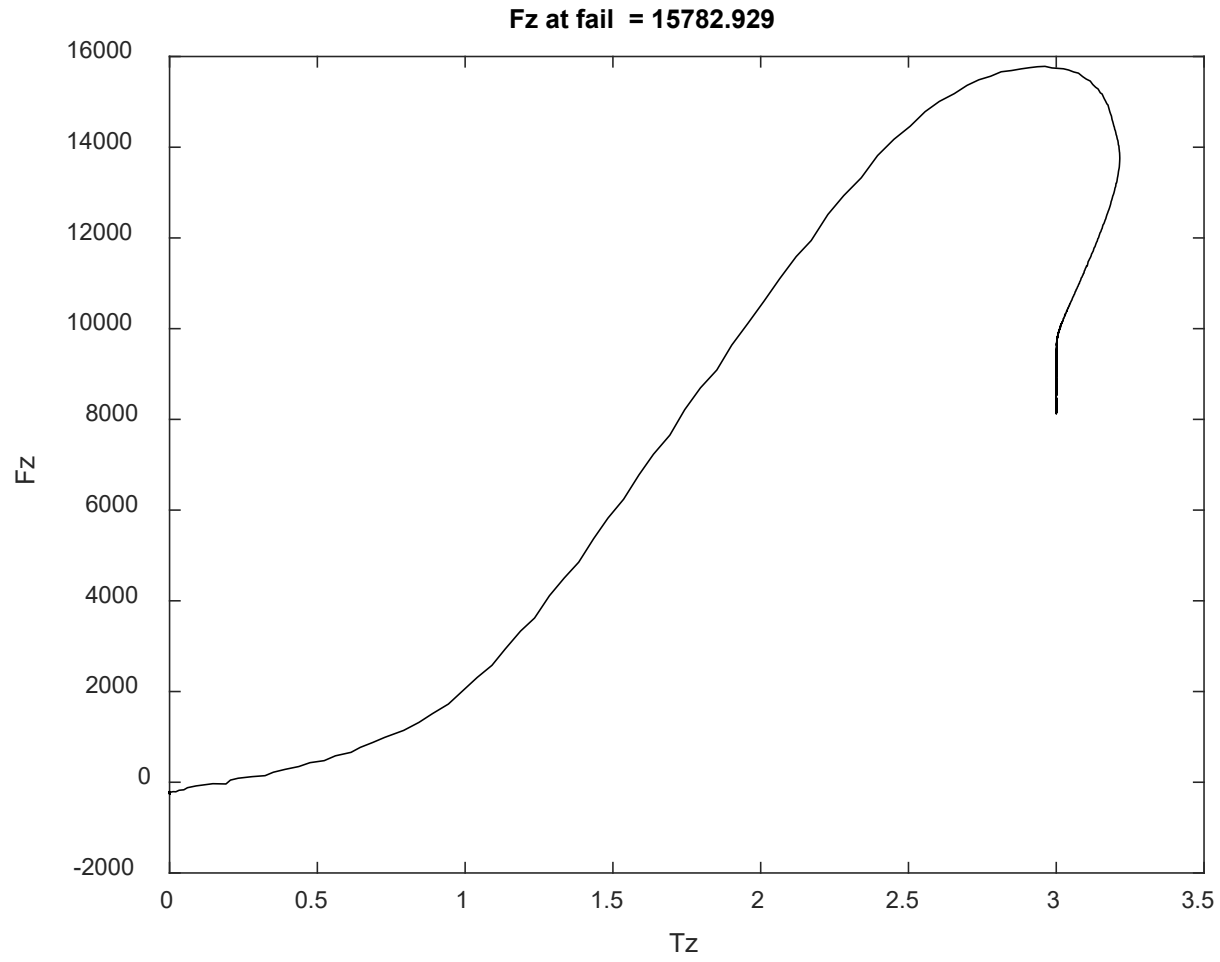Last Cycles of the 6DOF Dynamic Test at 0.1 Hz and 0.01 Hz:

Specimen 12 (Before Rim Lesion): T for translation, R for rotation, F for force, M for moment in/relative to x,y,z-axes

Calculations of Stiffness and Phase Angle:

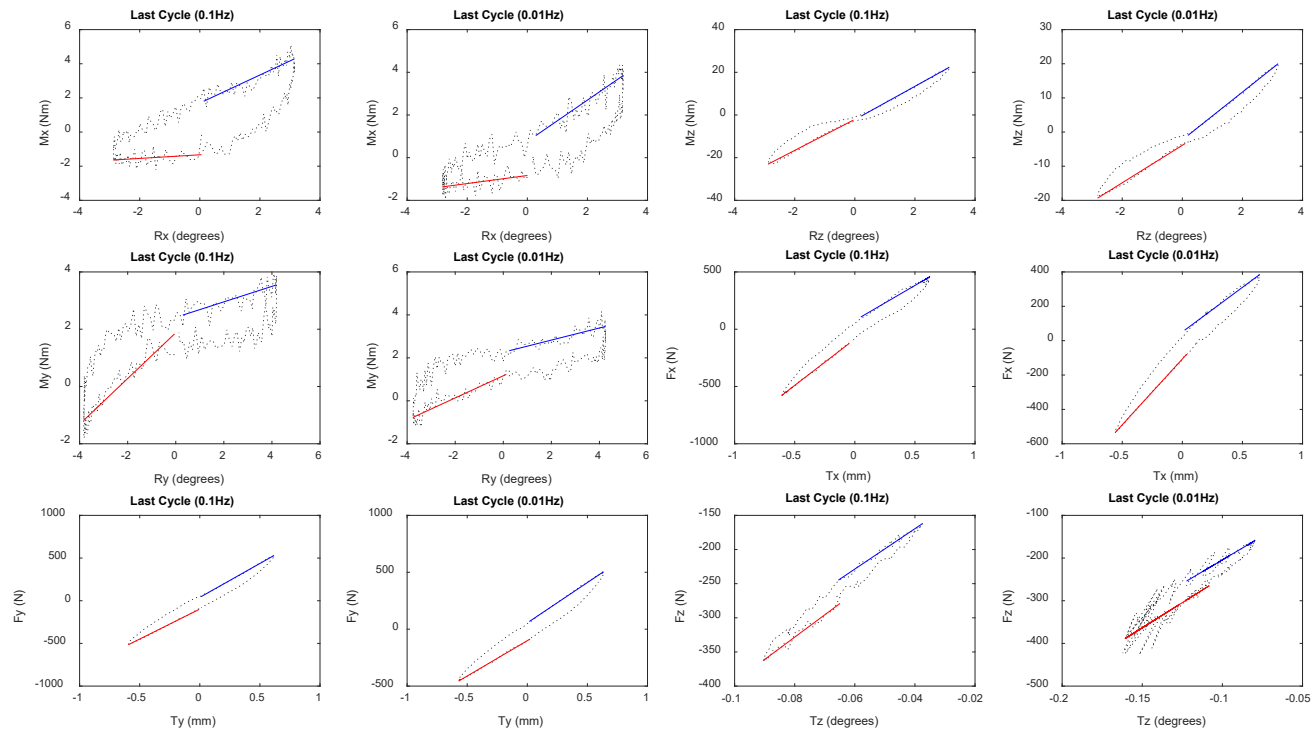| FileName	Test	Frequency	Stiffness_Positive_Direction	Stiffness_Negative_Direction	Phase
RLR12COB003Rx5E2	Rx	0.1	0.10657 Nm/degree	0.82263 Nm/degree	34.98054105
RLR12COB003Rx5E3	Rx	0.01	0.18909 Nm/degree	0.96787 Nm/degree	29.82377659
RLR12COB003Rz5E2	Rz	0.1	7.2683 Nm/degree	7.796 Nm/degree	8.002767641
RLR12COB003Rz5E3	Rz	0.01	5.4855 Nm/degree	6.9978 Nm/degree	8.724875711
RLR12COB004Ry5E2	Ry	0.1	0.79862 Nm/degree	0.27053 Nm/degree	29.37992068
RLR12COB004Ry5E3	Ry	0.01	0.51565 Nm/degree	0.28218 Nm/degree	32.23880351
RLR12COB6E1Tx5E2	Tx	0.1	807.7318 N/mm	611.4685 N/mm	8.762305684
RLR12COB6E1Tx5E3	Tx	0.01	765.6542 N/mm	519.038 N/mm	8.603922263
RLR12COB6E1Ty5E2	Ty	0.1	702.2501 N/mm	795.0321 N/mm	8.323643405
RLR12COB6E1Ty5E3	Ty	0.01	620.8792 N/mm	708.7975 N/mm	9.969293844
RLR12CON197Tz1E1M	Tz	0.1	3270.8791 N/mm	2957.1272 N/mm	8.167894413
RLR12CON197Tz1E2M	Tz	0.01	2355.6773 N/mm	2221.3501 N/mm	16.57916557

Specimen 12 (After Rim Lesion): T for translation, R for rotation, F for force, M for moment in/relative to x,y,z-axes

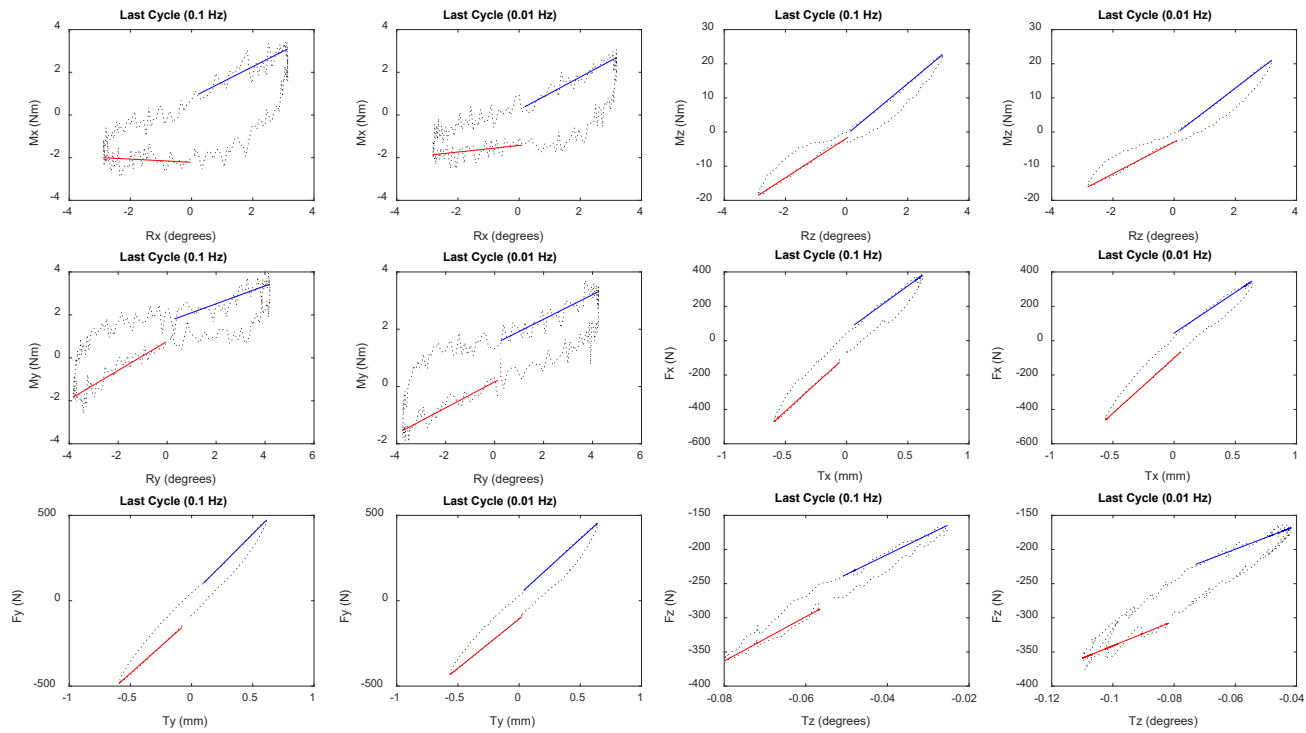Last Cycles of the 6DOF Dynamic Test at 0.1 Hz and 0.01 Hz:

Specimen 12 (After Rim Lesion): T for translation, R for rotation, F for force, M for moment in/relative to x,y,z-axes

Calculations of Stiffness and Phase Angle:

FileName	Test	Frequency	Stiffness_Positive_Direction	Stiffness_Negative_Direction	Phase
RLR12INB003Rx5E2	Rx	0.1	-0.073616 Nm/degree	0.72817 Nm/degree	41.0183991
RLR12INB003Rx5E3	Rx	0.01	0.15287 Nm/degree	0.76962 Nm/degree	37.42910104
RLR12INB003Rz5E2	Rz	0.1	5.8001 Nm/degree	7.4557 Nm/degree	8.710124176
RLR12INB003Rz5E3	Rz	0.01	4.6618 Nm/degree	6.8626 Nm/degree	9.111992444
RLR12INB004Ry5E2	Ry	0.1	0.67608 Nm/degree	0.41659 Nm/degree	28.74148348
RLR12INB004Ry5E3	Ry	0.01	0.4523 Nm/degree	0.42902 Nm/degree	30.27075369
RLR12INB6E1Tx5E2	Tx	0.1	646.5334 N/mm	519.5792 N/mm	9.244002649
RLR12INB6E1Tx5E3	Tx	0.01	644.1816 N/mm	475.0152 N/mm	9.134242965
RLR12INB6E1Ty5E2	Ty	0.1	637.1918 N/mm	718.8269 N/mm	8.322881231
RLR12INB6E1Ty5E3	Ty	0.01	578.7743 N/mm	652.0216 N/mm	9.743073863
RLR12INN197Tz1E1M	Tz	0.1	3246.1246 N/mm	2905.1629 N/mm	10.16068738
RLR12INN197Tz1E2M	Tz	0.01	1818.1355 N/mm	1714.033 N/mm	18.71321133

Failure Under Sudden Overload:

Fz at fail = 15750.4

Specimen 14 (Before Rim Lesion): T for translation, R for rotation, F for force, M for moment in/relative to x,y,z-axes

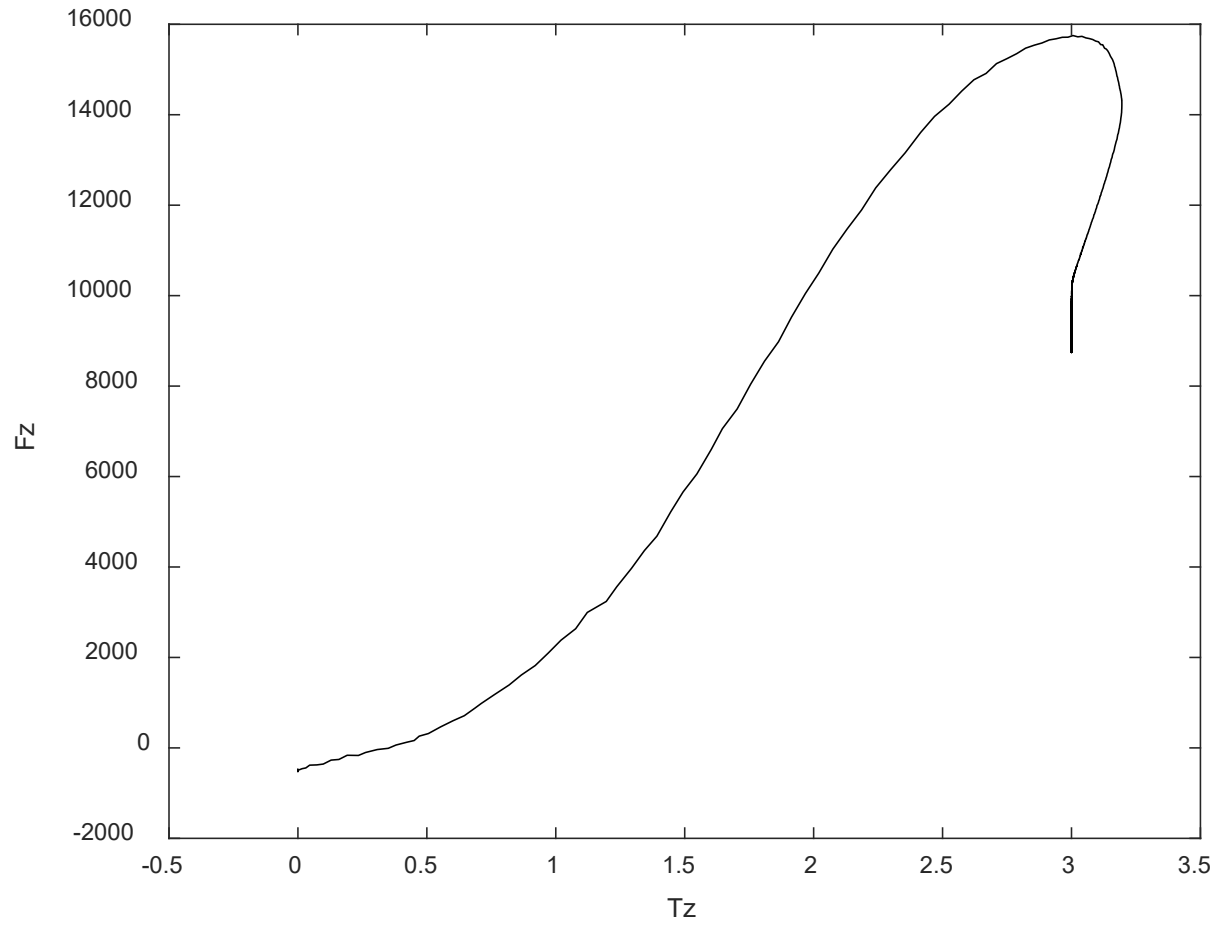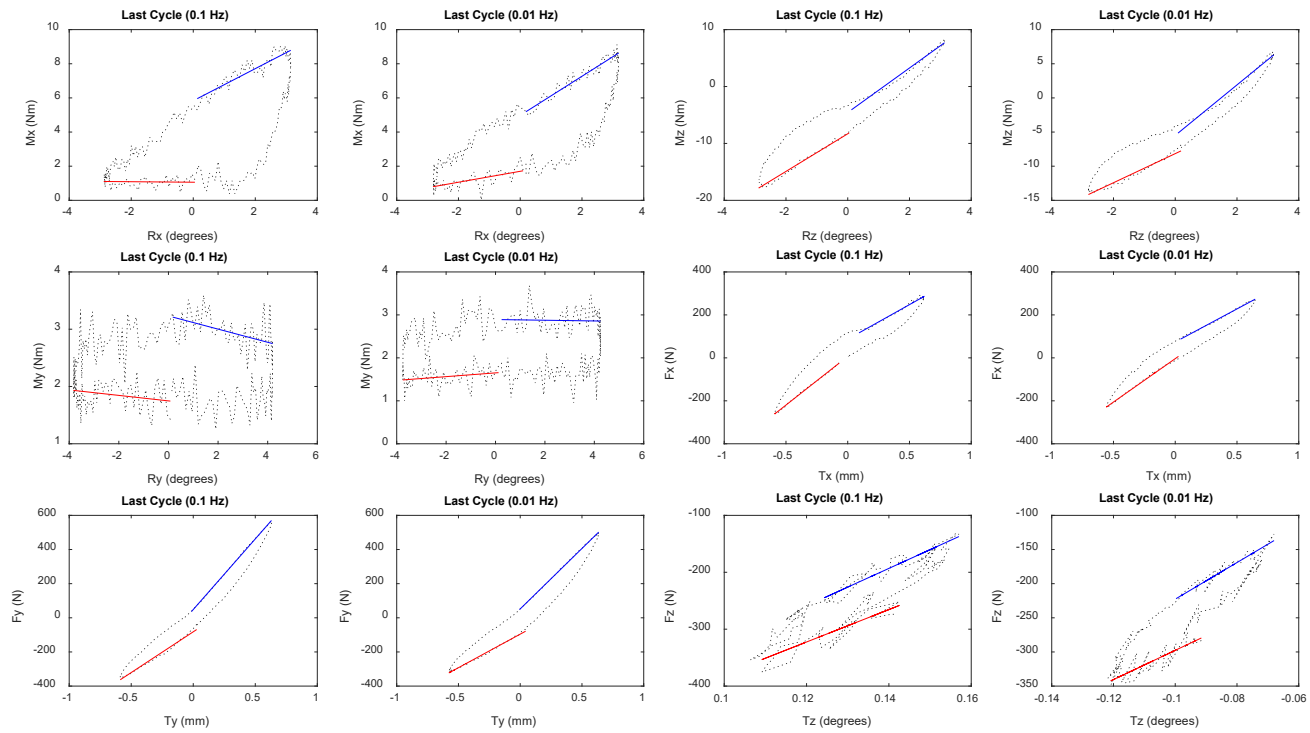Last Cycles of the 6DOF Dynamic Test at 0.1 Hz and 0.01 Hz:

Specimen 14 (Before Rim Lesion): T for translation, R for rotation, F for force, M for moment in/relative to x,y,z-axes

Calculations of Stiffness and Phase Angle:

FileName	Test	Frequency	Stiffness_Positive_Direction	Stiffness_Negative_Direction	Phase
RLR14COB003Rx5E2	Rx	0.1	-0.015055 Nm/degree	0.93996 Nm/degree	38.51551052
RLR14COB003Rx5E3	Rx	0.01	0.32016 Nm/degree	1.1449 Nm/degree	33.18558617
RLR14COB003Rz5E2	Rz	0.1	3.3071 Nm/degree	3.9098 Nm/degree	12.68919865
RLR14COB003Rz5E3	Rz	0.01	2.1303 Nm/degree	3.6972 Nm/degree	11.88804095
RLR14COB004Ry5E2	Ry	0.1	-0.047896 Nm/degree	-0.11488 Nm/degree	82.71373792
RLR14COB004Ry5E3	Ry	0.01	0.043676 Nm/degree	-0.0082119 Nm/degree	81.23642839
RLR14COB6E1Tx5E2	Tx	0.1	453.2725 N/mm	322.0564 N/mm	10.08629303
RLR14COB6E1Tx5E3	Tx	0.01	403.975 N/mm	307.9953 N/mm	10.72120341
RLR14COB6E1Ty5E2	Ty	0.1	477.3658 N/mm	827.1964 N/mm	8.696092256
RLR14COB6E1Ty5E3	Ty	0.01	393.1257 N/mm	708.0979 N/mm	10.88661505
RLR14CON188Tz1E1M	Tz	0.1	2849.7132 N/mm	3289.529 N/mm	23.89886502
RLR14CON188Tz1E2M	Tz	0.01	2139.1119 N/mm	2680.7562 N/mm	22.1573186

Specimen 14 (After Rim Lesion): T for translation, R for rotation, F for force, M for moment in/relative to x,y,z-axes

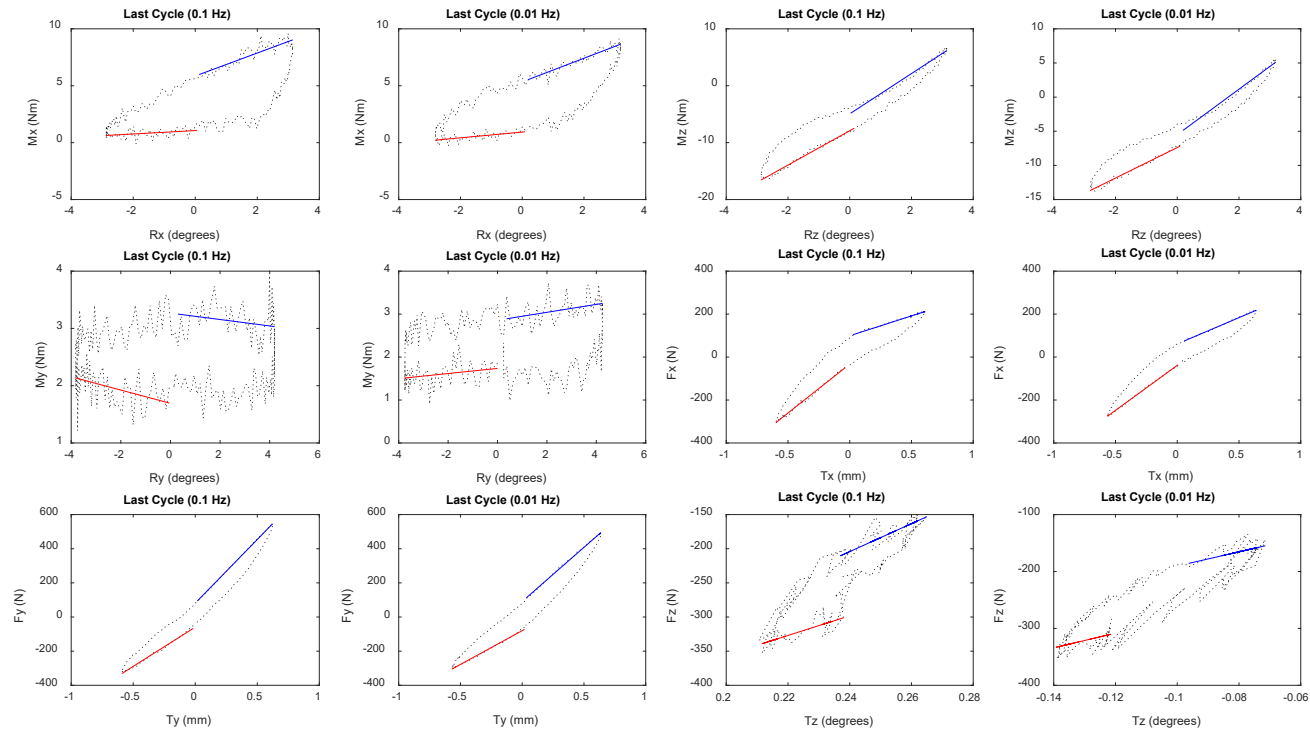Last Cycles of the 6DOF Dynamic Test at 0.1 Hz and 0.01 Hz:

Specimen 14 (After Rim Lesion): T for translation, R for rotation, F for force, M for moment in/relative to x,y,z-axes

Calculations of Stiffness and Phase Angle:

FileName	Test	Frequency	Stiffness_Positive_Direction	Stiffness_Negative_Direction	Phase
RLR14INB003Rx5E2	Rx	0.1	0.14949 Nm/degree	1.0101 Nm/degree	39.90758704
RLR14INB003Rx5E3	Rx	0.01	0.25278 Nm/degree	1.0393 Nm/degree	33.64064341
RLR14INB003Rz5E2	Rz	0.1	3.0172 Nm/degree	3.5386 Nm/degree	12.51293571
RLR14INB003Rz5E3	Rz	0.01	2.2333 Nm/degree	3.3284 Nm/degree	11.58918161
RLR14INB004Ry5E2	Ry	0.1	-0.11573 Nm/degree	-0.055935 Nm/degree	80.58108547
RLR14INB004Ry5E3	Ry	0.01	0.059292 Nm/degree	0.092109 Nm/degree	75.31276137
RLR14INB6E1Tx5E2	Tx	0.1	455.3864 N/mm	185.033 N/mm	13.70958105
RLR14INB6E1Tx5E3	Tx	0.01	419.2638 N/mm	244.8922 N/mm	12.15767506
RLR14INB6E1Ty5E2	Ty	0.1	459.6647 N/mm	745.877 N/mm	8.951046896
RLR14INB6E1Ty5E3	Ty	0.01	396.2192 N/mm	633.1242 N/mm	10.93770644
RLR14INN188Tz1E1M	Tz	0.1	1437.7871 N/mm	2047.3769 N/mm	29.3856257
RLR14INN188Tz1E2M	Tz	0.01	1285.1221 N/mm	1251.6812 N/mm	24.02603428

Failure Under Sudden Overload:

Fz at fail = 11806.218

Specimen 16 (Before Rim Lesion): T for translation, R for rotation, F for force, M for moment in/relative to x,y,z-axes

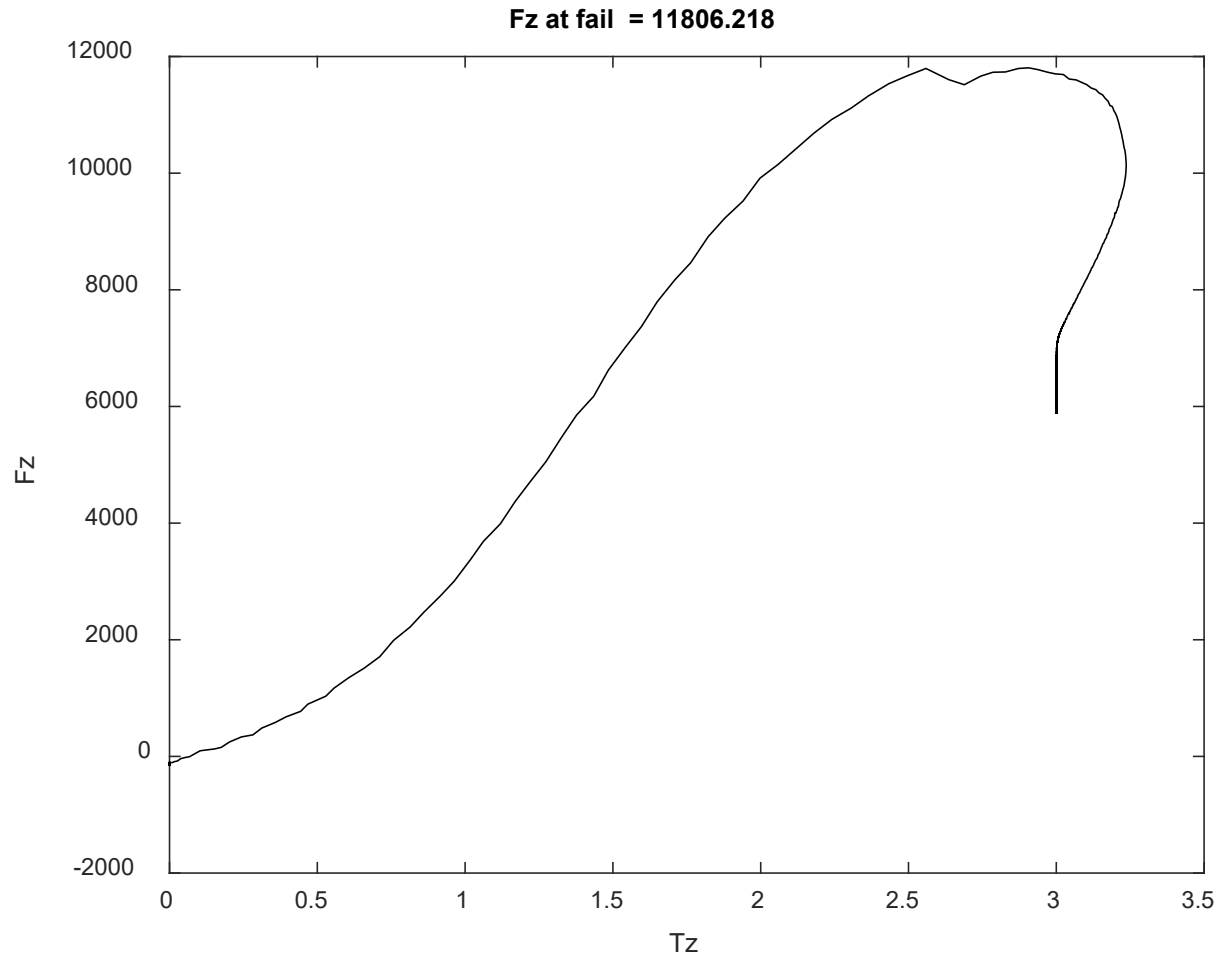Last Cycles of the 6DOF Dynamic Test at 0.1 Hz and 0.01 Hz:

Specimen 16 (Before Rim Lesion): T for translation, R for rotation, F for force, M for moment in/relative to x,y,z-axes

Calculations of Stiffness and Phase Angle:

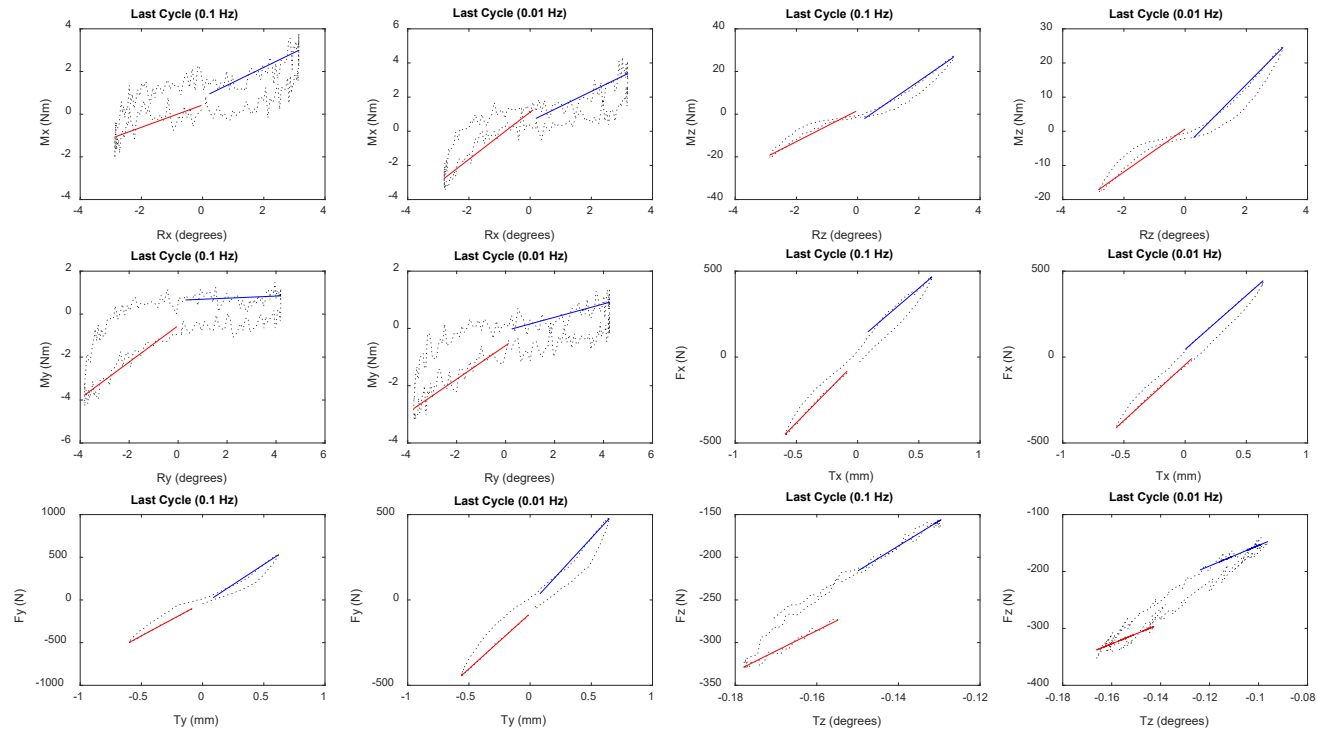| FileName	Test	Frequency	Stiffness_Positive_Direction	Stiffness_Negative_Direction	Phase
RLR16COB003Rx5E2	Rx	0.1	0.52279 Nm/degree	0.69985 Nm/degree	30.53831627
RLR16COB003Rx5E3	Rx	0.01	1.382 Nm/degree	0.87485 Nm/degree	25.1890629
RLR16COB003Rz5E2	Rz	0.1	7.2923 Nm/degree	9.8789 Nm/degree	5.393961112
RLR16COB003Rz5E3	Rz	0.01	6.2874 Nm/degree	9.0437 Nm/degree	6.267448406
RLR16COB004Ry5E2	Ry	0.1	0.84562 Nm/degree	0.049177 Nm/degree	35.22157667
RLR16COB004Ry5E3	Ry	0.01	0.58617 Nm/degree	0.23282 Nm/degree	31.27378882
RLR16COB6E1Tx5E2	Tx	0.1	725.2557 N/mm	610.717 N/mm	6.478647854
RLR16COB6E1Tx5E3	Tx	0.01	650.3483 N/mm	627.2228 N/mm	6.546921796
RLR16COB6E1Ty5E2	Ty	0.1	771.4362 N/mm	939.8582 N/mm	6.898166426
RLR16COB6E1Ty5E3	Ty	0.01	648.3255 N/mm	779.0588 N/mm	8.742491796
RLR16CON182Tz1E1M	Tz	0.1	2387.5663 N/mm	2939.9247 N/mm	7.114487471
RLR16CON182Tz1E2M	Tz	0.01	1754.2043 N/mm	1804.0989 N/mm	12.9433973

Specimen 16 (After Rim Lesion): T for translation, R for rotation, F for force, M for moment in/relative to x,y,z-axes

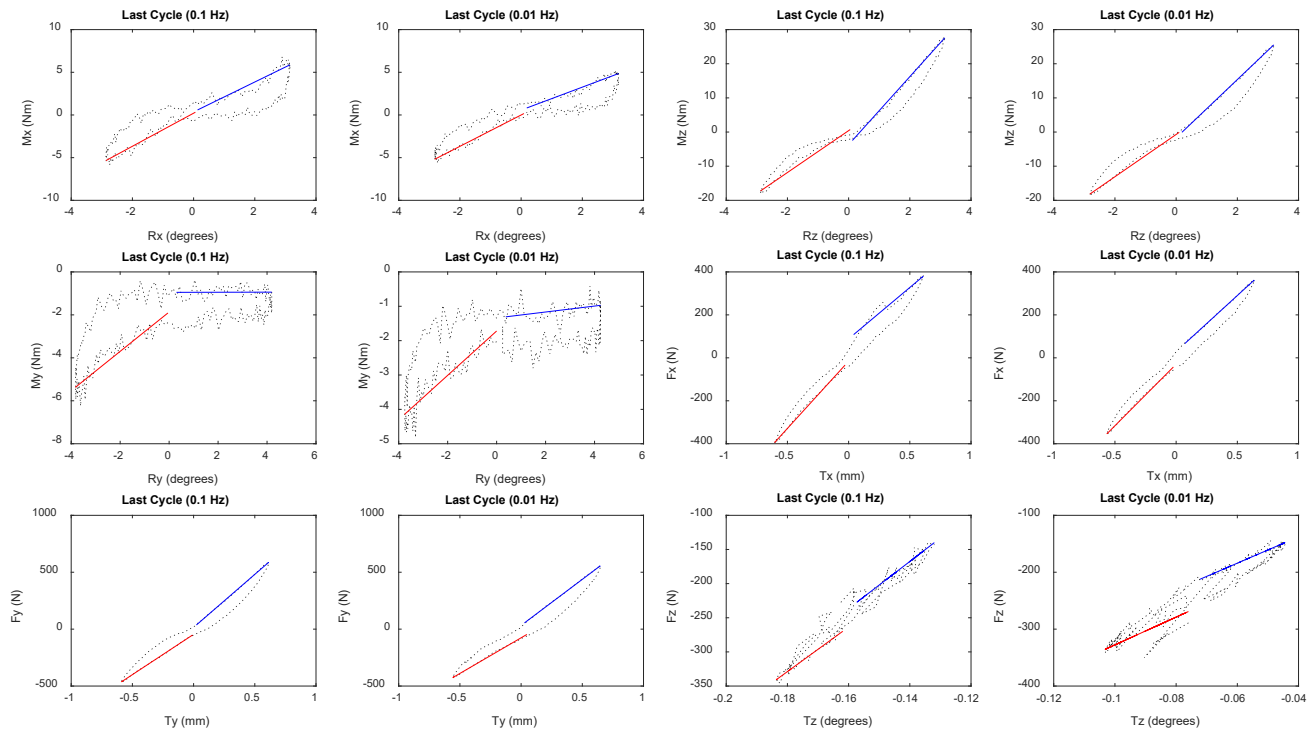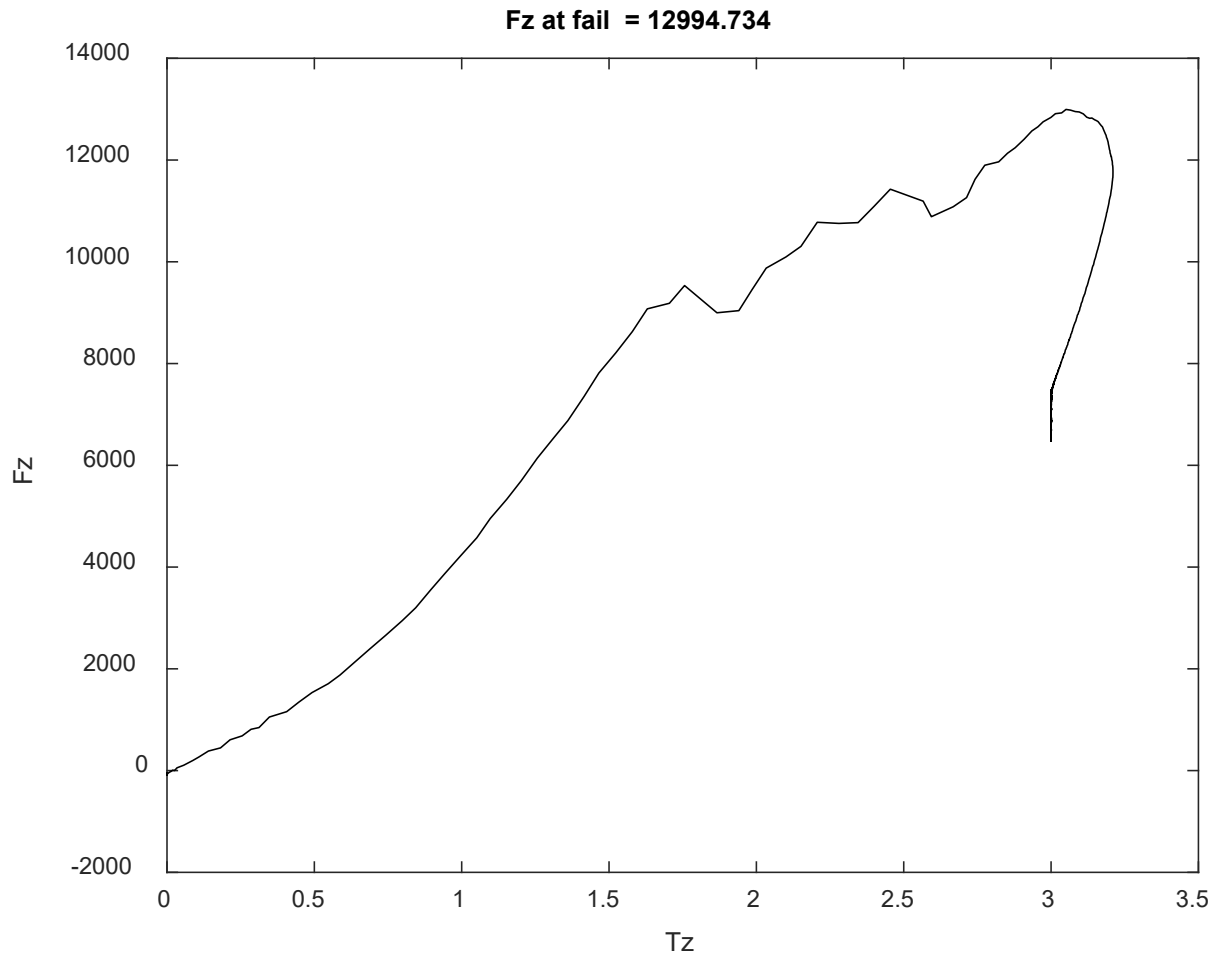Last Cycles of the 6DOF Dynamic Test at 0.1 Hz and 0.01 Hz:

Specimen 16 (After Rim Lesion): T for translation, R for rotation, F for force, M for moment in/relative to x,y,z-axes

Calculations of Stiffness and Phase Angle:

FileName	Test	Frequency	Stiffness_Positive_Direction	Stiffness_Negative_Direction	Phase
RLR16INB003Rx5E2	Rx	0.1	1.9378 Nm/degree	1.7512 Nm/degree	20.94646369
RLR16INB003Rx5E3	Rx	0.01	1.8362 Nm/degree	1.3441 Nm/degree	17.93030319
RLR16INB003Rz5E2	Rz	0.1	6.1358 Nm/degree	9.9562 Nm/degree	6.100842411
RLR16INB003Rz5E3	Rz	0.01	6.1919 Nm/degree	8.5324 Nm/degree	7.637887269
RLR16INB004Ry5E2	Ry	0.1	0.91596 Nm/degree	0.0022981 Nm/degree	39.29428219
RLR16INB004Ry5E3	Ry	0.01	0.64515 Nm/degree	0.086524 Nm/degree	35.79991524
RLR16INB6E1Tx5E2	Tx	0.1	626.0812 N/mm	478.0853 N/mm	7.463931359
RLR16INB6E1Tx5E3	Tx	0.01	572.6297 N/mm	521.5423 N/mm	6.377839161
RLR16INB6E1Ty5E2	Ty	0.1	708.5175 N/mm	932.3039 N/mm	7.393034234
RLR16INB6E1Ty5E3	Ty	0.01	626.4049 N/mm	809.6544 N/mm	9.00580793
RLR16INN182Tz1E1M	Tz	0.1	3263.9762 N/mm	3447.8985 N/mm	10.55420727
RLR16INN182Tz1E2M	Tz	0.01	2438.4829 N/mm	2319.5455 N/mm	11.41943812

Failure Under Sudden Overload:

Fz at fail = 12994.734

Specimen 3 (Before Radial Tear): T for translation, R for rotation, F for force, M for moment in/relative to x,y,z-axes

Last Cycles of the 6DOF Dynamic Test at 0.1 Hz and 0.01 Hz:

Specimen 3 (Before Radial Tear): T for translation, R for rotation, F for force, M for moment in/relative to x,y,z-axes
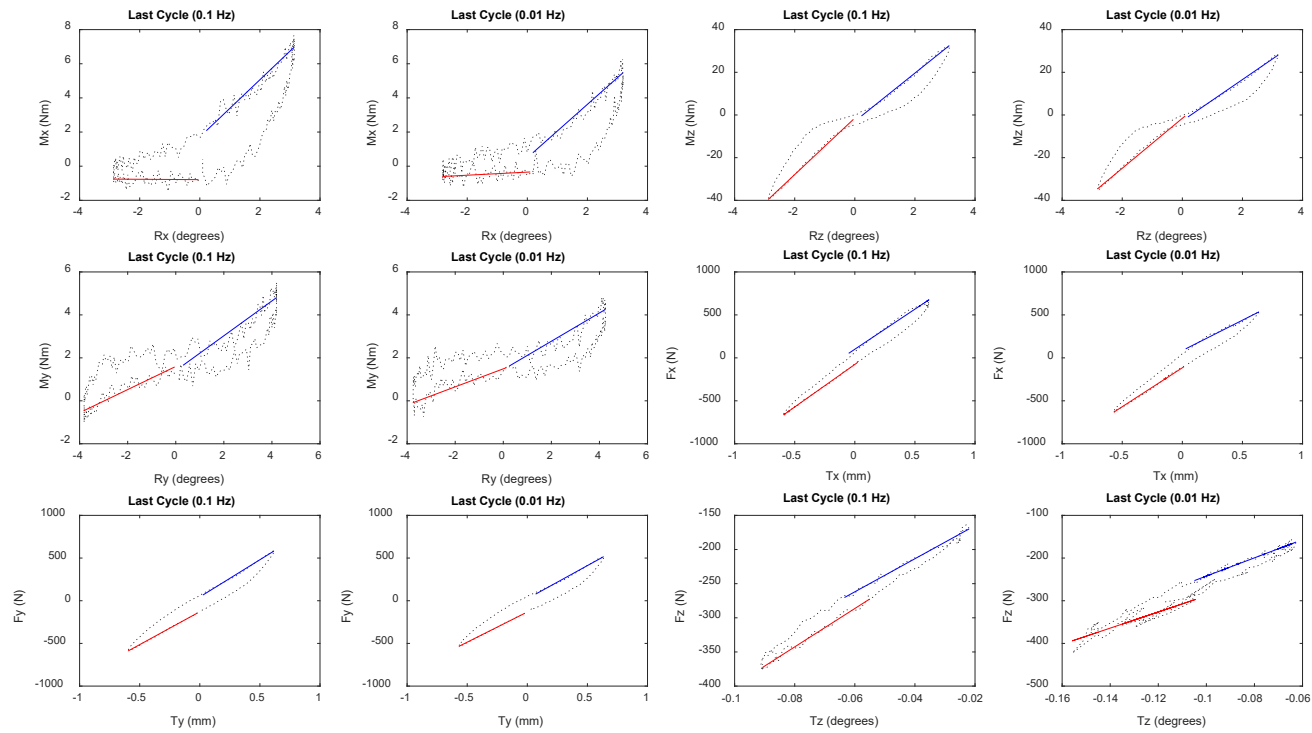
Calculations of Stiffness and Phase Angle:

FileName	Test	Frequency	Stiffness_Positive_Direction	Stiffness_Negative_Direction	Phase
RTR03COB003Rx5E2	Rx	0.1	-0.01078 Nm/degree	1.6754 Nm/degree	24.21942093
RTR03COB003Rx5E3	Rx	0.01	0.090879 Nm/degree	1.5626 Nm/degree	25.00608155
RTR03COB003Rz5E2	Rz	0.1	13.2506 Nm/degree	11.2862 Nm/degree	9.788139572
RTR03COB003Rz5E3	Rz	0.01	11.7096 Nm/degree	9.6637 Nm/degree	9.909799598
RTR03COB004Ry5E2	Ry	0.1	0.53861 Nm/degree	0.8108 Nm/degree	22.28022938
RTR03COB004Ry5E3	Ry	0.01	0.4192 Nm/degree	0.65872 Nm/degree	23.02419369
RTR03COB6E1Tx5E2	Tx	0.1	990.0105 N/mm	933.4152 N/mm	7.348448892
RTR03COB6E1Tx5E3	Tx	0.01	906.417 N/mm	706.0005 N/mm	8.101716303
RTR03COB6E1Ty5E2	Ty	0.1	770.7417 N/mm	871.8912 N/mm	10.06382233
RTR03COB6E1Ty5E3	Ty	0.01	706.6051 N/mm	775.5618 N/mm	11.15893299
RTR03CON205Tz1E1M	Tz	0.1	2809.0229 N/mm	2421.7308 N/mm	7.615370066
RTR03CON205Tz1E2M	Tz	0.01	1893.1896 N/mm	2134.1007 N/mm	9.91643553

Specimen 3 (After Radial Tear): T for translation, R for rotation, F for force, M for moment in/relative to x,y,z-axes

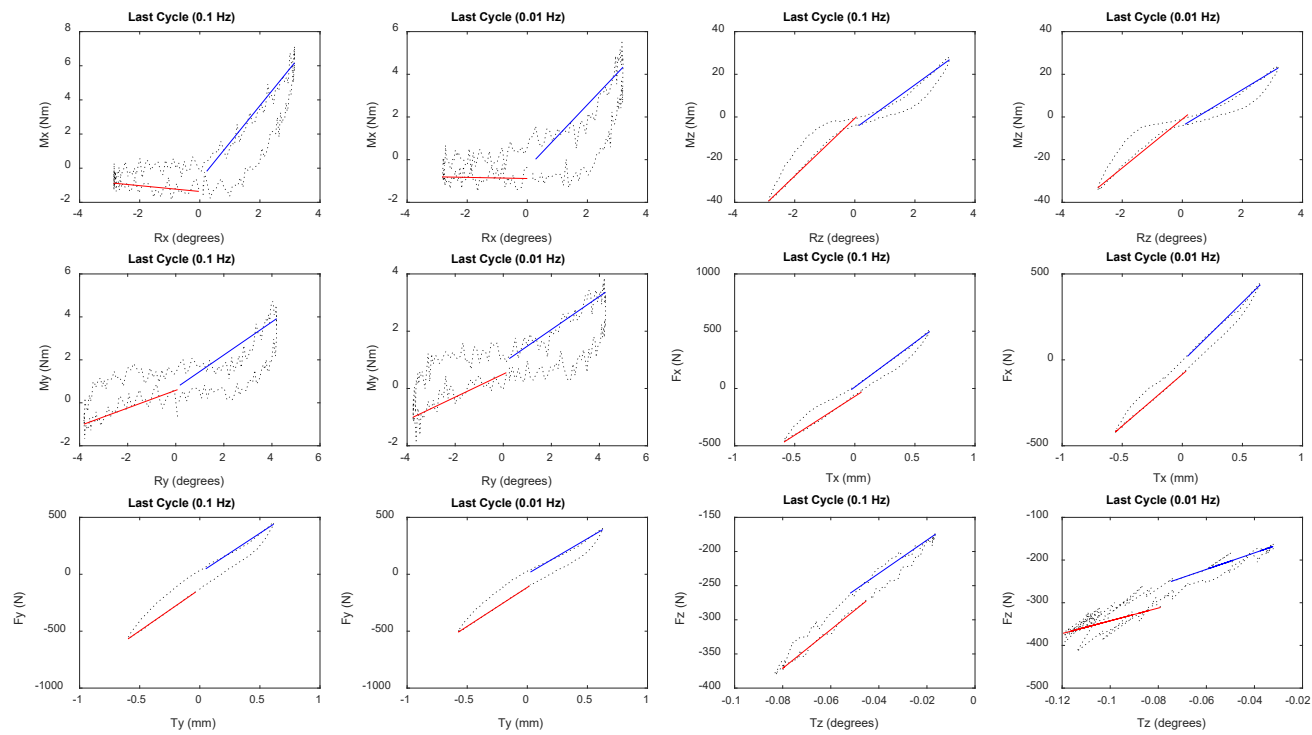Last Cycles of the 6DOF Dynamic Test at 0.1 Hz and 0.01 Hz:

Specimen 3 (After Radial Tear): T for translation, R for rotation, F for force, M for moment in/relative to x,y,z-axes

Calculations of Stiffness and Phase Angle:

FileName	Test	Frequency	Stiffness_Positive_Direction	Stiffness_Negative_Direction	Phase
RTR03INB003Rx5E2	Rx	0.1	-0.17014 Nm/degree	2.1734 Nm/degree	20.92594663
RTR03INB003Rx5E3	Rx	0.01	-0.026669 Nm/degree	1.4829 Nm/degree	25.84512317
RTR03INB003Rz5E2	Rz	0.1	13.4993 Nm/degree	10.2281 Nm/degree	8.82054353
RTR03INB003Rz5E3	Rz	0.01	11.4406 Nm/degree	8.5062 Nm/degree	8.96306956
RTR03INB004Ry5E2	Ry	0.1	0.41204 Nm/degree	0.77006 Nm/degree	27.33875938
RTR03INB004Ry5E3	Ry	0.01	0.40083 Nm/degree	0.57953 Nm/degree	29.88219913
RTR03INB6E1Tx5E2	Tx	0.1	676.6636 N/mm	779.7392 N/mm	7.562214733
RTR03INB6E1Tx5E3	Tx	0.01	602.0757 N/mm	688.8 N/mm	6.170640448
RTR03INB6E1Ty5E2	Ty	0.1	733.0147 N/mm	694.883 N/mm	9.64275869
RTR03INB6E1Ty5E3	Ty	0.01	685.0156 N/mm	619.8012 N/mm	9.7506598
RTR03INN205Tz1E1M	Tz	0.1	2837.3658 N/mm	2436.9821 N/mm	8.072383511
RTR03INN205Tz1E2M	Tz	0.01	1492.2764 N/mm	1932.051 N/mm	10.331592

Failure Under Sudden Overload:

Fz at fail = 18223.401

Specimen 5 (Before Radial Tear): T for translation, R for rotation, F for force, M for moment in/relative to x,y,z-axes

Last Cycles of the 6DOF Dynamic Test at 0.1 Hz and 0.01 Hz:

Specimen 5 (Before Radial Tear): T for translation, R for rotation, F for force, M for moment in/relative to x,y,z-axes
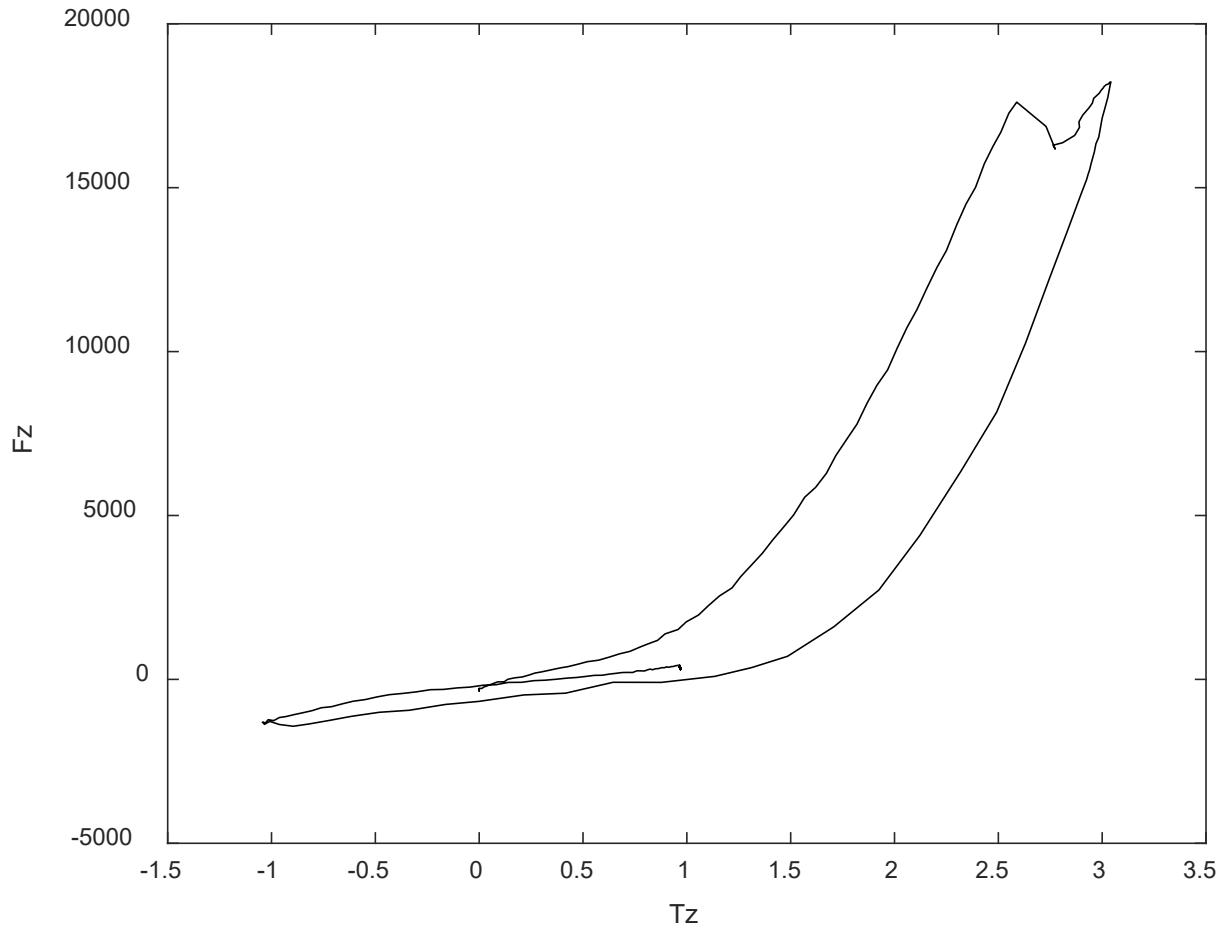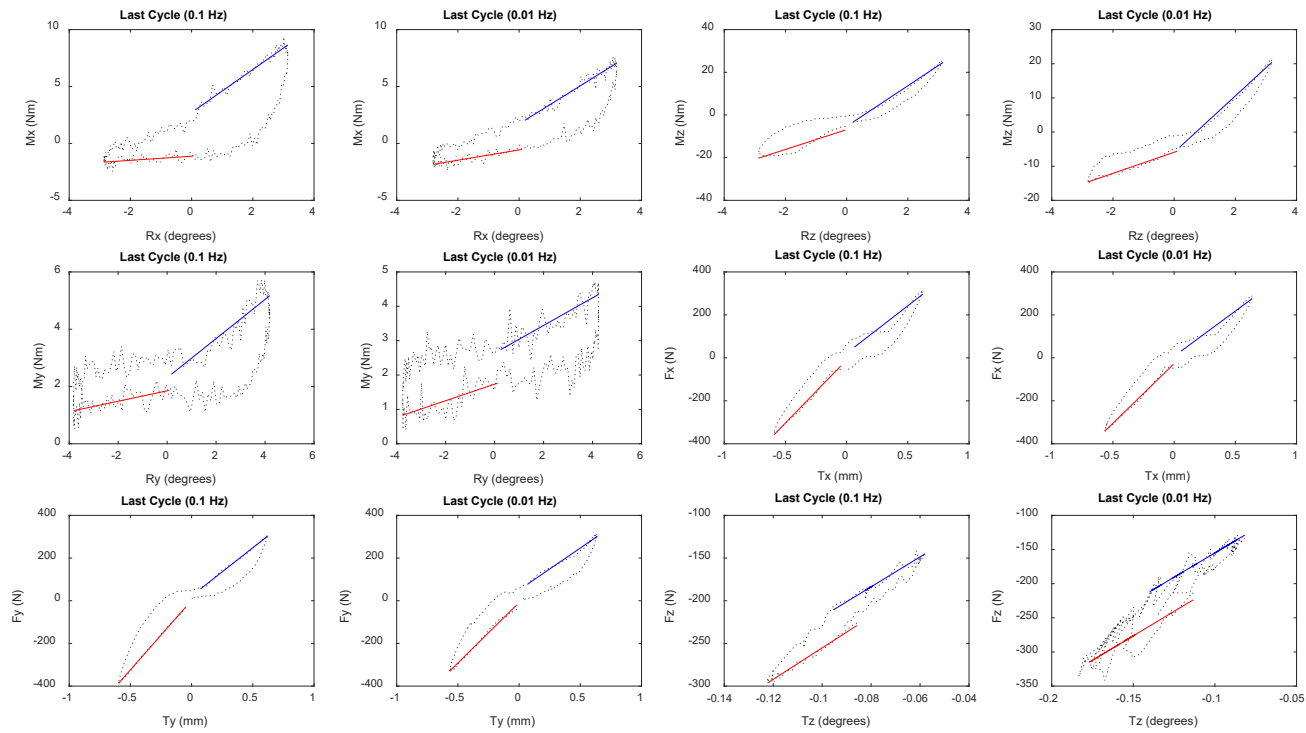
Calculations of Stiffness and Phase Angle:

FileName	Test	Frequency	Stiffness_Positive_Direction	Stiffness_Negative_Direction	Phase
RTR05COB003Rx5E2	Rx	0.1	0.18186 Nm/degree	1.8866 Nm/degree	31.2741366
RTR05COB003Rx5E3	Rx	0.01	0.45317 Nm/degree	1.6744 Nm/degree	25.00171669
RTR05COB003Rz5E2	Rz	0.1	4.6457 Nm/degree	9.5072 Nm/degree	12.24075534
RTR05COB003Rz5E3	Rz	0.01	3.0869 Nm/degree	8.2446 Nm/degree	10.33186582
RTR05COB004Ry5E2	Ry	0.1	0.1817 Nm/degree	0.68331 Nm/degree	40.20937051
RTR05COB004Ry5E3	Ry	0.01	0.24055 Nm/degree	0.40182 Nm/degree	42.44587675
RTR05COB6E1Tx5E2	Tx	0.1	587.6952 N/mm	441.4481 N/mm	10.48573279
RTR05COB6E1Tx5E3	Tx	0.01	555.3612 N/mm	420.6325 N/mm	10.6368335
RTR05COB6E1Ty5E2	Ty	0.1	651.3111 N/mm	451.7344 N/mm	11.76643045
RTR05COB6E1Ty5E3	Ty	0.01	565.5171 N/mm	392.6191 N/mm	13.11340045
RTR05CON166Tz1E1M	Tz	0.1	1843.3574 N/mm	1752.2264 N/mm	10.69493413
RTR05CON166Tz1E2M	Tz	0.01	1432.1102 N/mm	1423.9819 N/mm	13.1772621

Specimen 5 (After Radial Tear): T for translation, R for rotation, F for force, M for moment in/relative to x,y,z-axes

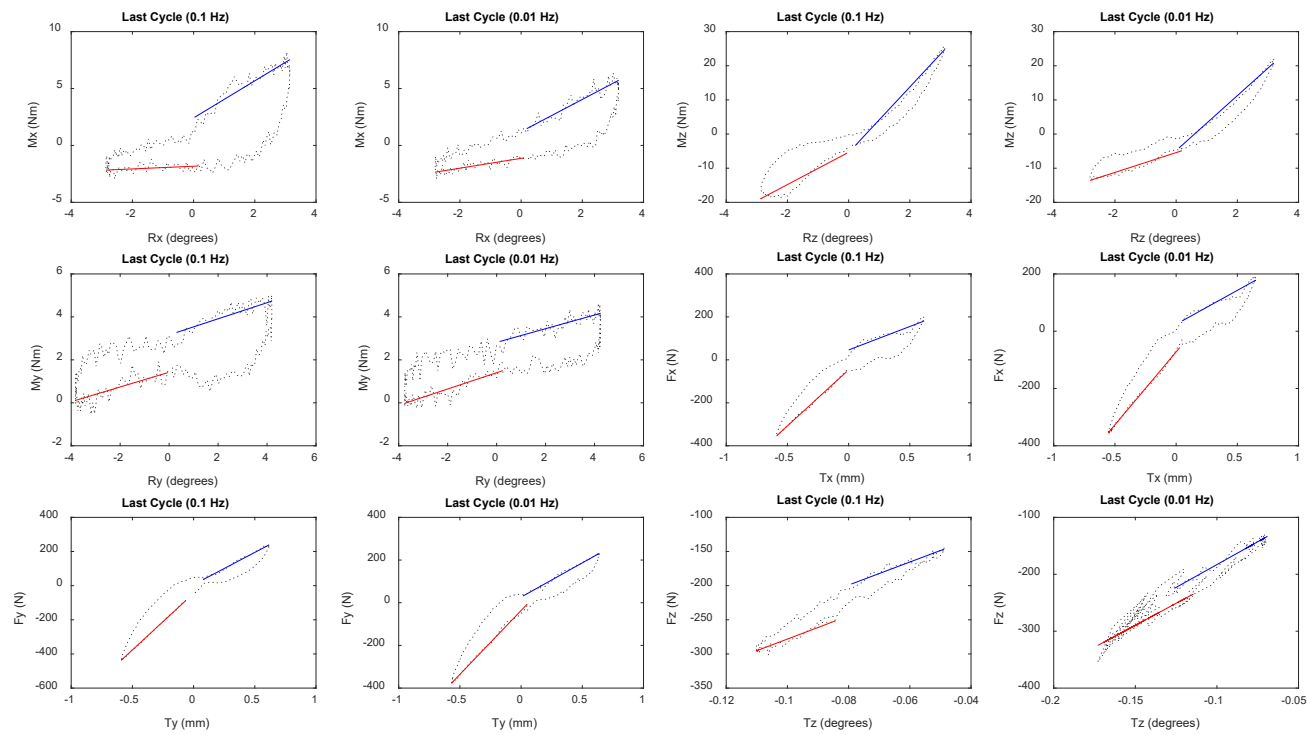Last Cycles of the 6DOF Dynamic Test at 0.1 Hz and 0.01 Hz:

Specimen 5 (After Radial Tear): T for translation, R for rotation, F for force, M for moment in/relative to x,y,z-axes

Calculations of Stiffness and Phase Angle:

FileName	Test	Frequency	Stiffness_Positive_Direction	Stiffness_Negative_Direction	Phase
RTR05INB003Rx5E2	Rx	0.1	0.11829 Nm/degree	1.6284 Nm/degree	34.37838587
RTR05INB003Rx5E3	Rx	0.01	0.43307 Nm/degree	1.4151 Nm/degree	28.76725465
RTR05INB003Rz5E2	Rz	0.1	4.7316 Nm/degree	9.6172 Nm/degree	11.46930254
RTR05INB003Rz5E3	Rz	0.01	2.9015 Nm/degree	8.0457 Nm/degree	10.15811132
RTR05INB004Ry5E2	Ry	0.1	0.34251 Nm/degree	0.3747 Nm/degree	41.32284024
RTR05INB004Ry5E3	Ry	0.01	0.37929 Nm/degree	0.31855 Nm/degree	37.69818139
RTR05INB6E1Tx5E2	Tx	0.1	522.3323 N/mm	218.2854 N/mm	12.02649548
RTR05INB6E1Tx5E3	Tx	0.01	509.42 N/mm	236.8043 N/mm	11.71627789
RTR05INB6E1Ty5E2	Ty	0.1	662.9961 N/mm	377.3613 N/mm	11.4575104
RTR05INB6E1Ty5E3	Ty	0.01	598.5218 N/mm	320.7388 N/mm	12.44704887
RTR05INN166Tz1E1M	Tz	0.1	1697.3776 N/mm	1684.4071 N/mm	10.63772643
RTR05INN166Tz1E2M	Tz	0.01	1543.7072 N/mm	1603.6512 N/mm	10.94573082

Failure Under Sudden Overload

Fz at fail = 12719

Specimen 7 (Before Radial Tear): T for translation, R for rotation, F for force, M for moment in/relative to x,y,z-axes

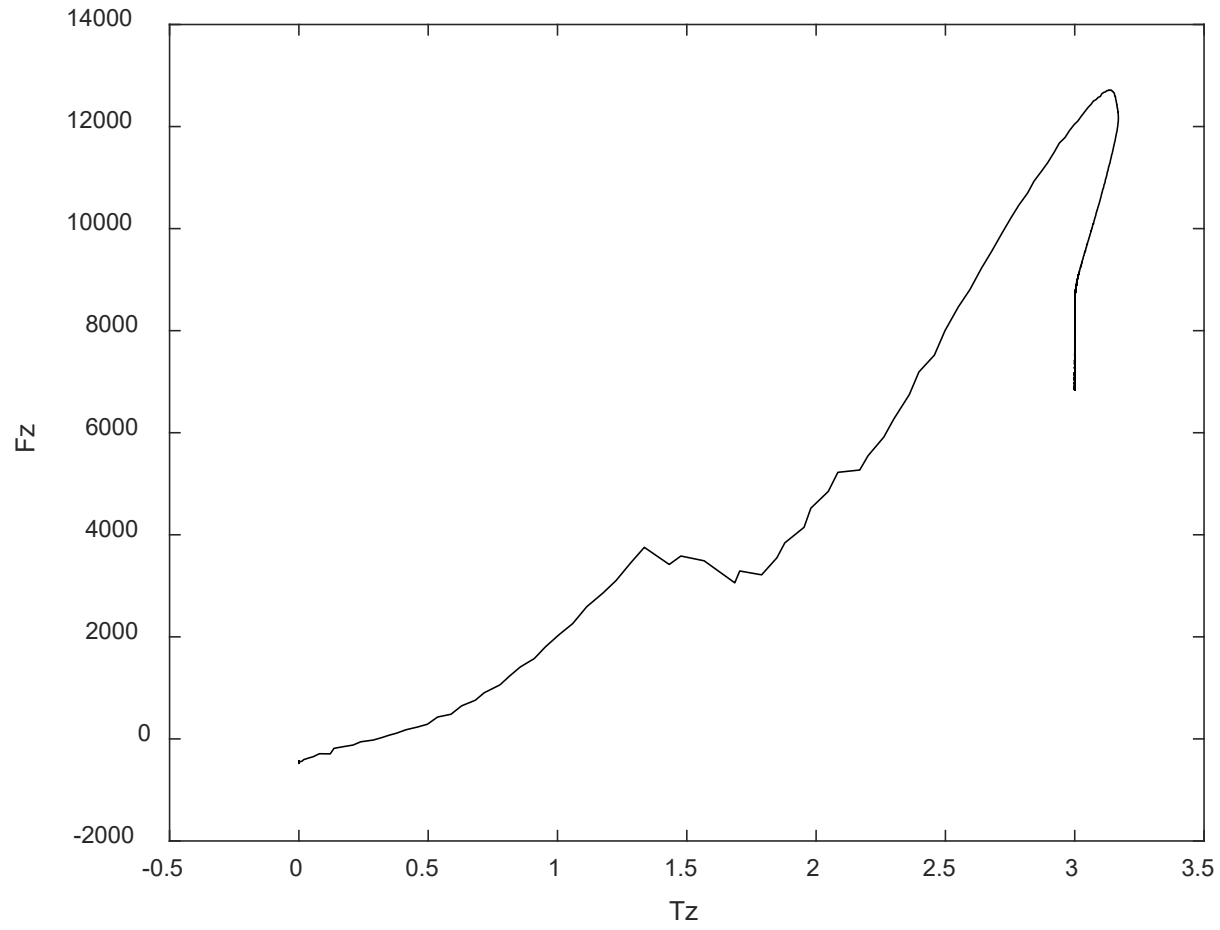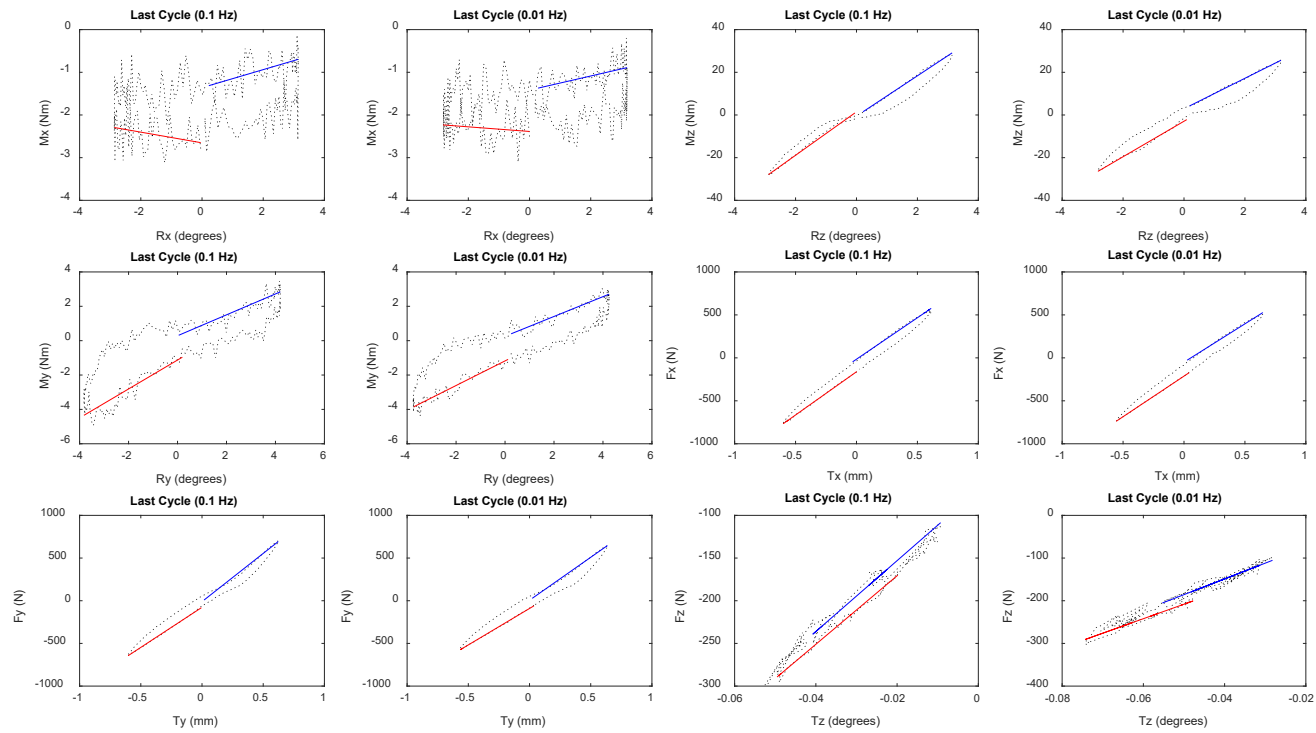Last Cycles of the 6DOF Dynamic Test at 0.1 Hz and 0.01 Hz:

Specimen 7 (Before Radial Tear): T for translation, R for rotation, F for force, M for moment in/relative to x,y,z-axes

Calculations of Stiffness and Phase Angle:

FileName	Test	Frequency	Stiffness_Positive_Direction	Stiffness_Negative_Direction	Phase
RTR07COB003Rx5E2	Rx	0.1	-0.12554 Nm/degree	0.21136 Nm/degree	60.84636844
RTR07COB003Rx5E3	Rx	0.01	-0.054128 Nm/degree	0.16529 Nm/degree	60.6931309
RTR07COB003Rz5E2	Rz	0.1	10.1834 Nm/degree	9.4337 Nm/degree	6.81526617
RTR07COB003Rz5E3	Rz	0.01	8.3168 Nm/degree	7.1347 Nm/degree	9.305357384
RTR07COB004Ry5E2	Ry	0.1	0.84128 Nm/degree	0.60883 Nm/degree	25.36769506
RTR07COB004Ry5E3	Ry	0.01	0.71577 Nm/degree	0.57628 Nm/degree	23.28853486
RTR07COB6E1Tx5E2	Tx	0.1	1005.8284 N/mm	965.4057 N/mm	6.391199393
RTR07COB6E1Tx5E3	Tx	0.01	944.7902 N/mm	892.2615 N/mm	6.452865498
RTR07COB6E1Ty5E2	Ty	0.1	939.2075 N/mm	1130.2379 N/mm	6.393044763
RTR07COB6E1Ty5E3	Ty	0.01	853.9975 N/mm	1006.0673 N/mm	7.81841547
RTR07CON151Tz1E1M	Tz	0.1	4014.5641 N/mm	4150.0823 N/mm	7.116975755
RTR07CON151Tz1E2M	Tz	0.01	3395.6183 N/mm	3689.1213 N/mm	7.341079081

Specimen 7 (After Radial Tear): T for translation, R for rotation, F for force, M for moment in/relative to x,y,z-axes

Last Cycles of the 6DOF Dynamic Test at 0.1 Hz and 0.01 Hz:

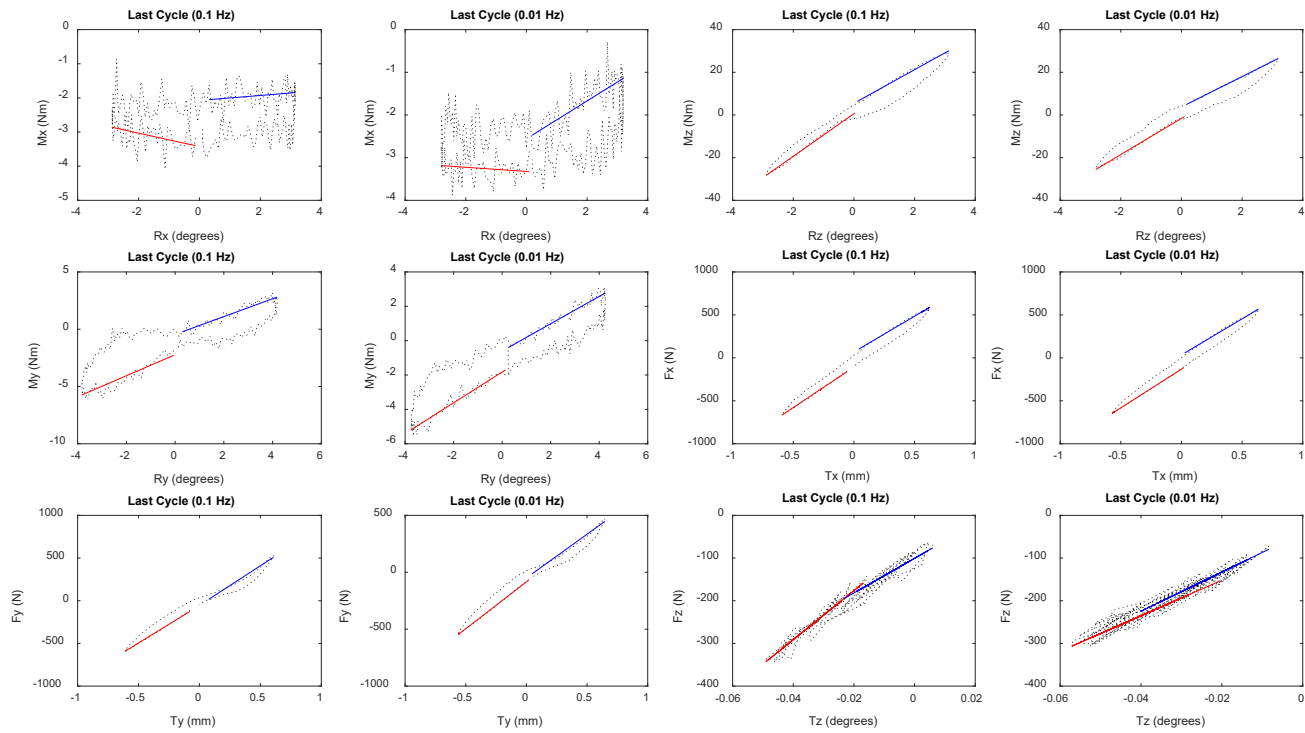Specimen 7 (After Radial Tear): T for translation, R for rotation, F for force, M for moment in/relative to x,y,z-axes

Calculations of Stiffness and Phase Angle:

FileName	Test	Frequency	Stiffness_Positive_Direction	Stiffness_Negative_Direction	Phase
RTR07INB003Rx5E2	Rx	0.1	-0.19666 Nm/degree	0.072844 Nm/degree	70.35942663
RTR07INB003Rx5E3	Rx	0.01	-0.049263 Nm/degree	0.44303 Nm/degree	65.03002122
RTR07INB003Rz5E2	Rz	0.1	9.9936 Nm/degree	7.8722 Nm/degree	8.60061301
RTR07INB003Rz5E3	Rz	0.01	8.48 Nm/degree	7.1146 Nm/degree	9.137449529
RTR07INB004Ry5E2	Ry	0.1	0.91784 Nm/degree	0.77755 Nm/degree	26.22833864
RTR07INB004Ry5E3	Ry	0.01	0.89599 Nm/degree	0.79423 Nm/degree	20.81883759
RTR07INB6E1Tx5E2	Tx	0.1	940.6589 N/mm	832.3502 N/mm	7.050229474
RTR07INB6E1Tx5E3	Tx	0.01	900.7822 N/mm	840.733 N/mm	6.664958434
RTR07INB6E1Ty5E2	Ty	0.1	875.3363 N/mm	926.409 N/mm	6.152239249
RTR07INB6E1Ty5E3	Ty	0.01	823.276 N/mm	768.2181 N/mm	6.645524989
RTR07INN151Tz1E1M	Tz	0.1	5737.9589 N/mm	4061.8538 N/mm	7.604423006
RTR07INN151Tz1E2M	Tz	0.01	4169.6325 N/mm	4588.0995 N/mm	8.782098036

Failure Under Sudden Overload:

Fz at fail = 11803.609

Specimen 9 (Before Radial Tear): T for translation, R for rotation, F for force, M for moment in/relative to x,y,z-axes

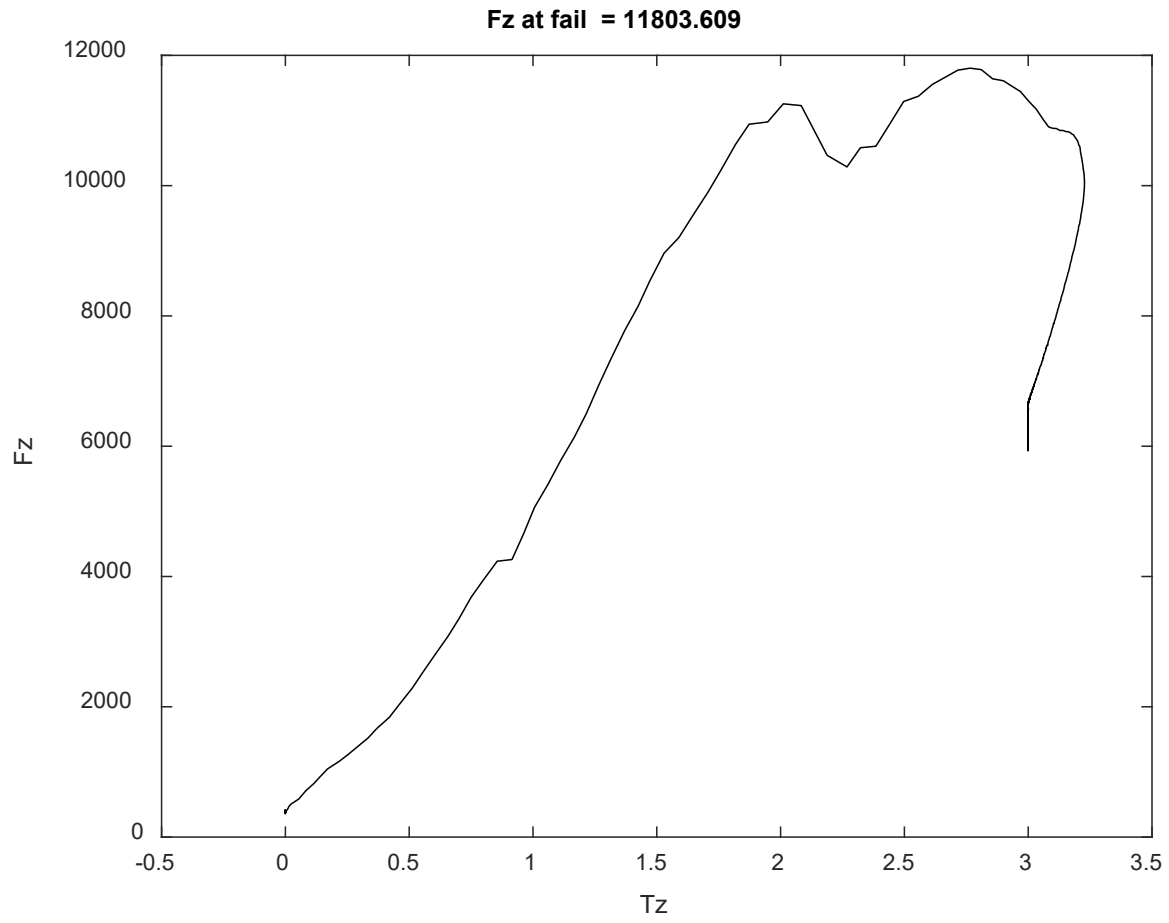Last Cycles of the 6DOF Dynamic Test at 0.1 Hz and 0.01 Hz:

Specimen 9 (Before Radial Tear): T for translation, R for rotation, F for force, M for moment in/relative to x,y,z-axes
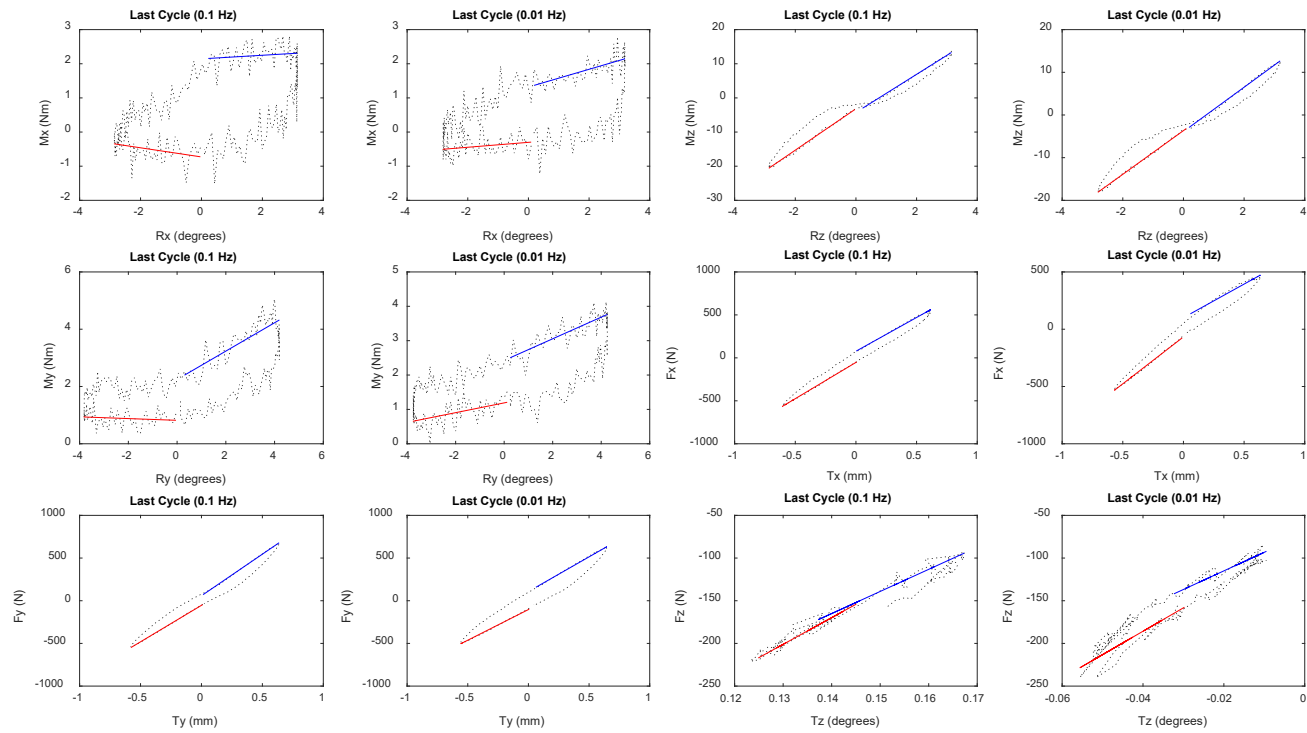
Calculations of Stiffness and Phase Angle:

FileName	Test	Frequency	Stiffness_Positive_Direction	Stiffness_Negative_Direction	Phase
RTR09COB003Rx5E2	Rx	0.1	-0.13392 Nm/degree	0.052665 Nm/degree	54.15091182
RTR09COB003Rx5E3	Rx	0.01	0.072046 Nm/degree	0.25997 Nm/degree	49.69265997
RTR09COB003Rz5E2	Rz	0.1	6.065 Nm/degree	5.5716 Nm/degree	7.046330695
RTR09COB003Rz5E3	Rz	0.01	5.1211 Nm/degree	5.1924 Nm/degree	7.430315962
RTR09COB004Ry5E2	Ry	0.1	-0.030538 Nm/degree	0.49495 Nm/degree	36.86492184
RTR09COB004Ry5E3	Ry	0.01	0.14216 Nm/degree	0.31481 Nm/degree	38.71712423
RTR09COB6E1Tx5E2	Tx	0.1	844.1984 N/mm	785.7799 N/mm	6.815758035
RTR09COB6E1Tx5E3	Tx	0.01	819.2119 N/mm	586.0478 N/mm	7.561212474
RTR09COB6E1Ty5E2	Ty	0.1	854.7949 N/mm	974.7363 N/mm	7.902045377
RTR09COB6E1Ty5E3	Ty	0.01	718.147 N/mm	812.7603 N/mm	11.1494052
RTR09CON117Tz1E1M	Tz	0.1	3124.0997 N/mm	2590.6468 N/mm	9.800228905
RTR09CON117Tz1E2M	Tz	0.01	2743.4297 N/mm	2177.9853 N/mm	14.9702862

Specimen 9 (After Radial Tear): T for translation, R for rotation, F for force, M for moment in/relative to x,y,z-axes

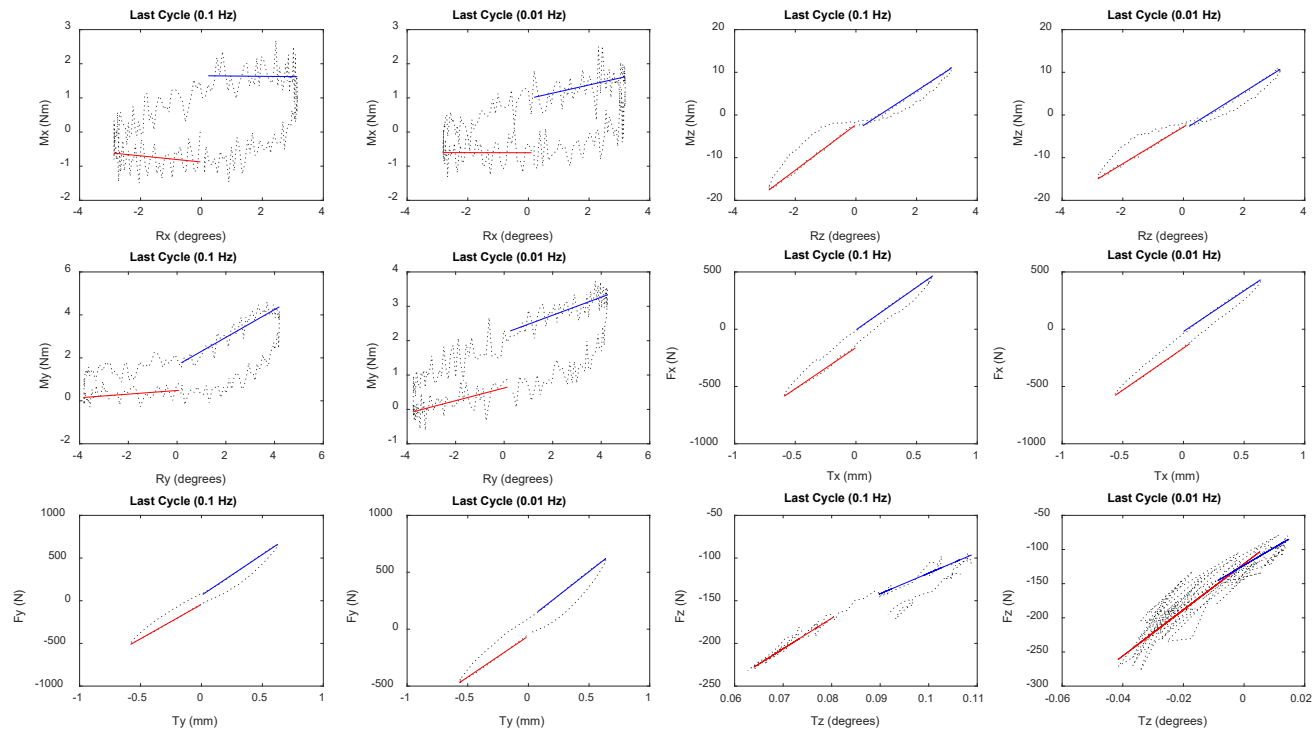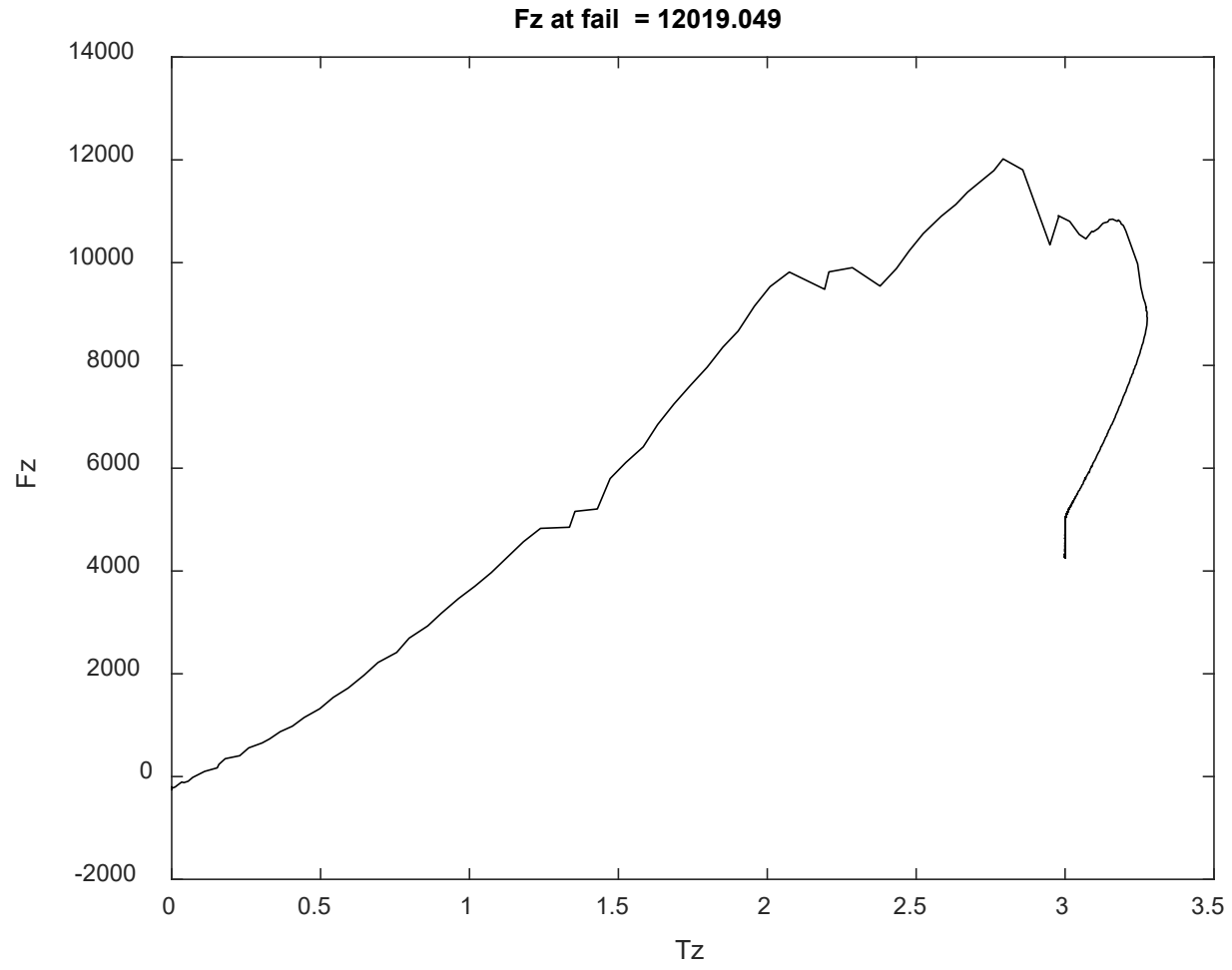Last Cycles of the 6DOF Dynamic Test at 0.1 Hz and 0.01 Hz:

Specimen 9 (After Radial Tear): T for translation, R for rotation, F for force, M for moment in/relative to x,y,z-axes

Calculations of Stiffness and Phase Angle:

FileName	Test	Frequency	Stiffness_Positive_Direction	Stiffness_Negative_Direction	Phase
RTR09INB003Rx5E2	Rx	0.1	-0.090143 Nm/degree	-0.0086869 Nm/degree	62.33459018
RTR09INB003Rx5E3	Rx	0.01	-0.0012615 Nm/degree	0.19991 Nm/degree	56.73996903
RTR09INB003Rz5E2	Rz	0.1	5.3364 Nm/degree	4.6269 Nm/degree	7.344470004
RTR09INB003Rz5E3	Rz	0.01	4.3088 Nm/degree	4.4465 Nm/degree	7.643955472
RTR09INB004Ry5E2	Ry	0.1	0.084497 Nm/degree	0.64763 Nm/degree	38.14338035
RTR09INB004Ry5E3	Ry	0.01	0.18435 Nm/degree	0.26192 Nm/degree	37.06177317
RTR09INB6E1Tx5E2	Tx	0.1	718.7091 N/mm	746.1274 N/mm	7.546119844
RTR09INB6E1Tx5E3	Tx	0.01	733.6339 N/mm	710.7087 N/mm	6.900224006
RTR09INB6E1Ty5E2	Ty	0.1	805.814 N/mm	956.2233 N/mm	7.939685716
RTR09INB6E1Ty5E3	Ty	0.01	718.935 N/mm	833.1175 N/mm	10.49245021
RTR09INN117Tz1E1M	Tz	0.1	3575.7722 N/mm	2408.1482 N/mm	9.957937307
RTR09INN117Tz1E2M	Tz	0.01	3375.4253 N/mm	2592.1938 N/mm	9.934642177

Failure Under Sudden Overload:

Fz at fail = 12019.049

Specimen 11 (Before Radial Tear): T for translation, R for rotation, F for force, M for moment in/relative to x,y,z-axes

Last Cycles of the 6DOF Dynamic Test at 0.1 Hz and 0.01 Hz:
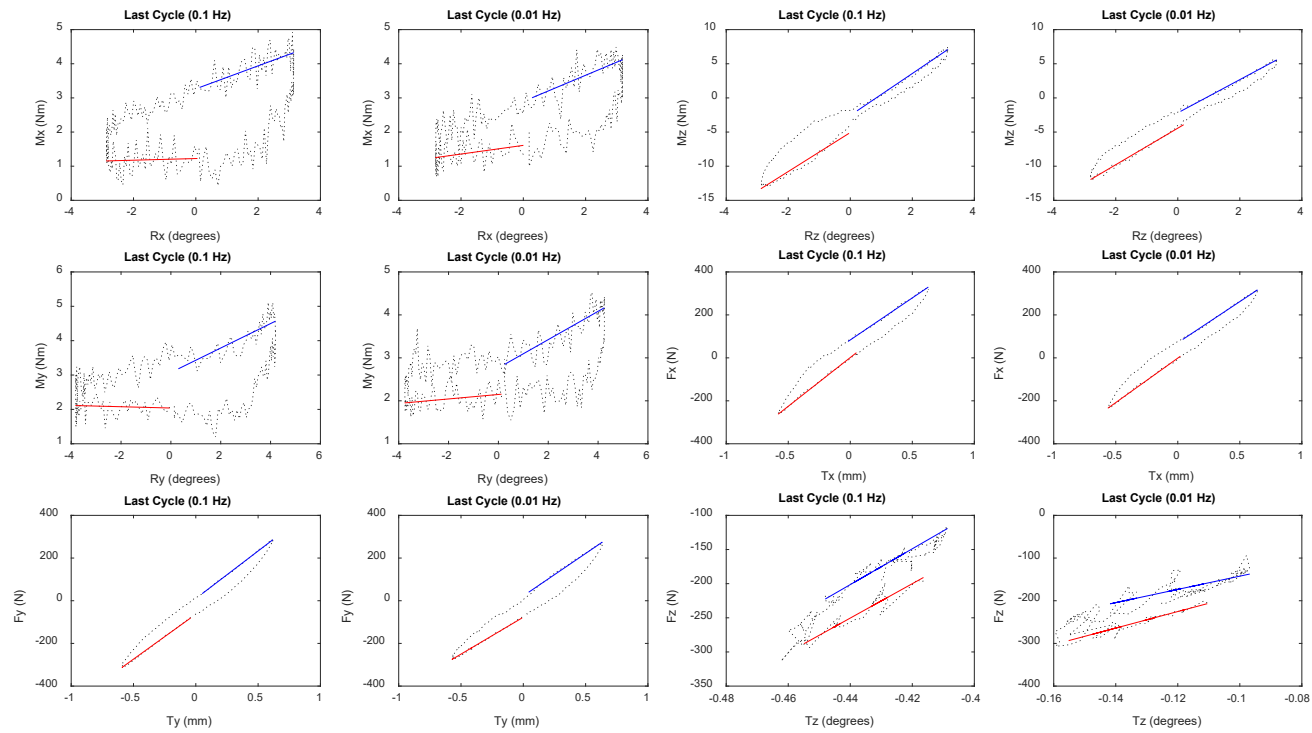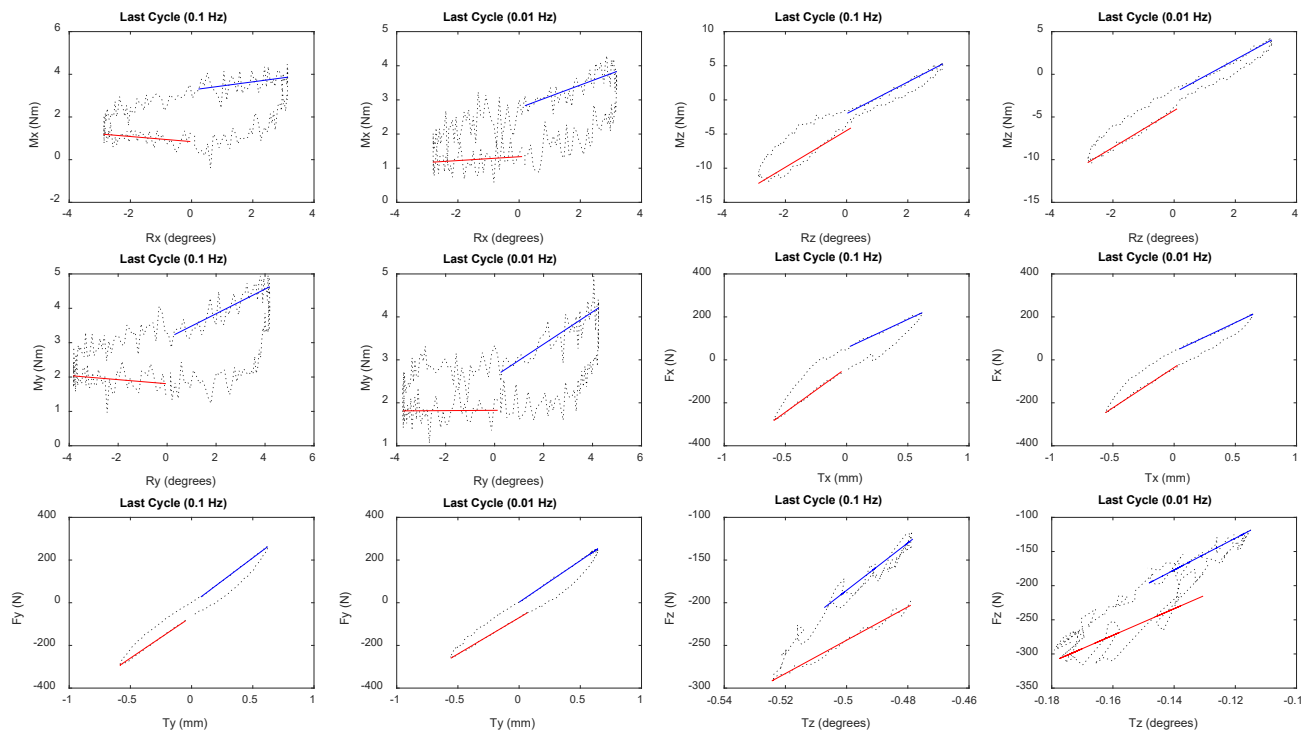
Specimen 11 (Before Radial Tear): T for translation, R for rotation, F for force, M for moment in/relative to x,y,z-axes

Calculations of Stiffness and Phase Angle:

FileName	Test	Frequency	Stiffness_Positive_Direction	Stiffness_Negative_Direction	Phase
RTR11COB003Rx5E2	Rx	0.1	0.024422 Nm/degree	0.33693 Nm/degree	51.68822206
RTR11COB003Rx5E3	Rx	0.01	0.12724 Nm/degree	0.38346 Nm/degree	41.00633264
RTR11COB003Rz5E2	Rz	0.1	2.8556 Nm/degree	3.0691 Nm/degree	10.57083368
RTR11COB003Rz5E3	Rz	0.01	2.6754 Nm/degree	2.4319 Nm/degree	9.172416408
RTR11COB004Ry5E2	Ry	0.1	-0.018856 Nm/degree	0.35578 Nm/degree	53.12641099
RTR11COB004Ry5E3	Ry	0.01	0.052191 Nm/degree	0.32927 Nm/degree	50.66562469
RTR11COB6E1Tx5E2	Tx	0.1	453.99 N/mm	391.5233 N/mm	11.29452255
RTR11COB6E1Tx5E3	Tx	0.01	414.128 N/mm	382.9907 N/mm	9.743458326
RTR11COB6E1Ty5E2	Ty	0.1	420.8214 N/mm	445.6321 N/mm	8.830215234
RTR11COB6E1Ty5E3	Ty	0.01	345.7398 N/mm	397.5122 N/mm	10.96335585
RTR11CON159Tz1E1M	Tz	0.1	2517.7171 N/mm	2621.6888 N/mm	20.76051694
RTR11CON159Tz1E2M	Tz	0.01	1936.7135 N/mm	1549.964 N/mm	18.55036932

Specimen 11 (After Radial Tear): T for translation, R for rotation, F for force, M for moment in/relative to x,y,z-axes

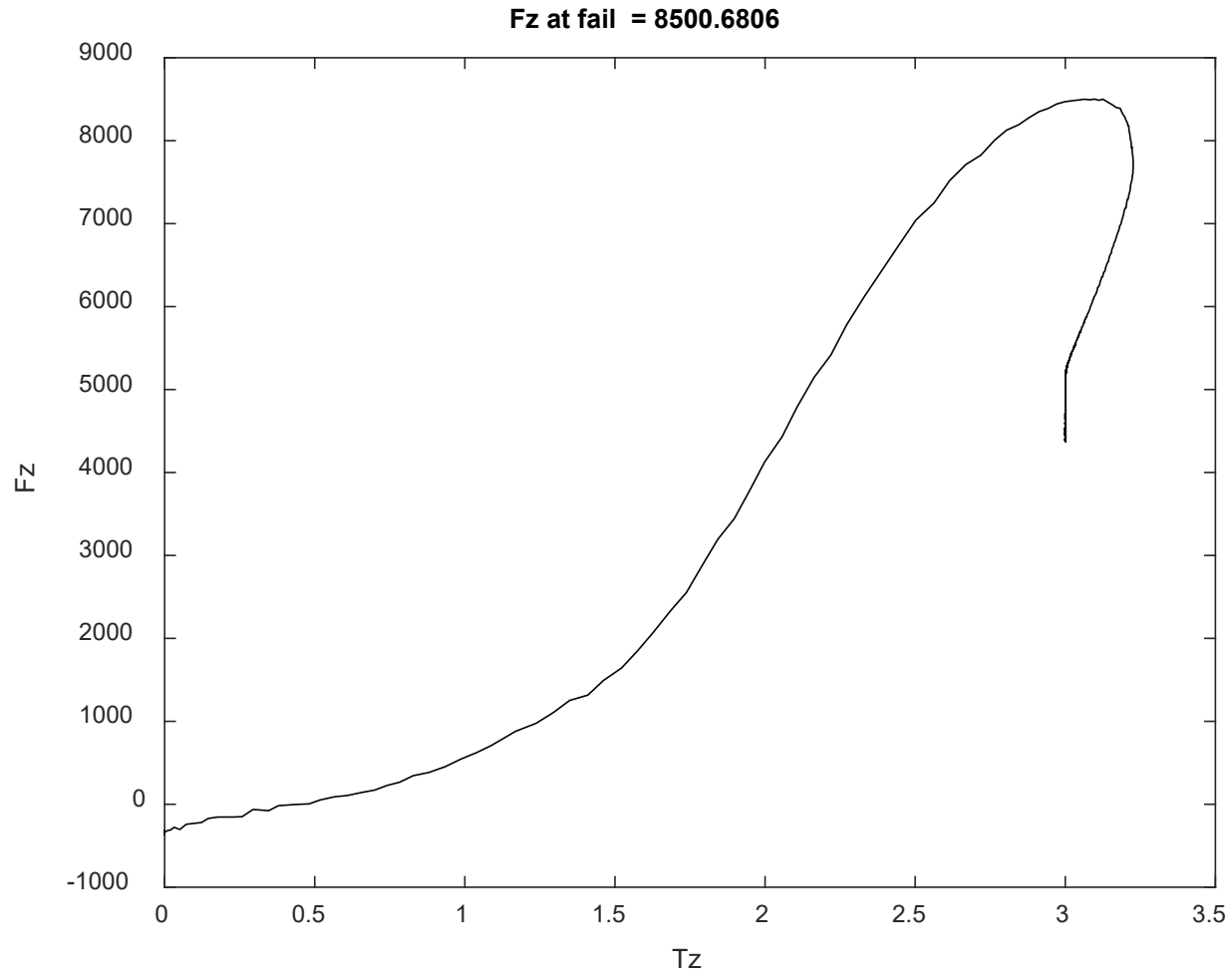Last Cycles of the 6DOF Dynamic Test at 0.1 Hz and 0.01 Hz:

Specimen 11 (After Radial Tear): T for translation, R for rotation, F for force, M for moment in/relative to x,y,z-axes

Calculations of Stiffness and Phase Angle:

FileName	Test	Frequency	Stiffness_Positive_Direction	Stiffness_Negative_Direction	Phase
RTR11INB003Rx5E2	Rx	0.1	-0.11982 Nm/degree	0.19063 Nm/degree	58.48457019
RTR11INB003Rx5E3	Rx	0.01	0.055859 Nm/degree	0.33397 Nm/degree	46.33062724
RTR11INB003Rz5E2	Rz	0.1	2.6856 Nm/degree	2.3194 Nm/degree	12.19441591
RTR11INB003Rz5E3	Rz	0.01	2.1591 Nm/degree	1.945 Nm/degree	9.984771241
RTR11INB004Ry5E2	Ry	0.1	-0.059393 Nm/degree	0.35831 Nm/degree	64.92604106
RTR11INB004Ry5E3	Ry	0.01	0.0032008 Nm/degree	0.37535 Nm/degree	51.35958293
RTR11INB6E1Tx5E2	Tx	0.1	412.3341 N/mm	266.202 N/mm	14.22316629
RTR11INB6E1Tx5E3	Tx	0.01	374.6108 N/mm	269.6833 N/mm	11.23696028
RTR11INB6E1Ty5E2	Ty	0.1	388.3412 N/mm	431.5361 N/mm	8.714758517
RTR11INB6E1Ty5E3	Ty	0.01	340.2563 N/mm	389.4944 N/mm	10.67422066
RTR11INN159Tz1E1M	Tz	0.1	1951.3877 N/mm	2776.7074 N/mm	14.07796818
RTR11INN159Tz1E2M	Tz	0.01	1949.9224 N/mm	2327.7049 N/mm	15.56293663

Failure Under Sudden Overload:

Fz at fail = 8500.6806

Specimen 13 (Before Radial Tear): T for translation, R for rotation, F for force, M for moment in/relative to x,y,z-axes

Last Cycles of the 6DOF Dynamic Test at 0.1 Hz and 0.01 Hz:

Specimen 13 (Before Radial Tear): T for translation, R for rotation, F for force, M for moment in/relative to x,y,z-axes
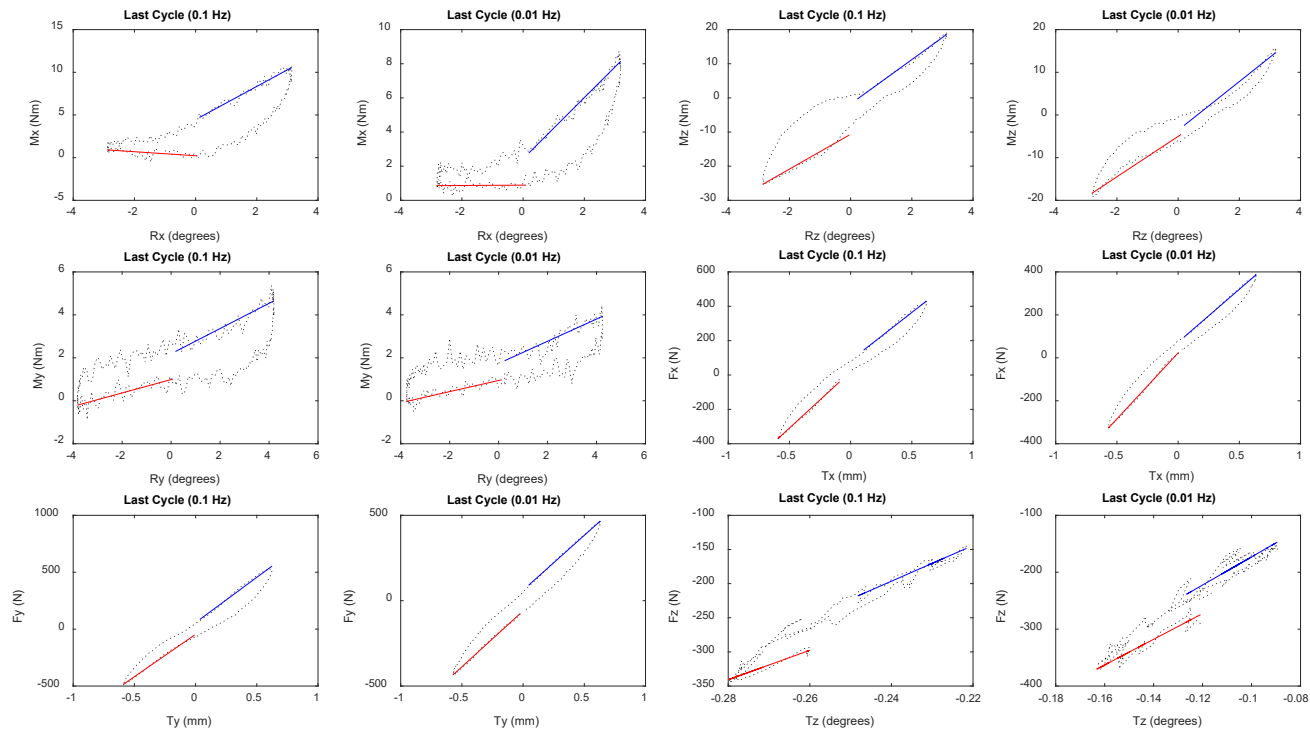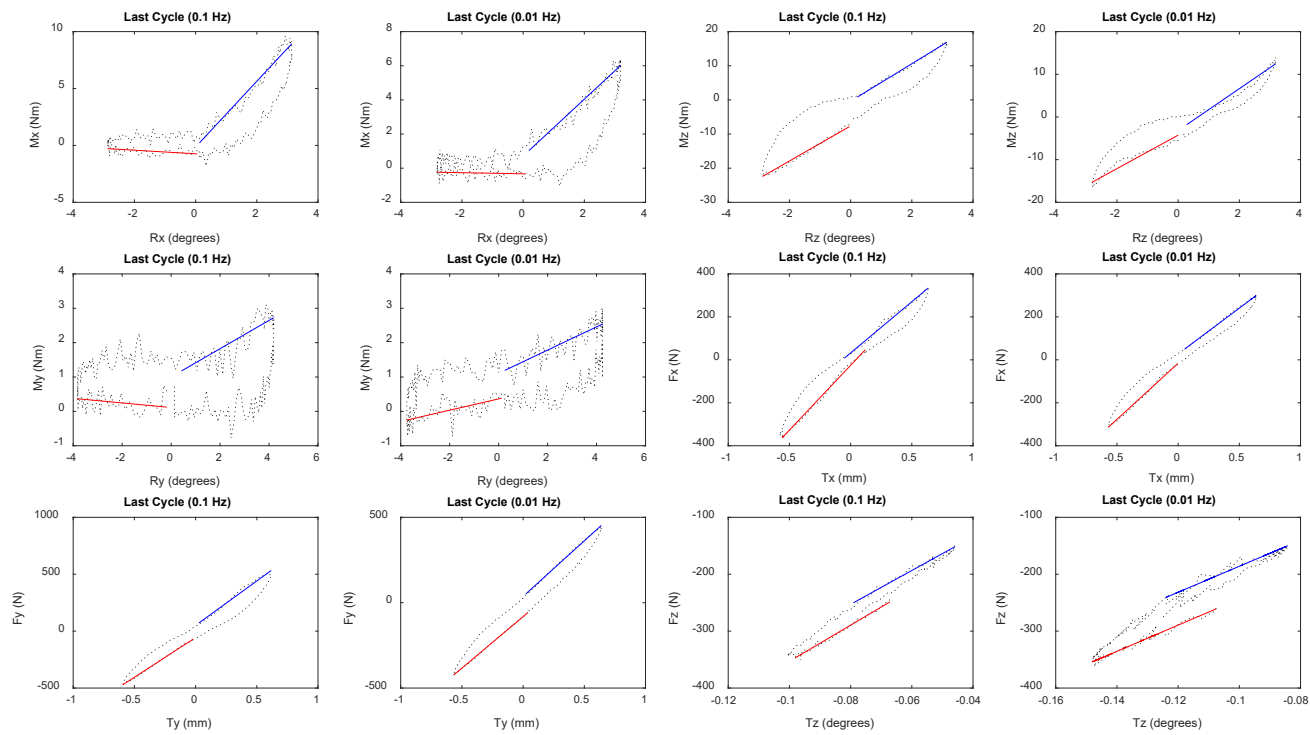
Calculations of Stiffness and Phase Angle:

FileName	Test	Frequency	Stiffness_Positive_Direction	Stiffness_Negative_Direction	Phase
RTR13COB003Rx5E2	Rx	0.1	-0.23661 Nm/degree	1.9421 Nm/degree	26.33237592
RTR13COB003Rx5E3	Rx	0.01	0.0099381 Nm/degree	1.7914 Nm/degree	23.92421352
RTR13COB003Rz5E2	Rz	0.1	5.1026 Nm/degree	6.4856 Nm/degree	15.28082348
RTR13COB003Rz5E3	Rz	0.01	4.7328 Nm/degree	5.7005 Nm/degree	10.66932381
RTR13COB004Ry5E2	Ry	0.1	0.31095 Nm/degree	0.58647 Nm/degree	36.2732084
RTR13COB004Ry5E3	Ry	0.01	0.2594 Nm/degree	0.51662 Nm/degree	31.95032842
RTR13COB6E1Tx5E2	Tx	0.1	656.0947 N/mm	556.4737 N/mm	8.505503926
RTR13COB6E1Tx5E3	Tx	0.01	614.7035 N/mm	493.1117 N/mm	7.405030826
RTR13COB6E1Ty5E2	Ty	0.1	745.1207 N/mm	794.8996 N/mm	9.890819744
RTR13COB6E1Ty5E3	Ty	0.01	655.0078 N/mm	641.9749 N/mm	9.424134816
RTR13CON190Tz1E1M	Tz	0.1	2156.3799 N/mm	2616.4071 N/mm	10.21553579
RTR13CON190Tz1E2M	Tz	0.01	2257.8438 N/mm	2470.4127 N/mm	11.19187455

Specimen 13 (After Radial Tear): T for translation, R for rotation, F for force, M for moment in/relative to x,y,z-axes

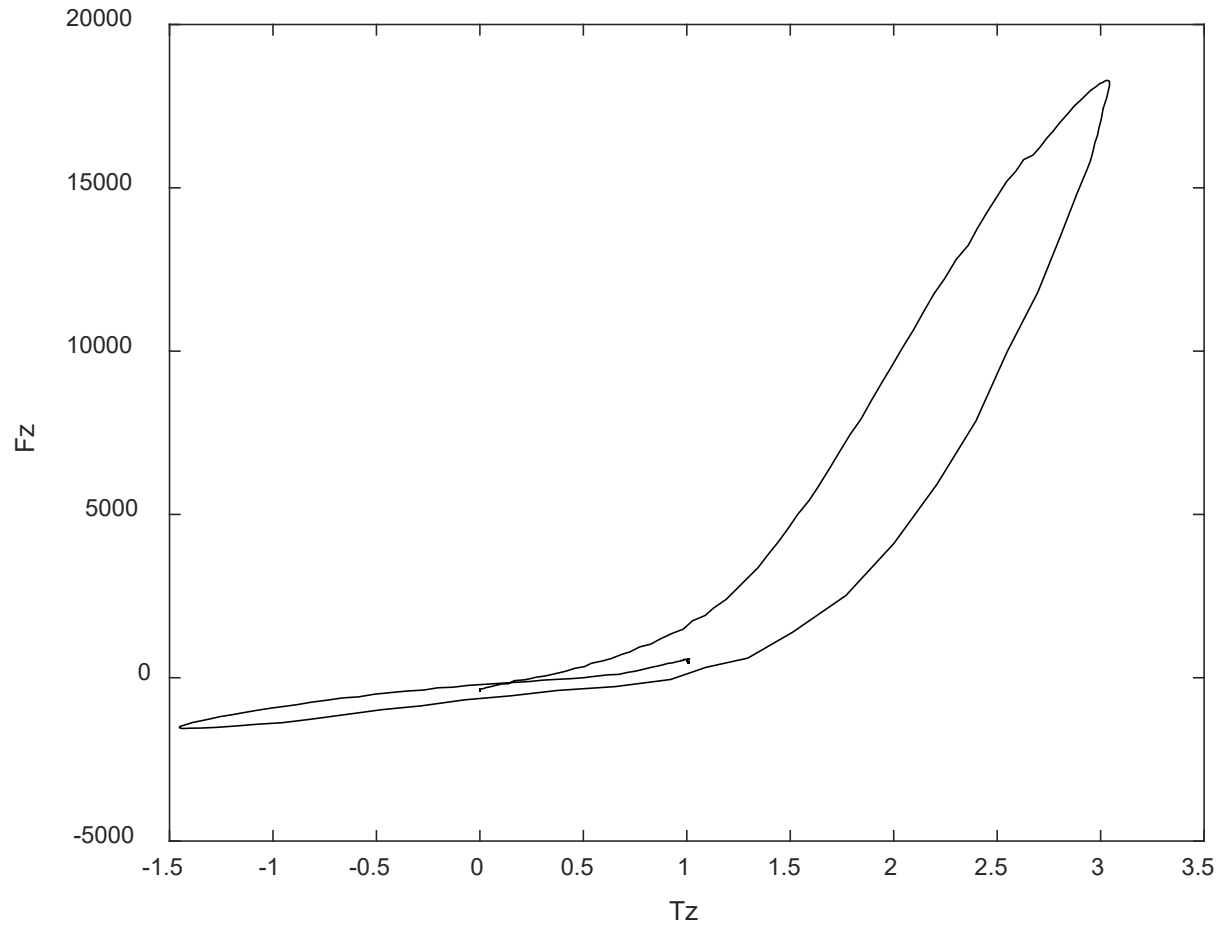Last Cycles of the 6DOF Dynamic Test at 0.1 Hz and 0.01 Hz:

Specimen 13 (After Radial Tear): T for translation, R for rotation, F for force, M for moment in/relative to x,y,z-axes

Calculations of Stiffness and Phase Angle:

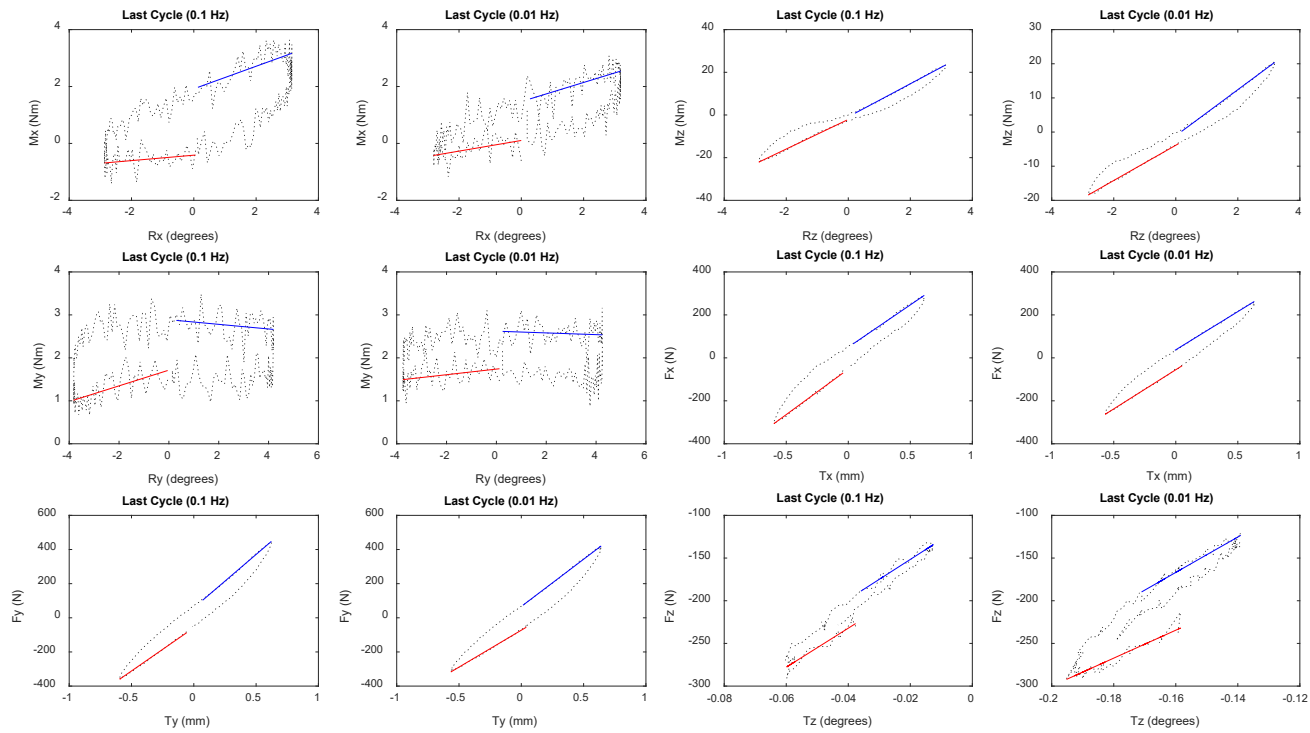| FileName	Test	Frequency	Stiffness_Positive_Direction	Stiffness_Negative_Direction	Phase
RTR13INB003Rx5E2	Rx	0.1	-0.15677 Nm/degree	2.8866 Nm/degree	21.32615239
RTR13INB003Rx5E3	Rx	0.01	-0.033303 Nm/degree	1.6659 Nm/degree	24.53913795
RTR13INB003Rz5E2	Rz	0.1	5.1371 Nm/degree	5.4853 Nm/degree	16.53183635
RTR13INB003Rz5E3	Rz	0.01	3.9212 Nm/degree	4.905 Nm/degree	11.76496199
RTR13INB004Ry5E2	Ry	0.1	-0.06682 Nm/degree	0.41182 Nm/degree	59.91255707
RTR13INB004Ry5E3	Ry	0.01	0.16435 Nm/degree	0.33801 Nm/degree	44.55611179
RTR13INB6E1Tx5E2	Tx	0.1	603.3498 N/mm	476.8006 N/mm	9.215812343
RTR13INB6E1Tx5E3	Tx	0.01	522.6657 N/mm	426.2076 N/mm	7.648875467
RTR13INB6E1Ty5E2	Ty	0.1	698.1726 N/mm	781.161 N/mm	9.863587106
RTR13INB6E1Ty5E3	Ty	0.01	603.5402 N/mm	650.501 N/mm	8.678469524
RTR13INN190Tz1E1M	Tz	0.1	3179.5767 N/mm	2970.361 N/mm	8.77119038
RTR13INN190Tz1E2M	Tz	0.01	2302.7228 N/mm	2282.1967 N/mm	11.59252743

Failure Under Sudden Overload:

Fz at fail = 18293.653

Specimen 15 (Before Radial Tear): T for translation, R for rotation, F for force, M for moment in/relative to x,y,z-axes

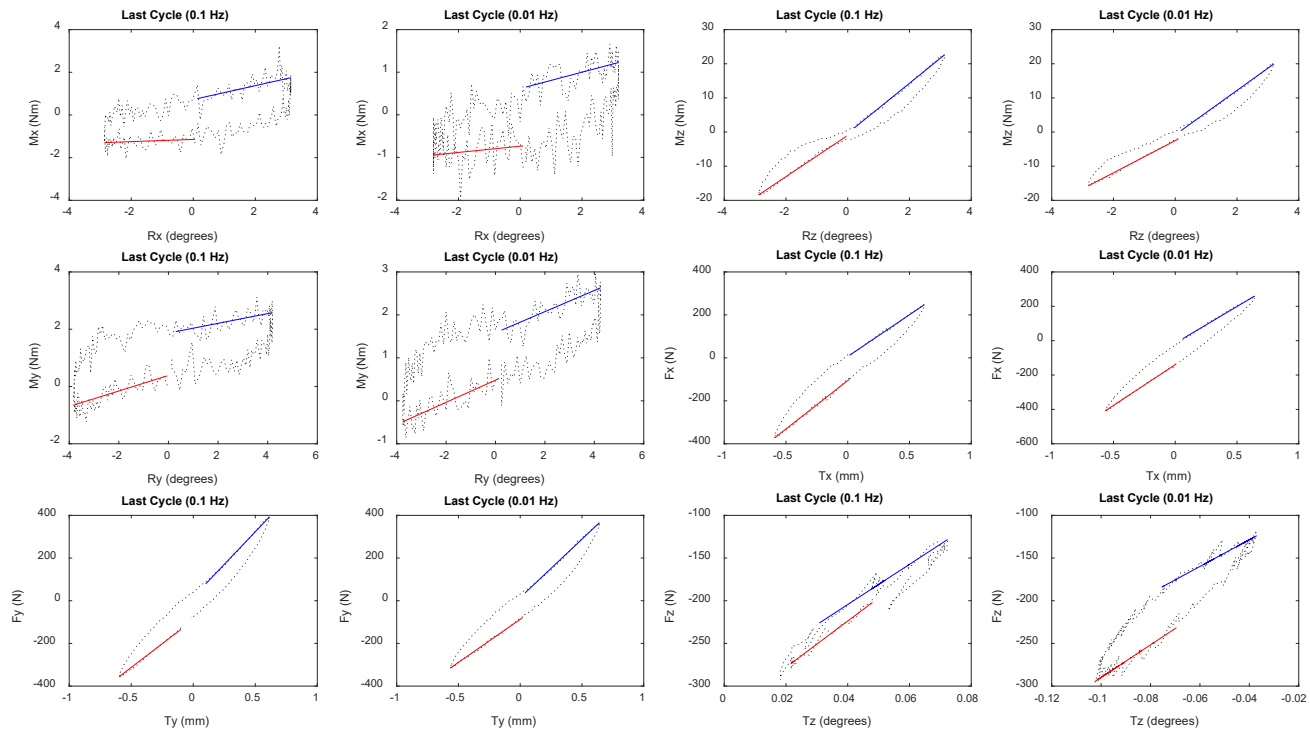Last Cycles of the 6DOF Dynamic Test at 0.1 Hz and 0.01 Hz:

Specimen 15 (Before Radial Tear): T for translation, R for rotation, F for force, M for moment in/relative to x,y,z-axes

Calculations of Stiffness and Phase Angle:

FileName	Test	Frequency	Stiffness_Positive_Direction	Stiffness_Negative_Direction	Phase
RTR15COB003Rx5E2	Rx	0.1	0.095348 Nm/degree	0.39639 Nm/degree	39.75791995
RTR15COB003Rx5E3	Rx	0.01	0.1871 Nm/degree	0.33545 Nm/degree	34.9659693
RTR15COB003Rz5E2	Rz	0.1	6.9276 Nm/degree	7.7382 Nm/degree	8.287237689
RTR15COB003Rz5E3	Rz	0.01	5.1626 Nm/degree	6.7405 Nm/degree	8.45460457
RTR15COB004Ry5E2	Ry	0.1	0.18295 Nm/degree	-0.05384 Nm/degree	68.17203886
RTR15COB004Ry5E3	Ry	0.01	0.065376 Nm/degree	-0.020086 Nm/degree	80.31133273
RTR15COB6E1Tx5E2	Tx	0.1	423.3405 N/mm	393.989 N/mm	10.99455436
RTR15COB6E1Tx5E3	Tx	0.01	364.7608 N/mm	355.5515 N/mm	10.19523765
RTR15COB6E1Ty5E2	Ty	0.1	506.3175 N/mm	625.2719 N/mm	9.598034635
RTR15COB6E1Ty5E3	Ty	0.01	432.526 N/mm	553.3341 N/mm	11.69855777
RTR15CON156Tz1E1M	Tz	0.1	2285.6388 N/mm	2331.3361 N/mm	10.45058077
RTR15CON156Tz1E2M	Tz	0.01	1635.9004 N/mm	2073.8249 N/mm	19.05714373

Specimen 15 (After Radial Tear): T for translation, R for rotation, F for force, M for moment in/relative to x,y,z-axes

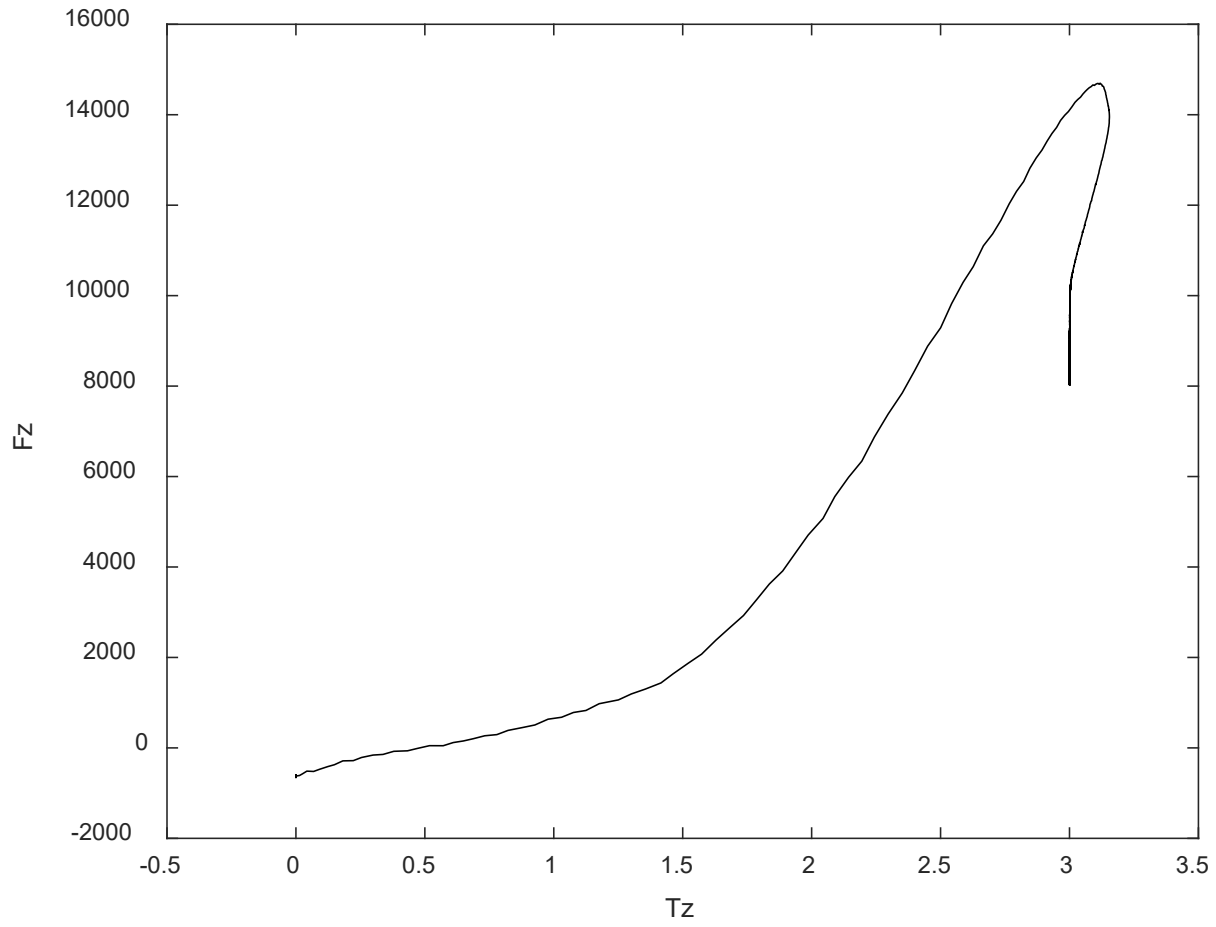Last Cycles of the 6DOF Dynamic Test at 0.1 Hz and 0.01 Hz:

Specimen 15 (After Radial Tear): T for translation, R for rotation, F for force, M for moment in/relative to x,y,z-axes

Calculations of Stiffness and Phase Angle:

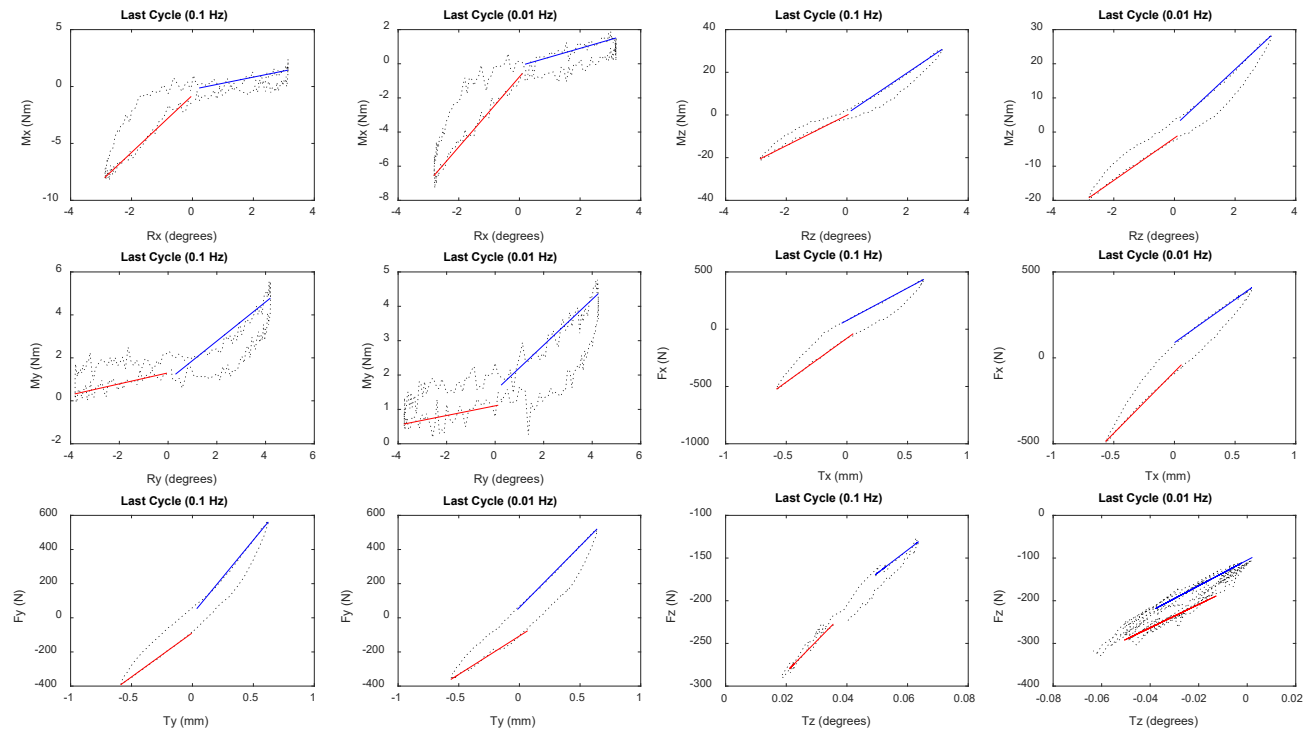| FileName	Test	Frequency	Stiffness_Positive_Direction	Stiffness_Negative_Direction	Phase
RTR15INB003Rx5E2	Rx	0.1	0.052836 Nm/degree	0.32512 Nm/degree	51.82999535
RTR15INB003Rx5E3	Rx	0.01	0.073403 Nm/degree	0.19256 Nm/degree	45.30050753
RTR15INB003Rz5E2	Rz	0.1	6.0369 Nm/degree	7.3216 Nm/degree	8.4283977
RTR15INB003Rz5E3	Rz	0.01	4.7041 Nm/degree	6.4968 Nm/degree	8.284218097
RTR15INB004Ry5E2	Ry	0.1	0.2706 Nm/degree	0.16986 Nm/degree	46.32643863
RTR15INB004Ry5E3	Ry	0.01	0.25848 Nm/degree	0.24597 Nm/degree	39.97736472
RTR15INB6E1Tx5E2	Tx	0.1	450.6827 N/mm	389.0485 N/mm	11.5348233
RTR15INB6E1Tx5E3	Tx	0.01	474.3474 N/mm	426.8389 N/mm	9.926409399
RTR15INB6E1Ty5E2	Ty	0.1	444.3289 N/mm	611.3714 N/mm	9.973957623
RTR15INB6E1Ty5E3	Ty	0.01	404.1211 N/mm	546.734 N/mm	11.03836106
RTR15INN156Tz1E1M	Tz	0.1	2711.5708 N/mm	2353.6276 N/mm	13.67112729
RTR15INN156Tz1E2M	Tz	0.01	1910.687 N/mm	1566.547 N/mm	19.28957486

Failure Under Sudden Overload:

Fz at fail = 14697.29

Specimen 17 (Before Radial Tear): T for translation, R for rotation, F for force, M for moment in/relative to x,y,z-axes

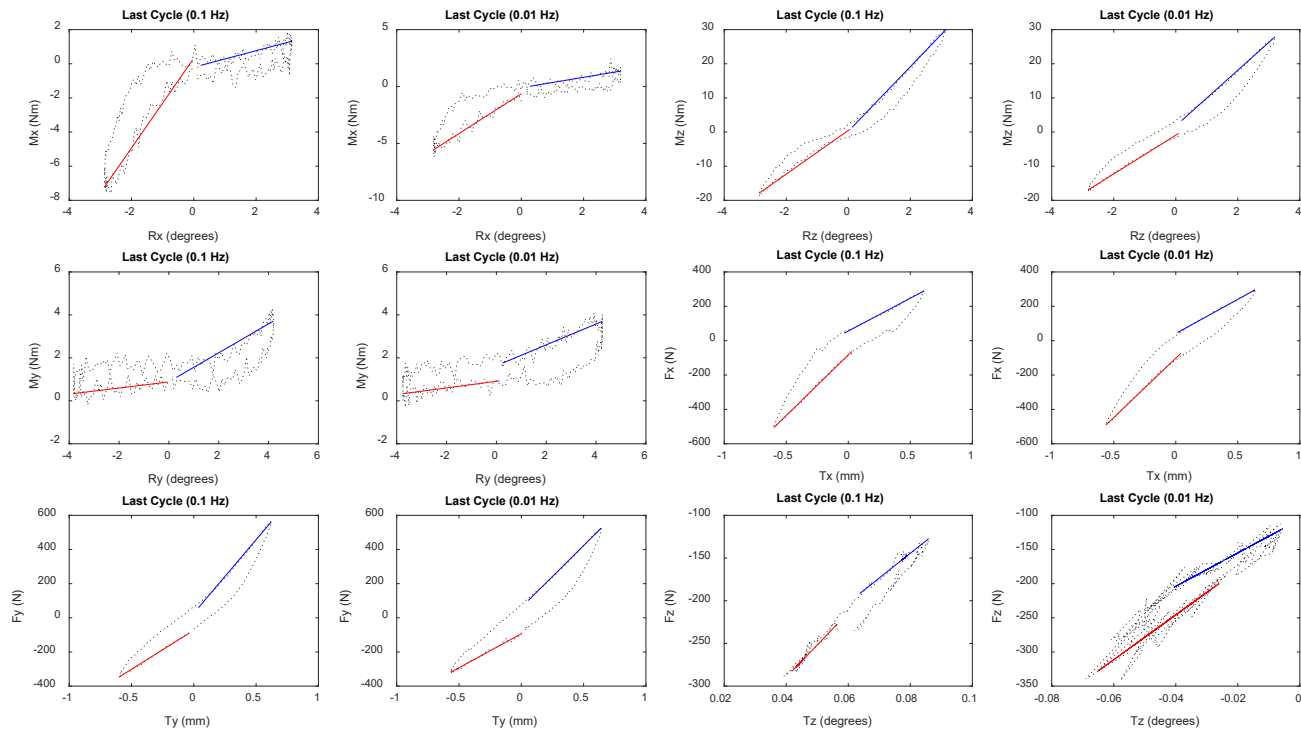Last Cycles of the 6DOF Dynamic Test at 0.1 Hz and 0.01 Hz:

Specimen 17 (Before Radial Tear): T for translation, R for rotation, F for force, M for moment in/relative to x,y,z-axes

Calculations of Stiffness and Phase Angle:

FileName	Test	Frequency	Stiffness_Positive_Direction	Stiffness_Negative_Direction	Phase
RTR17COB003Rx5E2	Rx	0.1	2.5134 Nm/degree	0.53877 Nm/degree	17.46416404
RTR17COB003Rx5E3	Rx	0.01	2.0534 Nm/degree	0.51245 Nm/degree	17.15520454
RTR17COB003Rz5E2	Rz	0.1	7.1405 Nm/degree	9.5861 Nm/degree	6.891484836
RTR17COB003Rz5E3	Rz	0.01	6.2076 Nm/degree	8.2858 Nm/degree	8.897600348
RTR17COB004Ry5E2	Ry	0.1	0.25618 Nm/degree	0.91006 Nm/degree	23.6338017
RTR17COB004Ry5E3	Ry	0.01	0.14096 Nm/degree	0.66504 Nm/degree	29.13367319
RTR17COB6E1Tx5E2	Tx	0.1	765.7737 N/mm	566.1334 N/mm	10.71253096
RTR17COB6E1Tx5E3	Tx	0.01	714.2398 N/mm	502.3091 N/mm	10.17780481
RTR17COB6E1Ty5E2	Ty	0.1	517.3361 N/mm	866.1912 N/mm	9.426158129
RTR17COB6E1Ty5E3	Ty	0.01	450.1726 N/mm	718.7039 N/mm	11.88699582
RTR17CON154Tz1E1M	Tz	0.1	3613.8001 N/mm	2714.8823 N/mm	7.742059473
RTR17CON154Tz1E2M	Tz	0.01	2732.6718 N/mm	2999.0148 N/mm	12.4666283

Specimen 17 (After Radial Tear): T for translation, R for rotation, F for force, M for moment in/relative to x,y,z-axes

Last Cycles of the 6DOF Dynamic Test at 0.1 Hz and 0.01 Hz:

Specimen 17 (After Radial Tear): T for translation, R for rotation, F for force, M for moment in/relative to x,y,z-axes

Calculations of Stiffness and Phase Angle:

FileName	Test	Frequency	Stiffness_Positive_Direction	Stiffness_Negative_Direction	Phase
RTR17INB003Rx5E2	Rx	0.1	2.6286 Nm/degree	0.48335 Nm/degree	19.13643409
RTR17INB003Rx5E3	Rx	0.01	1.7469 Nm/degree	0.45896 Nm/degree	18.78204673
RTR17INB003Rz5E2	Rz	0.1	6.3798 Nm/degree	9.4578 Nm/degree	6.892772514
RTR17INB003Rz5E3	Rz	0.01	5.6733 Nm/degree	8.1478 Nm/degree	8.861514123
RTR17INB004Ry5E2	Ry	0.1	0.14163 Nm/degree	0.6738 Nm/degree	32.83104683
RTR17INB004Ry5E3	Ry	0.01	0.15359 Nm/degree	0.48545 Nm/degree	36.76313742
RTR17INB6E1Tx5E2	Tx	0.1	705.1677 N/mm	382.0024 N/mm	12.43504029
RTR17INB6E1Tx5E3	Tx	0.01	691.0494 N/mm	397.8979 N/mm	11.0025928
RTR17INB6E1Ty5E2	Ty	0.1	457.2503 N/mm	861.208 N/mm	9.799017132
RTR17INB6E1Ty5E3	Ty	0.01	398.6627 N/mm	724.382 N/mm	12.46888639
RTR17INN154Tz1E1M	Tz	0.1	3782.0394 N/mm	2894.7166 N/mm	9.609550266
RTR17INN154Tz1E2M	Tz	0.01	3281.1898 N/mm	2443.041 N/mm	13.01903857

Failure Under Sudden Overload:

Fz at fail = 11883.35